Imaging the hemodynamics of pial collaterals and evaluating collateral therapeutics in rodent models of acute ischemic stroke

by

Junqiang Ma

A thesis submitted in partial fulfillment of the requirements for the degree of

Doctor of Philosophy

Neuroscience

University of Alberta

Abstract

Ischemic stroke is caused by blockage of a primary blood vessel supplying brain tissue. Cerebral collaterals are auxiliary vascular pathways in the cerebral circulation that can provide residual blood flow to partially maintain perfusion in ischemic tissue when primary vascular routes are blocked. Thus, it is collateral blood flow that slows down the progression of ischemic penumbra to irreversible ischemic damage. In this thesis, we investigated hemodynamic evolution of pial collaterals after stroke and provide preclinical evidence for a pair of pial collateral enhancement treatments (RIPerC and intravenous milrinone administration) to facilitate bench to bedside translation. To evaluate collateral flow during cerebral ischemia, laser speckle contrast imaging (LSCI) and two photon laser scanning microscopy (TPLSM) were used to image pial collaterals between the anterior cerebral artery (ACA) and the middle cerebral artery (MCA) in male Sprague Dawley rats during distal middle cerebral artery occlusion (dMCAo).

Ischemic stroke is age related and disproportionately affects the elderly. Aging leads to rarefaction of cerebral vessels and thereby accelerates ischemic injury by reducing penumbral blood flow via collaterals. Dynamic changes in pial collaterals after onset of cerebral ischemia may vary with age but have not been extensively studied. Therefore, in Chapter 2 we tested the hypothesis that retrograde pial collateral flow would be recruited immediately after dMCAo in both aged and young rats, but that aging would accelerate collateral failure over time and lead to more severe ischemic

damage. Our LSCI showed that cerebral collateral perfusion declined over time after stroke in aged and young rats, and that this decline was significantly greater in aged rats. TPLSM demonstrated that collateral failure is more severe in aged rats with significantly impaired pial collateral dynamics (reduced diameter, red blood cell velocity and red blood cell flux) relative to young adult rats. The accelerated collapse of pial collateral blood flow in aged rats exacerbated the insufficient perfusion of the penumbra and lead to greater ischemic damage than in young adult rats.

The dropout of collaterals during stroke is related to the progression of penumbra to irreversible ischemic infarct and impaired response to treatment. Enhancing cerebral pial collateral blood flow may therefore reduce ischemic damage. Remote ischemic perconditioning (RIPerC) involves inducing peripheral ischemia (typically in the limbs) during stroke and may reduce brain damage due to cerebral ischemia. In Chapter 3, we hypothesized that RIPerC treatment would induce a significant increase in blood flow through pial collaterals by enhanced dilation of pial collaterals relative to control rats. Our data clearly demonstrated that RIPerC significantly reduced early ischemic damage measured 6 h after stroke onset in both aged and young rats. This neuroprotective effect of RIPerC occurred at least in part due to the prevention of pial collateral collapse. While control rats exhibited an initial dilation followed by a progressive narrowing of pial arterioles after stroke, such constriction was prevented or reversed by RIPerC. Given the impairment in collateral blood flow observed in aged rats in Chapter 2, in Chapter 4 we examined the ability of RIPerC to drive collateral flow in aged animals.

Relative blood flow after dMCAO measured with LSCI suggested enhancement of blood flow in RIPerC treated aged stroke rats. Using TPLSM, we confirmed that RIPerC enhanced penumbral perfusion through pial collaterals and maintained retrograde blood flow from ACA to distal MCA segments. This improved flow was associated with reduced early ischemic damage in RIPerC treated aged rats.

Milrinone is a potent selective phosphodiesterase 3 (PDE3) inhibitor that inhibits cAMP specific PDE3 in both cardiac myocytes and vascular smooth muscle cells. PDE3 inhibitors may therefore have a cerebral vasodilatory effect with concomitant augmentation of cardiac output. We hypothesized that systemic pharmacotherapy with milrinone lactate would be effective for augmenting pial collateral flow and reducing cerebral ischemic damage. Using LSCI, we found that milrinone increased collateral flow acutely. Moreover, continuous subacute administration of milrinone was well tolerated. However, no significant reduction in infarct volume was found after five days of treatment.

In conclusion, the data herein demonstrates that aging has a detrimental effect on pial collateral flow during ischemic stroke. New therapeutic strategies aiming at modulating cerebral collateral flow, including RIPerC and milrinone, have translational potential as collateral therapeutics to reduce ischemic damage.

Preface

This thesis is an original work by Junqiang Ma. All animal researched was conducted in accordance with Canadian Council on Animal Care guidelines. All animals used protocols were approved by the University of Alberta Animal Care and Use Committee (AUP361, Ian Winship)

Chapter 2 of this thesis has been accepted for publication by Translational Stroke Research as Junqiang Ma, Yonglie Ma, Ashfaq Shuaib, and Ian R. Winship, "Impaired collateral flow in pial arterioles of aged rats during ischemic stroke". Junqiang Ma was responsible for experimental design, data collection and analysis as well as the manuscript composition. Yonglie Ma assisted with data collection and analysis. Dr. Ashfaq Shuaib contributed to experimental design, concept formation and manuscript edits. Dr. Ian R Winship was the supervisory author and was involved with experimental design, concept formation, manuscript composition and manuscript edits.

Chapter 3 of this thesis has been published as Junqiang Ma, Yonglie Ma, Bin Dong, Mischa V Bandet, Ashfaq Shuaib, and Ian R Winship," Prevention of the collapse of pial collaterals by remote ischemic perconditioning during acute ischemic stroke" Journal of Cerebral Blood Flow and Metabolism. 2017 Aug, volume 37(8), pages 3001–3014. Junqiang Ma was responsible for data collection and analysis as well as the manuscript composition. Yonglie Ma and Bin Dong assisted with data collection. Mischa V Bandet assisted with data collection and analysis. Dr. Ashfaq Shuaib contributed to experimental design, concept formation and manuscript edits. Dr. Ian R Winship was the supervisory author and was involved with experimental design, concept formation, manuscript composition and manuscript edits.

Chapter 4 of this thesis is in preparation for publication as Junqiang Ma, Yonglie Ma, Ashfaq Shuaib, and Ian R. Winship. Junqiang Ma was responsible for experimental design, data collection and analysis as well as the manuscript composition. Yonglie Ma assisted with data collection and analysis. Dr. Ashfaq Shuaib contributed to experimental design, concept formation and manuscript edits. Dr. Ian R Winship was the supervisory author and was involved with experimental design, concept formation, manuscript composition and manuscript edits.

Chapter 5 of this thesis forms part of a research collaboration between Dr. Ian R. Winship and Dr. Fred Colbourne both at the University of Alberta. Junqiang Ma was responsible for data collection and analysis as well as the manuscript composition. Yonglie Ma assisted with data collection and analysis. Dr. Fred Colbourne contributed to experimental design and manuscript edits. Ian R Winship was the supervisory author and was involved with experimental design, concept formation, manuscript composition and manuscript edits.

Acknowledgment

First and foremost, I would like to express my deepest gratitude and sincerest thanks to my supervisor, Dr. Ian Winship for his guidance, for his patience as well as for his encouragement throughout my Ph.D. education in the last 4 and half years. Thank you for taking a chance on me as your student and providing me with opportunities for professional development to grow as a researcher.

I also would like to thank my supervisory committee members, Dr. Ashfaq Shuaib and Dr. Ken Butcher, for their time, their constructive suggestions, and valuable feedback. I am also grateful to Dr. Fred Colbourne, who has also provided me with much needed academic advice.

I must thank our laboratory technician, Yonglie Ma, who helped me with my research, you have been my rock during these past years. I would also like to thank my lab mate, Eszter Wendlandt, who helped me with my coursework when I was struggling. I would not have been able to go through the course PTHER 567 without you. I would like to express my thanks to my lab mate, Mischa Bandet, for his technical assistance, your help is greatly appreciated. Thank you also to my other lab mates, Sam Joshva, John W. Paylor, Anna Wiersma and Somnath Gupta for your support and friendship throughout the course of my graduate studies. I would like to acknowledge the help I got from our laboratory technicians, Patricia Kent, Jocelyn Madeira and Bin Dong as well as the staff at the Neurochemical Research Unit and Neuroscience and Mental Health Institute. It is my fortune that I got a wonderful opportunity to work with all of you.

Of course, thanks and gratitude must go to my family. They do not speak English and have no idea what neuroscience is, but they provide me with endless love, and understanding which gave me the confidence to come abroad to pursue my Ph.D. degree.

Last by not the least, I would like to acknowledge the Li Ka Shing Foundation, for covering tuition and stipends during my PhD study in Canada. Without their support, I would never have had a chance to start my Ph.D. program. This generous sponsorship has changed my life profoundly.

While research life is challenging, it was and will be undoubtedly exciting. Thank you to everyone I have met along the way.

Table of Contents

List of Figures

Chapter 1

General Introduction

1.1. Stroke Epidemiology

Stroke is a devastating cerebrovascular disease caused by blockage or rupture of a blood vessel supplying the brain [1]. It is one of the main causes of death and the leading cause of long term disability worldwide [2,3]. Each year stroke is responsible for the deaths of approximately 5.5 million people around the world [4]. Stroke is age related and disproportionately affects the elderly, with risk of stroke doubling every decade after the age of 55 in both sexes [5–7]. Patients who survive after a stroke typically live with significant functional limitations that greatly impair activities in their daily life [8]. Notably, elderly stroke patients exhibit significantly worse functional recovery and higher mortality compared to younger patients [5–7].

1.2. Ischemic Stroke

Ischemic stroke accounts for 85% of all strokes, with the remainder of cases classified as hemorrhagic strokes or transient ischemic strokes [8]. Ischemic stroke occurs as a result of blockage of a blood vessel supplying the brain, while hemorrhagic stroke occurs when a vessel in the brain ruptures. During acute ischemic stroke, there are two major zones of injury that can be identified after the obstruction of the artery. The zone closest to the occluded artery is called the ischemic core, while a zone more peripheral to the occlusion is called the ischemic penumbra. Neurons in the ischemic core die within minutes, causing irreversible brain damage. Tissues surrounding the nonviable infarct core in the penumbra remain alive despite reduced cerebral blood flow, but are at risk for progressing into infarction [9]. The delayed nature of cell death in the penumbra leaves a unique window of opportunity for therapeutic interventions that attempt to save this tissue from death [4,10].

1.3. Cerebral Collaterals

Cerebral collaterals are auxiliary vascular pathways in the cerebral circulation that can partially maintain blood flow to ischemic tissue when primary vascular routes are blocked [11–14].Thus, it is collateral blood flow that defines the degree of ischemia in the penumbra. Cerebral collaterals can be classified as primary or secondary. Primary collaterals refer to the circulatory anastomoses that constitute the circle of Willis and allow blood flow exchange between anterior and posterior circulation and between the hemispheres [15]. Secondary collaterals include the pial collaterals, which are also called leptomeningeal collaterals [16]. Pial collaterals are anastomotic connections located on the cortical surface which connect distal branches of the anterior cerebral artery (ACA), middle cerebral artery (MCA), and posterior cerebral artery (PCA) [16,17]. The pial collaterals are therefore alternative circulatory routes to deliver blood to the ischemic penumbra after occlusion of the principal supplying artery (e.g. the MCA) during cortical stroke [16]. Rarefaction of cerebral collaterals with aging has been reported in preclinical models [18]. Such rarefaction would reduce aged animals' ability to maintain blood flow during ischemia, resulting in increasing risk of neuronal loss in brain regions where vessel rarefaction is prominent [18,19].

Collateral status at the time of occlusion (i.e., number and diameter) is also the strongest independent predictor of final infarct volume in patients and is considered crucial for clinical decision making in stroke treatment [14,20–24]. Blood flow through the pial collaterals defines the degree of ischemia in the penumbra of cortical infarcts [16,25]. The hemodynamic evolution of the collateral circulation is also important since collaterals are thought to be time limited and can fail over time [26–28]. The dropout of collaterals during stroke is related to the progression of penumbra to irreversible ischemic infarct and impaired response to treatment [26–28]. However, much about the dynamics of collateral blood flow and the potential of collateral flow enhancement as a treatment for ischemic stroke remain to be investigated. Moreover, the consequences of aging on the dynamics of the pial collateral circulation has not been well described.

1.4. Stroke Treatment & Important of Cerebral Collaterals

The treatment of acute ischemic stroke has entered a new era because of the consistent success of intravenous recombinant tissue plasminogen activator (IV r-tPA) and endovascular therapies (for example, thrombotic removal of the clot with guidance from Digital subtraction Angiography (DSA)) [25]. Both IV r-tPA and endovascular therapies can rescue penumbral tissue by recanalizing occluded cerebral arteries. However, even when recanalization is successful, some patients show lack of histological and neurologic benefit, possibly because the penumbral tissue had already progressed into the irreversibly damaged ischemic core due to insufficient collateral flow to sustain tissue viability until recanalization [25]. Patients with better collateral flow are more likely to have viable tissue at the time of recanalization [12,13,24]. Moreover, retrograde collateral flow may improve transportation of thrombolytic agents, such as intravenous recombinant tissue plasminogen activator (IV r-tPA), to the ischemic penumbra, increasing access to more areas of the thrombus and aiding in recanalization [13,25,29]. The data from the ESCAPE (Endovascular treatment for Small Core and Anterior circulation Proximal occlusion with Emphasis on minimizing CT to recanalization times) study, which included multiphase CT angiography, demonstrated a strong association between pre-treatment cerebral pial collaterals and favorable post stroke outcome after recanalization [30]. New data from DAWN (DWI or CTP Assessment with Clinical Mismatch in the Triage of Wake-Up and Late Presenting Strokes Undergoing Neurointervention with Trevo) and DEFUSE3 (Endovascular Therapy Following Imaging Evaluation for Ischemic Stroke) trials that evaluated patients following late thrombectomy (6 to 24 hours after stroke onset) reported significant benefits of endovascular treatment, in some cases even greater than in similar trials of early thrombectomy treatment [31,32]. Notably, patients with "slow-growing infarcts" due to good collateral circulation (identified by cerebral blood flow imaging) were selected into DAWN and DEFUSE3 trials [31–33]. Because these patients had sufficient collateral circulation to maintain tissue viability, they presented with large volumes of salvageable brain tissue that could be benefit from recanalization even up to 24 hours post stroke [33]. Moreover, lower rates of hemorrhagic transformation after recanalization occurred in patients with good collaterals [16,34,35]. After intra-arterial thrombolysis, only 2.78% of patients with good pial collaterals suffered a significant hemorrhage compared to 25% of those with poor collateral flow [16,35].

1.5. Cerebral Collateral Imaging

Collateral circulation is a key variable in determining prognosis and response to recanalization therapy during acute ischemic stroke, therefore, accurate imaging techniques are essential to define the anatomy, physiology of collateral circulation and to evaluate the benefits of collateral therapeutics [13,26]. This section will briefly outline some of the methods used to image blood flow in the clinical and pre-clinical setting.

1.5.1. Collateral Blood Flow Imaging in Humans

Numerous imaging methods have been developed to directly or indirectly evaluate collateral circulation. Direct assessment of collateral circulation can be performed via angiography techniques, which can visualize individual vessel distal to occlusion. Angiographic techniques include cerebral Digital Subtraction Angiography (DSA), Computed Tomographic Angiography (CTA), Magnetic Resonance angiography (MRA), and Transcranial Doppler sonography (TCD) [13,36]. Indirect methods such as CT perfusion, MR perfusion, and MR perfusion imaging of arterial spin labeling can be used to measure cerebral blood flow and indirectly estimate status of collateral circulation by measuring perfusion of ischemic tissues downstream of occluded artery [36]. At present, there is no consensus on which imaging should be performed in clinical practice, and different trails of endovascular treatment used different techniques to evaluate collaterals of patients [37]. Below we will briefly discuss these imaging techniques for collateral blood flow during stroke.

1.5.1.1. Digital Subtraction Angiography (DSA)

The high spatial and temporal resolution of DSA makes it the gold standard in assessing the presence and extent of all levels of collaterals including the circle of Willis and pial collaterals [38,39]. It is an invasive technique in which endovascular access is obtained by a catheter advanced through the puncture of common femoral artery to the proximal cranial circulation, such as the internal carotid artery or other artery of interest [36,39,40]. After contrast injection, DSA allows direct, real-time visualization of cerebral vasculature during arterial, parenchymal and venous phases under X-ray [36,40]. Therefore, a dynamic analysis of cerebral blood flow can be performed. The limitation of DSA is that it is impossible to simultaneously examine collaterals of anterior and posterior cerebral circulation, because images are acquired during injection of contrast by one single artery at a time [36,41]. Additionally, because it is invasive, greater expertise and time is needed to perform DSA, and it is not routinely used to evaluate collaterals for thrombolytic treatment decision making, especially in the acute clinical setting [39]. However, the advent of endovascular treatment such as thrombectomy in recent years has increased the utility of DSA, since endovascular access is needed for treatment.

1.5.1.2. Computed Tomographic (CT)

Given the widespread availability of CT and its tolerability for most stroke patients, CT is the most commonly used technique for stroke related imaging [13,39]. CT-based methods comprise both direct and indirect approaches, CTA and CTP, to evaluate cerebral collateral circulation.

The relatively non-invasive nature of CT-angiography (CTA) for identifying site of vascular occlusion and grading of collateral blood flow appears as an attractive alternative to DSA [42]. CTA is performed by standard CT scanner to acquire high resolution, thin slice cerebral vasculature CT images during the administration of intravenous iodinated contrast bolus injection [13,36]. With 3D image reconstruction, CTA allows 3D resolution of cerebral vasculature [13,43]. CTA is highly effective in assessing patency of the circle of Willis, with more than 90% agreement with DSA [38,44]. With proper post acquisition processing, collateral filling distal to the vascular occlusion can be visualized for pial collateral assessment [36,39]. However, retrograde blood flow via pial collaterals after stroke may be delayed as compared with normal anterograde flow [38]. There is a risk to underestimate the degree of collateral flow if image acquisition with CTA is done before contrast arrives in the pial vessels [37]. Recently, multiphase CTA, also named dynamic CTA, has been developed to address this issue [37,45]. The goal of multiphase CTA is to acquire rapid scans throughout the whole brain over multiple time points after contrast injection, enabling identification of pial collateral flow in a more time resolved manner [39,43,46]. The first image acquisition phase is set at the same time as the peak arterial phase, as the latter two phases coincide with peak venous and late venous phases [39,43,46]. Multiphase CTA can be quickly performed at the patient's arrival and requires less i.v. contrast material as compared to conventional CTA [41–43]. Multiphase CTA also provides better resolution of cerebral vasculature with hemodynamic information [42]. About 30% of patients diagnosed with "poor" collaterals with conventional CTA demonstrate adequate collateral if acquired with multiphase CTA [36,47].

CTP is an imaging technique capable of differentiating penumbra and ischemic core based on cerebral perfusion by generation of maps of cerebral blood volume (CBV), mean transit time (MTT), and cerebral blood flow (CBF) [43,48–50]. Although CTP dose not directly assess the number and size of pial collaterals, it provides blood flow and perfusion which are affected by the effectiveness of collateral supply [39]. Therefore, CTP helps to characterize status of collateral network [41,43,51].

1.5.1.3. Magnetic Resonance Imaging (MRI)

Similar to CT, MRI can be used with a number of direct and indirect approaches, including magnetic resonance angiography (MRA), magnetic resonance perfusion (MRP) and MRI Arterial spin labeling (ASL) to access cerebral collateral circulation [37]. However, it cannot be used in patients with magnetic appliances such as pacemakers or artificial joints [13,52].

MRA is a sensitive technique using magnetic resonance imaging approach to directly map cerebral vasculature, especially for the circle of Willis [13,53,54]. High field MRI allow for high resolution angiography to access pial collaterals for cerebral vascular disease [41,55]. Unlike CTA and DSA, MRA does not need radiation. Moreover, the contrast medium (gadolinium) for contrast enhanced MRA is generally safe, although some reports suggest risk of nephrogenic systemic fibrosis in patients with kidney function impairment [13,56].

MRP, also known as perfusion-weighted imaging, can indirectly assess the performance of collateral flow based on the perfusion information of cerebral tissues [39], though it does quantify the number or size of collaterals directly. A variety of different MRP parameters have been used to evaluate collateral status [57–60]. However, there is still no consensus about which is the most appropriate [57–60].

MRI arterial spin labeling (ASL) is a promising non-contrast perfusion imaging method capable of blood flow quantification which depends on the magnetic labeling of arterial water [41]. Pial collaterals can be identified on ASL images as linear hyper intense regions in the peripheral area of the ischemic penumbra [39]. Furthermore, ASL can also distinguish blood flow direction between anterograde and retrograde based on different post label imaging delays [39,61]. A retrospective study with acute ischemic stroke patients showed collateral flow detected by ASL strongly correlated with good clinical outcome [39,62,63]. In general, ASL is an alternative technique that could be used to characterize pial collateral status [37,39,64]. However, the long acquisition time of ASL has limited its use clinically [65].

1.5.1.4. Transcranial Doppler ultrasonography (TCD)

Transcranial Doppler ultrasonography (TCD) is a non-invasive, reliable screening and monitoring tool to evaluate collateral circulation around the circle of Willis [13,14,53]. TCD use transcranial ultrasound beam to sample over particular cerebral blood vessels [13]. Thus, stroke patients are not exposed to repeated doses of contrast agents and radiation during collateral circulation monitoring [13]. By analyzing the waveforms shifts caused by velocity of moving particles inside vessels, TCD can provide real time collateral status and cerebral blood flow velocity with a low cost [13]. However, the quality of images and accuracy of TCD measurements are highly dependent on the experience of the operator [38,52,53].

1.5.2. Collateral Blood Flow Imaging in Laboratory Animals

Clinical studies of cerebral collaterals are limited by safety, feasibility and the access to imaging modalities and heterogeneity of patients and treatment options [13]. Continuously monitoring the natural evolution of pial collaterals in humans after stroke is unrealistic in the clinical setting, where the progress of stroke is time sensitive and access to thrombolysis or thrombectomy for restoring blood flow of occlusive vessel is prioritized. Experimental stroke models offer greater experimental control and could play a crucial role for facilitating a deeper understanding of techniques to increase collateral flow and the modulatory mechanisms of cerebral collateral circulation [37]. Although clinical techniques like DSA, CT, MRI and TCD could also be used in animals for pre-clinical studies of cerebral collateral flow, they have several limitations including inadequate spatial resolution for small pial collaterals in rodents, high cost, and limited availability [37,66]. Below we will discuss two imaging techniques, laser speckle contrast imaging (LSCI) and two photon laser scanning microscopy (TPLSM), which are available for use in preclinical studies and provide high spatial resolution and nearly real time temporal resolution for assessing cerebral pial collaterals.

1.5.2.1. Laser Speckle Contrast Imaging (LSCI)

LSCI is a technology capable of elucidating in real time the hemodynamic evolution of cerebral blood flow in ischemic cortex with high spatial temporal resolution in a two dimensional, wide field of view [67,68]. When illuminating a surface with coherent laser light, it will appear granular to the observer. This effect is commonly known as the speckle effect. A scattering of the laser light by moving particles, such as blood cells in pial vessels on the cortical surface, will cause fluctuations of the speckle pattern. If these fluctuations are recorded by camera with fixed exposure time, the pattern will appear blurred (Figure 1-1). Such blurring is generally quantified as speckle contrast, a measure of relative changes in blood flow. The speckle contrast value (*K*) is defined as the ratio of the standard deviation to the mean intensity ($K = \sigma_s/I$) in a small region of the speckle image (typically 5× 5 or 7x7 pixels). Speckle contrast can be plotted to generate a LSCI map of blood flow (Figure 1-1). Speckle contrast and motion of the scattering particles (red blood cells) are inversely related [13]. *K* value ranges from 0 to 1. When red blood cells (RBC) are moving very fast in vessels, the speckle *K* will be very close to 0 and vice versa, when no blood flow in vessels, then *K* is approaching to 1 [13]. LSCI has been used in middle cerebral artery occlusion (MCAo) rodent models to measure dynamic change of cortical blood flow and pial collateral circulations after stroke [27,28,37]. Although LSCI provides sensitive mapping of blood flow on cortical surface and speckle contrast value *K* are indicative of RBC motion, the exact quantitative relationship between *K* and blood flow velocity are still undefined [37,69]. Therefore, LSCI is best used to describe relative blood flow changes rather than absolute quantification [13,37,70,71].

Armitage et al. were the first to use LSCI to precisely map the robust anastomotic connections between the ACA and MCA which are recruited after thromboembolic MCA. Their data showed that these collateral connections were dynamic but most persisted at least for 24 hours in rats [27]. Later, Wang et al. reported that based on dynamic changes in LSCI maps, the recruitment of collaterals after intraluminal suture MCAO could be classified in to three different kinds: persistent, impermanent, and transient pial collaterals. Persistent pial collaterals were found in normal healthy brain areas, while the impermanent and transient ones were associated with penumbra that had moderate and severe ischemia [28,37]. LSCI for cortical surface vessels blood flow measurement has been used to measure changes in blood flow during collateral flow augmentation therapies. For example, LSCI was used to demonstrate that transient aortic occlusion is capable of augmenting collateral blood flow in two different stroke models in rats, the thromboembolic MCAO and an intraluminal proximal MCA occlusion with a silicone rubber coated monofilament [11,72].

1.5.2.2. Two Photon Laser Scanning Microscopy (TPLSM)

TPLSM is an optical imaging technique permits precise quantitative measurement of RBC direction of flow (which is not possible with LSCI) and velocity in single vessels [13,37]. After intravenous injection of fluorescent dye, plasma is labelled thus allowing cortical microcirculation with depth resolution up to 1mm be visualized and imaged using two photon fluorescence microscopy through cranial window preparations [37]. Precise vessel diameter measurements can be obtained from maximum intensity projections of image stacks collected through the cortex [73]. To determine RBC velocity, line scans can be performed in the lumen of identified arterioles or capillaries. As RBCs do not take up fluorescent dye, they are detectable as non-fluorescent streaks in plots of the line scan images where the slope of streaks represents RBC velocity (Figure 1-2). Vessel diameter and RBC velocity collected from a single vessel can then be combined to calculate RBC flux, which provides an overall measure of flow through each individual collateral vessel.

TPLSM can provide important insight on the rules regulating cerebral blood flow in many different studies [13,74–77]. Shih et al. visualized blood vessels and neurons in the somatosensory cortex of anesthetized rats with in vivo two-photon laser scanning microscopy to examine changes flow through penetrating arterioles and the microcirculation in the healthy brain and after focal ischemia [78–80]. Using TPLSM, these studies showed that the pre-occlusion flux of RBCs through a single occluded penetrating vessel is directly correlated with the volume of infarction within that region. Thus, TPLSM quantitatively demonstrated the relationship between occlusion of vessels and infarct, and demonstrated with high resolution that occlusion of penetrating vessels with larger diameters and therefore with greater flux led to larger microinfarcts [80]. Similarly, Tennant et al. [81] used in vivo two-photon imaging to track micro vessels before and after stroke and evaluate the impact of chronic hyperglycemia on vascular dynamics post stroke. Imaging was performed before stroke and on days 3, 7, 14, and 28 after the stroke. TPLSM data showed that chronic hyperglycemia significantly affected the vascular dynamics after ischemic stroke, especially in superficial vessels in the peri-infarct cortex. The data showed that dilation of peri-infarct micro vessels occurred in both diabetic and non-diabetic mice. In diabetic mice vessels remained dilated until 14 days post stroke, however, whereas the vessels of nondiabetic mice returned to baseline diameters on day 7 post stroke. Diabetic mice showed a significant increase in blood flow velocity (relative to baseline values) at 3 days after stroke, and this enhancement remained until 14 days post stroke. By contrast, blood flow velocity in nondiabetic mice did not increase after stroke and velocities remained lower than diabetic mice at all imaging time points. When RBC flux was calculated from blood flow velocity and vessel diameter, a significant increase in RBC flux in superficial periinfarct microvessels was observed in diabetic at 3 days post stroke that returned to baseline at 7th day post stroke [81]. TPLSM has also been used in studies of collateral blood flow. Luo et al [82] used femtosecond laser pulses to occlude the target a pial arteriole of the MCA in vivo and documented leptomeningeal anastomoses with TPLSM. They reported that such occlusion caused dynamic changes of the leptomeningeal anastomoses diameter and the RBC velocity and confirmed reversal of blood flow direction reflecting input from ACA arterioles.

1.6. Cerebral Collateral Enhancement Treatment

As discussed above, good pial collateral circulation is associated with improved outcome after recanalization. Based on these data, it seems promising that enhancing collateral blood flow by pharmacological or mechanical means may have a therapeutic role in the acute or hyper-acute (even pre-hospital) phase of ischemic stroke by maintaining blood supply in the ischemic penumbra and reducing cell death in this at-risk [13]. In recent years, the concept of the tissue viability window has been raised to guide acute stroke treatment. Progression of brain ischemia is dynamic and influenced by the location of occluded artery, completeness of occlusion and the extent of the collateral circulation [83]. While the time window guided treatment selection of 4.5h for r-tPA treatment and 6h for endovascular treatment is simply accounting on the time from stroke onset, the tissue window guided treatment selection use advanced imaging techniques to accurately access stroke progression and identify a suitable time window for recanalization treatment in patients [31,32,83]. In 2018, two clinical trials, DAWN and DEFUSE-3, demonstrated that thrombectomy improved outcomes up to 24 h from stroke onset for selected acute ischemic stroke patients who had small ischemic core, slow growth rate of infarct, and a large penumbra [31,32,84]. With effective treatments to enhance cerebral collateral flow, more penumbra could be kept alive and more patients would be eligible for recanalization therapy even with longer delays from time of onset. Several methods for enhancing collateral cerebral blood flow have been tested in preclinical and clinical studies, including mild hypertension induction, sphenopalatine ganglion stimulation, partial aortic occlusion, external counter pulsation, and remote ischemic per-conditioning [14,16,43,85,86]. Here we will briefly introduce these cerebral collateral enhancement treatments after stroke and discuss the strength of their supporting evidence in preclinical and clinical studies.

1.6.1. Induced Mild Hypertension

Cerebral autoregulation is impaired in ischemic stroke patients, therefore, changes in systemic blood pressure during stroke may have a linear effect on cerebral blood flow in penumbral regions [16,53,87]. It is well known that blood pressure reduction in ischemic patients after stroke can lead to worse neurological outcome [13,88]. However, elevated blood pressure in hypertensive patients is also known to be associated with increased risk of hemorrhagic transformation [89–92]. It is reported that the risk of hemorrhagic transformation increases with each 10 mm Hg rise in systolic blood pressure from 140 to 180 mm Hg [93,94]. The 2018 Guidelines for the Early Management of Patients With Acute Ischemic Stroke therefore recommended hypotension should be corrected to maintain systemic perfusion, but in order to prevent hemorrhage transformation, blood pressure should be lowered to below 185/110 mm Hg if this value is exceeded prior to r-tPA therapy [95]. Conversely, while hypertension (particularly chronic hypertension) can lead to increased risk of hemorrhage, artificially inducing mild hypertension may help to increase flow through pial collateral channels, enhance cerebral blood flow, maintain penumbra perfusion and protect neuronal function [13,53,96–98]. Neuroprotection by mild induced hypertension has been demonstrated in animal studies [13]. Reduction of infarction by increasing blood pressure was first reported with angiotensin administration in rats after transient middle cerebral artery occlusion (MCAO) in 1996 [99]. More recently, Shin et al. induced mild hypertension with intravenous phenylephrine

1 hour after ischemic onset in mice with transient distal middle cerebral artery occlusion (dMCAo) [13,16,100]. Although phenylephrine is a selective a1-agnoist with systemic vasoconstriction causing hypertension, it has very limit constrict effect on cerebral arteries due to the low density of a1 receptors in the brain [37,53]. Treated mice displayed decreased infarction and pial collateral flow augmentation that was confirmed by laser speckle flowmetry [43,100]. Clinical applications of mild hypertension induction therapy are still under investigation [53]. Preliminary clinical studies have suggested that inducing mild hypertension may reduce volume of hypo-perfused tissue and increase neurological function as measured by NIHSS scores [13,16,97,101,102]. However, as noted above, blood pressure is often elevated during stroke clinically, therefore, addition hypertension induction may increase risk of intracerebral hemorrhage [12,13,16,98]. Large, randomized trials of mild hypertension induction therapy are needed to better assess its safety and effects on collateral channels and neurological outcome.

1.6.2. Sphenopalatine Ganglion Stimulation

Sphenopalatine ganglion (SPG) is a parasympathetic ganglia located in the pterygopalatine fossa, which is found behind the bony structure of the nose [103]. The SPG can be accessed from the oral cavity under local anesthesia [85], and electrical stimulation of SPG after MCAO can activate postganglionic parasympathetic fibers and has been shown to induce vasodilation and ipsilateral hemispheric blood flow enhancement in a number of animal studies [14,16,37,104–107]. Stimulation of SPG has been shown to freeze the penumbra, reduce infarct size, and improve behavioral outcomes after ischemic stroke in rats [14,43,106,108–110]. A pilot clinical study on SPG stimulation (Implant for Augmentation of CBF trial 1, ImpACT-1) was launched in 2009 to study the safety, efficacy and tolerability of sphenopalatine ganglion stimulation accessed from the oral cavity in ischemic stroke patients within 24 hours of onset [85,111]. Data collection was completed in June, 2018 and the results show SPG stimulation is safe for acute ischemic stroke patients within 24 hours of onset [112,113]. A trend for benefit in function outcome was observed, especially for patients with imaging evidence of cortical involvement at presentation [112,113].

1.6.3. Partial Aortic Occlusion

Partial occlusion of the abdominal aorta attempts to increase perfusion of ischemic territories and enhance cerebral blood flow by diverting blood flow from the periphery [13]. Noor et al. demonstrated that partial aortic occlusion reduced infarction size when used alone and had further neuroprotection when combined with r-tPA treatment in the thromboembolic MCAo rat model [13,14,114]. The Winship lab used LSCI to image pial collateral circulation and demonstrated that transit aortic occlusion increased cerebral blood flow in rats after thromboembolic MCAo via ACA-MCA anastomoses for at least 75mins after transit aortic occlusion [11,16,37]. A dual balloon catheter system capable of partially occluding the aortic lumen by as much as 80% above and below renal arteries has been developed for use in patients with acute stroke (NeuroFlo, CoAxia, USA;) [14,38,53,85]. In a preclinical study, Hammer et al. used the intra-aortic NeuroFlo catheter in a non-stroke porcine model to study the effect of partial aortic occlusion on cerebral perfusion. The data suggested that cerebral blood flow of normal adult pigs increased with inflation of suprarenal balloon and remained elevated at least 90min after deflation without adversely affecting cardiac performance [85,115,116]. The Safety and Efficacy of NeuroFlo in Acute Ischemic Stroke (SENTIS) trial randomly tested aortic occlusion in acute ischemic stroke patients within 14 hours of symptom onset and found that transit aortic occlusion is safe with no difference in serious adverse events as compared to controls who were given standard treatments [11,13,14,16,85,117–121]. The primary efficacy endpoint for SENTIS trial was neutral, although with a trend for reduced mortality in NeuroFlo treated group. (11.2% vs 16.3%; OR 1.60; 95% CI 0.91 to 2.83; p=0.086) [38,43,106,117,120]. However, post-hoc subgroup analyses suggested that transit aortic occlusion had significant benefit in patients aged over 70 years, patients treated in an early window (within 5 hours of symptom onset) and patients with moderate stroke severity (NIHSS score of 8–14) [16,117,118,120–122]. These findings indicate that appropriate patient selection is important for NeuroFlo treatment to benefit [85]. Further investigation that combine NeuroFlo with recanalization therapies are warranted to address the penumbral freezing effect of transit aortic occlusion.

1.6.4. External Counter Pulsation

External counter pulsation is a noninvasive treatment which can increase cardiac output and augment blood flow to vital organs including the brain [38]. It operates by applying electrocardiogram triggered air filled cuffs around the lower extremities and buttocks. During diastole, cuffs from lower extremities to buttocks are triggered sequentially with inflation pressure up to 250mmHg [53,85,123–125]. Such inflation of air cuffs augment blood flow to aortic artery from lower limbs and create retrograde pressure wave at the same time, leading to the elevation of blood pressure. The cuffs are deflated before the start of systole lowering peripheral vascular resistance during systole by making a relative empty vascular bed in lower limbs [53,123,126–128]. External counter pulsation treatment has been piloted in acute ischemic stroke patients and induced improvement in neurological outcome [14,129]. The results also suggested that external counter pulsation is associated with cerebral blood flow enhancement in the ipsilateral and contralateral hemisphere after stroke, which may indicate collateral flow augmentation to the ischemic region [38,127,130–132]. However, well designed and large scale RCTs are still needed for further investigation [85,133].

1.6.5. Remote Ischemic Per-Conditioning (RIPerC)

Ischemic conditioning was introduced in the 1980s [134] as a treatment to induce an organ's endogenous mechanism of protection against ischemic injury by the application of repetitive, sub-lethal, transit ischemic periods before or after more severe ischemic insults (referred to as local pre- and post-conditioning, respectively). A significant breakthrough in the study of ischemic conditioning as a protective therapy was the discovery that ischemic conditioning (repetitive, short periods of ischemic/reperfusion) induced at a non-vital organ remote to the site of severe ischemia (termed “remote ischemic conditioning”), such as the limb in the case of cerebral ischemia, can also protect vital target organs compared to unconditioned occlusion controls [135]. Crucially, remote ischemic conditioning can be applied prior to stroke (termed remote ischemic preconditioning), after the onset of ischemia (termed remote ischemic per-conditioning (RIPerC), or at the time of reperfusion (termed remote ischemic post-conditioning) [136]. RIPerC has promise as an acute ischemic stroke treatment that can be applied during target organ ischemia whether patients receive reperfusion treatment (e.g. r-tPA) or not [135].

Preliminary preclinical and clinical data suggest that RIPerC may be neuroprotective [8,137–144]. However, relatively little is known about the underlying protective mechanisms of RIPerC. The neuroprotective effect of RIPerC works by multiple mechanisms, potentially including improvement of cerebral blood flow [135,140,145]. Hoda et al. studied RIPerC using the autologous thromboembolic MCA occlusion mouse model with CBF measurement by laser Doppler flowmetry and LSCI [139–141]. These studies suggested that RIPerC was effective alone and in combination with i.v. r-tPA to enhance cerebral blood flow in young male, ovarectomized females and aged male mice (12 months old) [139–141,146,147]. Kitagawa reported that diameter of pial collaterals are larger in RIPerC treated transient MCAo mice than control MCAo mice with latex compound perfusion at 24 hour post stroke [148]. A research group in Denmark conducted the first randomized trial to examine adjunctive neuroprotective effects of RIPerC in acute stroke patients in the prehospital setting prior to r-tPA treatment [135,137,144]. Four cycles of 5mins occlusion and 5mins reperfusion of upper limb by manual cuff inflation of RIPerC treatment was administered by paramedics to patients with stroke symptoms presentation during transportation in the ambulance [137,144]. Less than half of patients received full conditioning regiment due to a transportation time that was too short [140,145,146]. Only patients who had MRI based acute ischemic stroke evidence and were eligible for r-tPA treatment were included for further analysis [137,144,146]. The primary endpoint was penumbral salvage assessed by MRI, and the secondary endpoints were infarct growth, final infarct size and functional outcome assessed with modified Rankin Scale after 3 months [135,137,144,146]. No intolerable discomfort and adverse events caused by RIPerC were reported [144,146]. The MRI study demonstrated no significant effect in of RIPerC on penumbral salvage, infarct growth and final infarct size or functional outcome after RIPerC [144–146]. However, after adjustment for baseline severity of hypo-perfusion, there was evidence of tissue protection by RIPerC in post hoc MRI data analysis with voxel based logistic regression method [144–146]. Thus, there is some evidence that pre hospital RIPerC may be neuroprotective [145]. However, this finding should be interpreted with caution since voxel based analysis of tissue survival was not a prespecified endpoint [144,146]. Notably, RIPerC treated patients showed higher proportion of TIA diagnosis and lower NIHSS score at admission than controls [144,146]. Therefore, more patients in the RIPerC group did not receive r-tPA treatment and were excluded from further analysis [144,146]. The higher proportion of TIA in RIPerC group may indicate that RIPerC increased the chance of prehospital reperfusion and is neuroprotective alone even without r-tPA [137,144–146]. However, stroke symptom severity was not assessed before RIPerC treatment, and an initial stroke severity imbalance of RIPerC treatment group and control group during randomization process could not be ruled out [137,144–146]. In general, prehospital RIPerC seems safe, tolerable and feasible with a likely benefit on tissue survival [144]. Further studies with a more optimized design to determine stroke symptom severity before RIPerC should be conducted to prove clinical effect of RIPerC.

1.7. General Objectives and Hypotheses:

This thesis aims to further our understanding regarding hemodynamic evolution of pial collaterals after stroke and provide preclinical evidence on a pair of pial collateral enhancement treatments (RIPerC and intravenous milrinone administration) to facilitate bench to bedside translation.

As one of the most significant health problems worldwide, ischemic stroke negatively affects patients and their family, and results in significant expense to the healthcare system. However, the clinical therapeutic options are still limited and mostly rely on vessel recanalization by intravenous r-TPA or endovascular therapy. Clinical evidence shows that collateral status at the time of occlusion (i.e., number and diameter) is the strongest independent predictor of final infarct volume [14,20–24]. The hemodynamic evolution of the collateral circulation is also important since collaterals are thought to be time limited and can fail over time [26–28]. Rarefaction of cerebral collaterals with aging[18], but the consequences of aging on the dynamics of the pial collateral circulation has not been well defined.

Altered collateral dynamics with aging are important considering that aging is one of the risk factors for ischemic stroke and the brain of the elderly has worse ischemic tolerance [149–152]. Thus, in the first set of experiments described in this thesis (Chapter 2), we used in vivo imaging to assess the impact of aging on hemodynamic evolution of pial collaterals circulation post dMCAo with SD rats. We hypothesized that retrograde pial collateral flow is recruited immediately after dMCAo in both aged and young rats, but aging would accelerate collateral failure over time, leading to more severe cerebral ischemic damage.

Next we examined new treatment to improve collateral blood flow. The dropout of collaterals during stroke is related to the progression of penumbra to irreversible ischemic infarct and impaired response to treatment [26–28]. Enhancing cerebral pial collateral blood flow by mechanical or pharmacological means may therefore be helpful in stroke therapy, especially before recanalization treatment.

The goals of Chapter 3 and Chapter 4 were to determine whether RIPerC is a viable method for augmenting pial collateral flow and reducing infarction after dMCAo in young adult (Chapter 3) and aged (Chapter 4) rats. We hypothesized 1) that RIPerC treatment would induce a significant increase in blood flow through pial collaterals by continued dilation of pial collaterals while pial collaterals in control rats would exhibit progressive constriction; and 2) Prevention of collateral failure by RIPerC would persist in aged rats and provide neuroprotection.

Chapter 5 examined milrinone treatment as a collateral therapeutic. Milrinone is a potent selective phosphodiesterase 3 (PDE3) inhibitor that inhibits cAMP specific PDE3 in cardiac myocytes and vascular smooth muscle cells [153]. The inotropic effect of milrinone is largely attribute to PDE3 inhibition, leading to intracellular cyclic AMP accumulation and an increase of cyclic AMP dependent protein kinase A (PKA). PKA not only phosphorylates the myofilament proteins which can promote action of myosin and actin, but also phosphorylates calcium channels causing trans-sarcolemmal calcium influx. Both of these lead to cardiac contractility enhancement and cardiac output augmentation [154–156]. The vasodilatation effect of milrinone is mediated by increasing of cAMP in vascular smooth muscle which stimulates calcium uptake into the sarcoplasmic reticulum, reducing the affinity of troponin C to calcium available for contraction, and thus relaxing vascular tone [157–160]. PDE3 is highly expressed in cerebral arteries smooth muscle cells. Therefore, after ischemic stroke, milrinone may enhance penumbra perfusion through dilating cerebral pial collaterals while maintain systemic hemodynamic at the same time due to enhancing cardiac output. Therefore, in Chapter 5, we hypothesized that systemic collateral pharmacotherapy with milrinone lactate is effective for augmenting pial collateral flow and reducing cerebral ischemic damage.

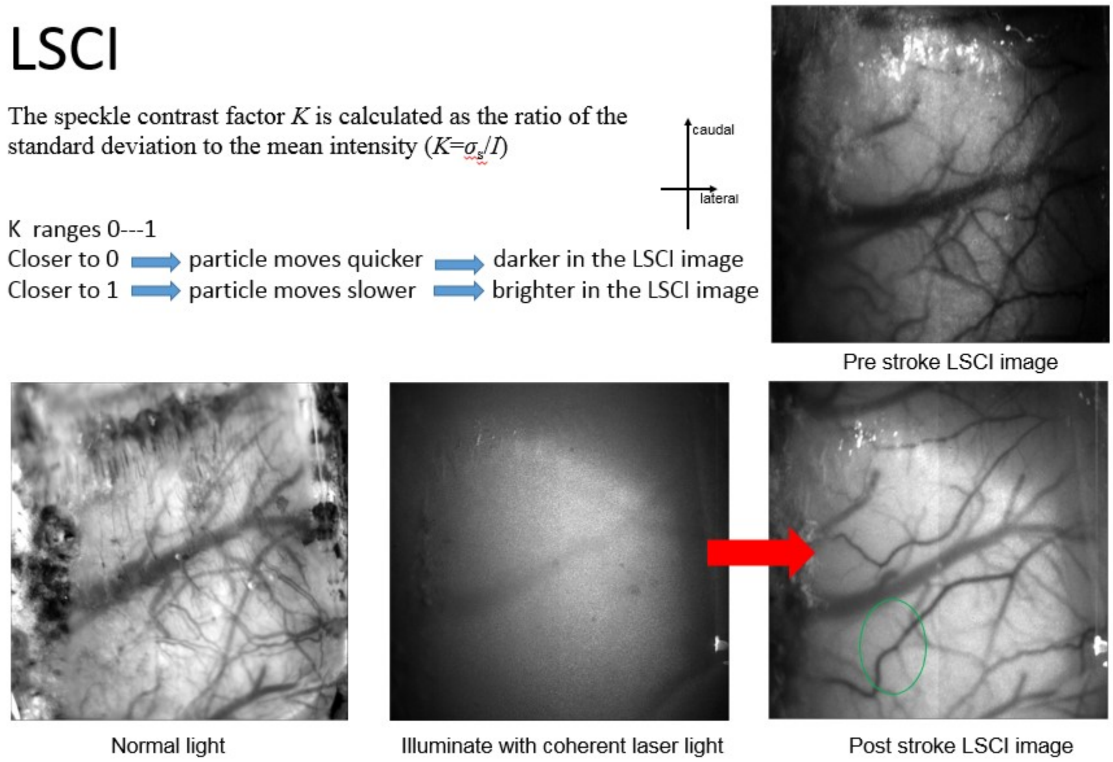

Figure 1- 1 Mechanism of Laser speckle contrast imaging.

When illuminating a surface with coherent laser light, it will appear granular to the observer. This effect is commonly known as the speckle effect. A scattering of the laser light by moving particles, such as blood cells in pial vessels on the cortical surface, will cause fluctuations of the speckle pattern. If these fluctuations are recorded by camera with fixed exposure time, the pattern will appear blurred. Such blurring is generally quantified as speckle contrast, a measure of relative changes in blood flow. The speckle contrast value (K) is defined as the ratio of the standard deviation to the mean intensity ($K = \sigma s/I$) in a small region of the speckle image (typically 5× 5 or 7 x 7 pixels). Speckle contrast can be plotted to generate a LSCI map of blood flow. Speckle contrast and motion of the scattering particles (red blood cells) are inversely related. K value ranges from 0 to 1. When red blood cells (RBC) are moving very fast in vessels, the speckle K will be very close to 0 and vice versa, when no blood flow in vessels, then K is approaching to 1.

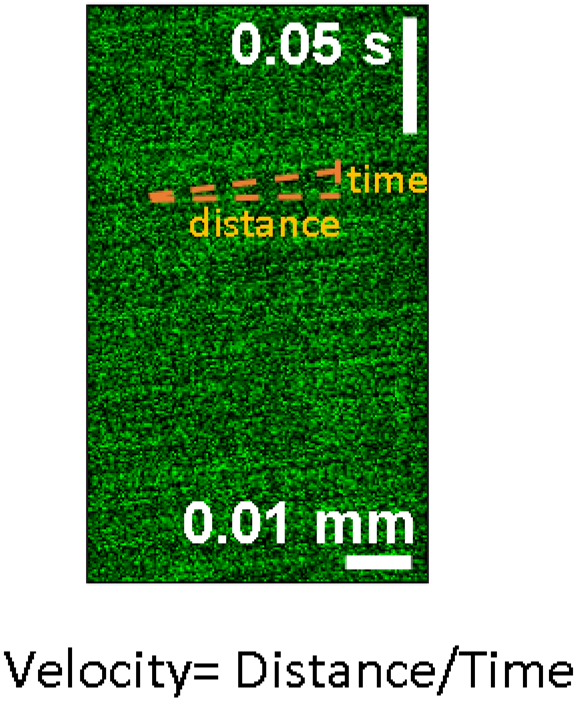

Figure 1- 2 Representative linescan to determine RBC velocity.

As RBCs do not take up fluorescent dye, they are detectable as non-fluorescent streaks in plots of the line scan images where the slope of streaks represents RBC velocity.

Chapter 2

Impaired collateral flow in pial arterioles of aged rats during ischemic stroke

2.1. Introduction

Stroke disproportionately affects the elderly, with risk of stroke doubling every decade after the age of 55 in both sexes [5–7]. Moreover, elderly stroke patients exhibit significantly worse functional recovery and higher mortality compared to younger patients [5–7]. Thus, preclinical studies of the pathophysiology of stroke should be performed in aged animals whenever possible.

After occlusion of a cerebral vessel, tissue surrounding the nonviable infarct core in the penumbra remains viable due to blood flow via the cerebral collateral circulation [16]. Cerebral collaterals are auxiliary vascular pathways that can partially maintain blood flow to ischemic tissue when primary vascular routes are blocked [11,12,14,161]. Pial (or leptomeningeal) collaterals are anastomotic connections on the cortical surface that connect distal branches of the anterior cerebral artery (ACA) and posterior cerebral artery (PCA) with distal branches of the middle cerebral artery (MCA) [16,17]. Clinically, blood flow through the pial collaterals defines the degree of ischemia in the penumbra of cortical infarcts, and thus influences infarct growth, prognosis and response to therapy [25,29,161,162]. Among recent trials of endovascular thrombectomy [163–167], data from the ESCAPE trial, that included multiphase CT angiography, demonstrated a strong association between robust pial collateral flow before recanalization and favorable outcome after recanalization [30,163]. The DAWN and DEFUSE3 trials that evaluated patients following late thrombectomy (6 to 24 hours after stroke onset) reported significant benefits of delayed endovascular treatment [31,32]. Notably, patients with "slow-growing infarcts" due to good collateral circulation were selected into DAWN and DEFUSE3 trials [31–33].

Thus, collaterals are a primary predictor of stroke prognosis and response to treatment, but the interactions between collateral dynamics and aging are not known. Rarefaction of cerebral collaterals with aging has been reported in preclinical models [18], and in some cases collateral therapies have reported differential efficacy based on age [117]. However, age-related changes in the dynamics of collateral flow are not well described, particularly at the level of visually identified pial collaterals. Here, laser speckle contrast imaging (LSCI) and two photon laser scanning microscopy (TPLSM) were used to evaluate the dynamics of pial collateral circulation in young adult (2 months) and aged (16 months) rats during the first 4.5 h after distal middle cerebral artery occlusion (dMCAo). Retrograde collateral flow was apparent immediately after dMCAo. While collateral vessels narrowed over time in both groups, overall flow was more impaired and failed over time in aged rats relative to adult young rats.

2.2. Materials and Methods:

Male *Sprague–Dawley rats* (young group: 2-3 months of age; aged group: 16-18 months of age) were used. Prior to experimental procedures, animals were housed in pairs on a 12-h day/night cycle and had access to food and water ad libitum. Procedures conformed to guidelines established by the Canadian Council on Animal Care and were approved by the Health Sciences Animal Care and Use Committee at the University of Alberta. Procedures and results reporting is consistent with the ARRIVE guidelines [168].

The experimental timeline is illustrated in Figure 2-1(a). A total of 13 aged rats and 12 young adult rats underwent implantation of an imaging window. Two rats (1 aged, 1 young adult) were excluded due to poor quality cranial windows and image quality (prior to post-stroke imaging), and one aged rat died during imaging. Thus, the data set for the aged and young adult groups include 11 rats each.

2.2.1. Anesthesia and Monitoring

Light anesthesia was induced using an induction chamber with 4–5% isoflurane (in 70% nitrogen and 30% oxygen) prior to intraperitoneal injections of urethane (1.25 g/kg, divided into four doses delivered at 30-min intervals). Isoflurane was discontinued after the first urethane injection, and rats remained anaesthetized until euthanasia. During all surgery and imaging, temperature was maintained at 36.5–37.5C with a thermostatically controlled warming pad and heart rate, oxygen saturation, and breath rate were monitored using a pulse oximeter (MouseOx, STARR Life Sciences).

2.2.2. Cranial Window

LSCI and TPLSM were performed through cranial windows implanted after craniotomy. A midline incision was made on the scalp to expose the surface of the skull. A 5*5 mm section of the skull over the distal regions of the right MCA territory was thinned until translucent using a dental drill (frequently flushing with saline to dissipate heat) and then gently removed. The dura matter was removed, then the cranial window was covered with a thin layer of 1.3% low melt agarose and sealed with a glass coverslip as previously described [11,169].

2.2.3. dMCAo

Cerebral ischemia was induced by bilateral common carotid artery (CCA) ligation in addition with distal MCA ligation [26,170]. Distal MCA ligation and imaging protocols were performed by different individuals, and surgeons inducing ischemia were blind to the experimental group for each rat. CCAs were accessed through ventral midline cervical incisions and ligated with 4–0 prolene sutures below the carotid bifurcation. A temporal incision was then made and the right temporalis muscle was gently separated from the bone. A burr hole of 1.5 mm in diameter was made through the squamosal bone, the dura was removed, and the cortical MCA was visualized. The exposed distal MCA was isolated with a loose square knot by atraumatic 9–0 prolene suture above the rhinal fissure before stroke. After pre-stroke imaging, the knot was ligated to induce permanent dMCAo.

2.2.4. LSCI

LSCI measures real time changes in cerebral blood flow with high spatial and temporal resolution over a wide field of view [171–173]. To collect LSCI data, rats were secured in ear bars on a custom-built stereotaxic plate under a Leica SP5 MP laser scanning microscope. A Thorlabs LDM 785S laser (20 mW, wavelength of 785 nm) was used to illuminate the rat cortex at approximately 30 ° incidence. Stacks of 101 sequential images (1024 × 1024 pixels) were acquired at 20 Hz (5 ms exposure time) during each imaging session. All processing and analysis of laser speckle images were performed using ImageJ software (NIH) by a blinded experimenter. Maps of speckle contrast were made from the collected images of raw speckling by determining the speckle contrast factor K for each pixel in an image. K is calculated as the ratio of the standard deviation to the mean intensity ($K = \sigma_s/I$) in a small (5 × 5 pixels) region of the speckle image [171–173]. Plots of K show maps of blood flow with darker vessels illustrating faster blood flow velocity [174,175]. For quantification of penumbral flow, K was measured in a contiguous ROI consisting of an 800 × 800 pixel square positioned to include the distal MCA and ACA segments. Because cerebral blood flow (CBF) velocity in selected region of interest was inversely proportional to the square of speckle contrast value K [176,177].

$$v \propto \frac{1}{K^2}$$

Therefore, $1/K^2$ is also used to illustrate CBF velocity change in LSCI figures [174,178].

2.2.5. TPLSM

TPLSM was performed using a Leica SP5 MP TPLSM and Coherent Chameleon Vision II pulse laser tuned to 800 nm. Blood plasma was labelled with fluorescein isothiocyanate–dextran (70,000 MW, Sigma-Aldrich) injected (0.3 mL (5% (w/v) in saline, 0.2 mL supplements as required) via the tail vein [73,81]. Z-stacks through the first 0.15mm of cortical tissue were acquired through the cranial window using a 10 × water dipping objective (Leica HCX APO L10×/0.3 W) and vessel diameter measurements were made from maximum intensity projections of these stacks using ImageJ plug-in (full-width at half-maximum algorithm) [179]. For acquisition of red blood cell (RBC) velocity, line scans were performed in the lumen of arterioles over a length of 50-100 pixels at scan rates of 1200Hz. While the repeated imaging schedule (30-min intervals) did not allow a comprehensive analysis of blood flow velocity in all vessels within these regions of interest, RBC velocity was via line scans in three identifiable arterioles (>0.05mm diameter) per region. RBC velocity was determined from line scan images by calculating the slope of streaks [73,81]. RBC flux, which provides an overall measure of flow through each vessel, was calculated using the following equation:

$$\text{Flux}=(\pi/8)(d^2)(v)$$

where v is the RBC velocity along the central axis of the vessel, and d is the vessel diameter.

2.2.6. Hemotoxylin and Eosin Staining (H&E staining)

All rats were euthanized 6 h after induction of the dMCAo. Tissue damage was assessed in digital images of H&E stained cryosections by a blinded experimenter using ImageJ (NIH) software. Volume of tissues showing early ischemic damage were calculated for each tissue slice using the indirect method[180,181] to control for tissue distortion due to edema using the following equation:

$$\text{Volume of ischemic damage \% hemisphere} = \mathbf{[\ \Sigma(A_C\text{-}A_{NI})/\ \Sigma(A_C)]*100}$$

where A_C is the area of the hemisphere contralateral to stroke in a given tissue slice and A_{NI} is the area of the non-injured tissue in the ipsilateral stroke (affected) hemisphere of the same slice.

2.2.7. Statistical Analysis

Statistical analyses were performed using Graph Pad Prism (GraphPad software, San Diego, CA, US). RBC velocity and RBC flux data exhibited a right skewed distribution. To reduce skewness, a cubed root transformation was applied. The cubed root transform was selected as it is a standard transform for right skewness, and can be applied to zero values (which occurred in some instances for velocity measurements). Normality was confirmed for all blood flow data sets (i.e. LSCI data in Figure 2-3 and TPLSM data in Figure 2-5) using the D'Agostino-Pearson normality test. Two-way analysis of variance (ANOVA) with repeated measures were used to compare the time course of aged and young rats on LSCI measures (speckle value, relative blood flow) and TPLSM measures (vessel diameter, RBC velocity, and RBC flux). Post hoc comparisons were performed using Bonferroni multiple comparisons test. Volumes of ischemic tissue infarct (% of contralateral hemisphere) and physiological parameters (pulse, respiratory rate and oxygen saturation) were compared using an unpaired Student's t-test. Values are expressed as mean ± S.E.M. Sample size was estimated using published and unpublished data that suggested 10 rats was sufficient to detect a 10% difference in vessel diameter using TPLSM (μ_1=100, μ_2=90, σ_s=7.8%, β=0.80, α= 0.05).

2.3. Results:

LSCI and TPLSM were used to assess changes of pial collateral flow immediately before and for 4.5h after dMCAO (at intervals of 30 mins, Figure 2-1(a)). Physiological parameters remained stable throughout imaging (Figure 2-1 (b-d)). LSCI and TPLSM were used to create high-spatiotemporal resolution maps of blood flow in pial vessels in the region of ischemia, including measures of regional flow (LSCI) as well as pial vessel diameter, RBC velocity, and RBC flux (TPLSM) (Figure 2-2) [11].

2.3.1. LSCI Reveals Reduced Penumbral Blood Flow in Aged Rats relative to Young Rats

Figure 2-3 shows LSCI derived maps of speckle contrast showing flow changes over 270 min (4.5 h) post stroke for aged and young rats. Immediately after dMCAo, robust anastomotic connections between distal segments of the ACA and MCA were observed in both groups. However, pial collaterals were more robust in young rats (Figure 2-3(b), note the number of visible vessels following dMCAo in young vs. aged rats) and penumbral blood flow in young rat persisted through the imaging sessions in young rats. In aged rats, penumbral flow decreased during the imaging period (as indicated by a consistent increase in speckle contrast during the imaging period in the aged rats, and relatively few visible pial vessels, Figure 2-3(a)). Speckle contrast normalized to pre-dMCAo values is shown in Figure 2-3(c). Two-way ANOVA revealed a significant main effect of Time and Age on speckle contrast, as well as a significant Time X Age interaction (all $P < 0.0001$). Posthoc comparisons confirmed that speckle contrast was significantly greater in aged rats relative to young rats at all time-points after 30min post-dMCAo. A more proportional measure of blood flow can be attained by determining the inverse square of the speckle contrast values (Figure 2-3(d)) [174,178]. While blood flow of young rats remained between 60%-80% of baseline (pre-dMCAo) during all imaging sessions, flow in aged rats dropped rapidly to less than 40% and remained low throughout imaging. Again, a two-way ANOVA revealed a significant main effect of Time and Age on speckle contrast, as well as a significant Time X Age interaction (all P <0. 0001). Post hoc comparisons confirmed significantly reduced flow in aged animals (relative to young animals) at all time-points after 60 minutes post-dMCAo.

2.3.2. TPLSM Reveals Dynamic Changes in Pial Arteriole Diameter, RBC Velocity, and Flux after dMCAo

TPLSM revealed a reduction in pial arteriole diameter over time after dMCAo in both groups (representative images in Figure 2-4, group quantification in Figure 2-5a). Two-way ANOVA confirmed a significant Time X Age interaction in pial arteriole diameter ($P < 0.0001$). Notably, aged rats show more rapid "collapse" or narrowing of pial arterioles relative to young rats. Interestingly, diameters at the completion of imaging were not different between experimental groups, and post hoc comparisons only revealed a significant difference in MCA segment diameters at 90 min after dMCAo, suggesting that the dynamics of collateral failure are accelerated in aged rats but the degree of collateral narrowing is comparable. Figure 2-5(b) shows mean changes in red blood cell (RBC) velocity relative to baseline (pre-dMCAo). There was a significant main effect of Time and Age ($P<0.0001$ and $P=0.0061$, respectively) and a significant Age x Time interaction ($P=0.0002$). Posthoc comparisons confirmed that RBC velocity in pial arterioles downstream of anastomoses was significantly reduced in aged rats relative to young rats at all time points after 120 min post-dMCAo. Finally, because the oxygen and nutrient carrying capacities of a blood vessel are proportional to their RBC flux [75,182], mean RBC flux for arteriole segments downstream of collateral anastomoses in aged and young rats are shown in Figure 2-5(c). Analysis of RBC flux between groups revealed a significant main effect of Time ($P<0.0001$) and Age ($P=0.0057$), and a significant Age X Time interaction ($P=0.0159$). Post hoc comparisons confirmed significantly reduced RBC flux in aged rats relative to young rats at all time points after 90 min post-dMCAo.

2.3.3. Early Ischemic Damage in Aged Rats and Young Rats.

Figure 2-6 shows that a significant larger volume of early ischemic damage was found in aged rats relative to young rats ($P<0.001$).

2.4. Discussion:

Aging is a multifaceted process associated with cellular, metabolic, and structural changes in the brain [183,184]. Many factors, such as increased oxidative stress, pro-inflammatory cytokine expression, and reduced cell survival have been considered important factors contributing to increased ischemic brain injury in aged animals [183,185].

The effects of age on cerebral circulation is an additional factor to be considered. Although there is some debate in the field [186–190], most published literature suggest that there is a rarefaction of cerebral arterioles and decrease in capillary density in aged humans, aged nonhuman primates and different species of aged rodents (such as Wistar, Wistar-Kyoto, spontaneously hypertensive, Brown-Norway, and F344 rats) [19,191–195]. An age-related decrease in the number of venules and arteriole-to-arteriole anastomoses has also been reported in both Brown-Norway and F344 rats [19]. Such rarefaction would reduce aged animals ability to maintain blood flow during ischemia, resulting in increasing risk of neuronal loss in brain regions where vessel rarefaction is prominent [19]. Increasing age is also associated with significantly decreased lumen diameter at the arteriole level and more tortuous cerebral vessels [186,196,197]. The net result of these alterations in the cerebral circulation is increased vascular resistance, which leads to impaired tissue perfusion and larger infarcts [198]. A loss of collateral number and diameter and increased tortuosity has been observed in aged mice, resulting in a 6-fold increase in calculated resistance and 3-fold increase in severity of infarct volume after MCAO in 24- versus 3-months-old-mice [18,20]. These studies used postmortem cerebral artery micro-angiography to estimate rarefaction, however, so collateral extent and compensatory flow were not directly verified during ischemia. However, age related biochemical alterations in the peripheral and mesenteric collaterals suggest altered hemodynamics in the days following stroke. Specifically, endothelial nitric oxide synthase (eNOS) signaling appears to be dysfunctional in endothelial cells in mice three days after MCAO, as indicated by increased protein nitrosylation and reduced concentration of phosphorylated endothelial nitric oxide synthase [18]. Moreover, expression of vasodilator-stimulated phosphoprotein (VASP) is altered in collateral wall cells [18]. Decreases in phospho-eNOS (necessary for eNOS activation) and phospho-VASP (which undergoes phosphorylation when NO is increased) would impair collateral remodeling during this subacute period, but reduced eNOS could also impair vasodilation and could lead to reduced collateral diameter during acute stroke. This would agree with preclinical and clinical studies in the peripheral and cerebral circulation that suggest impaired vasodilation and vasoreactivity with aging [199–201].

Collateral status at the time of occlusion (i.e., number and diameter) is the strongest independent predictor of final infarct volume and is considered crucial for clinical decision making in stroke treatment [14,20–24]. The hemodynamic evolution of the collateral circulation is also important since collaterals are thought to be time limited and can fail over time [26,169,202].The dropout of collaterals during stroke is related to the progression of penumbra to irreversible ischemic infarct and impaired response to treatment [26,169,202]. However, the effects of aging on the dynamics of collaterals circulation are not well defined. The data presented here show that pial collaterals are patent immediately after ligation of a distal branch of MCA, with clear retrograde flow to ischemic territories. LSCI showed that cerebral collateral perfusion was impaired after stroke ("collateral failure") in both aged and young rats, but this decline was more severe in aged rats. TPLSM showed that pial arterioles narrowed to around 80% of pre-stroke diameter at 4.5h post stroke in both young and aged rats, but that this collateral constriction was accelerated in aged rats. More specifically, the narrowing of pial vessels occurred over 90 minutes post-stroke in aged rats, while more gradual narrowing occurred over the full 270 minute imaging period in young rats. Notably, RBC velocity remained near baseline values (though the direction of flow was reversed) in young rats, such that overall RBC flux downstream of pial anastomoses was stable over the imaging period. Contrasting this, RBC velocity declined steadily in aged rats after ischemic onset. Thus, while arteriole vessel narrowing reached comparable endpoints, RBC velocity and the overall flux of blood through pial arterioles was significantly reduced at time points after 120 and 90 minutes, respectively, after occlusion in aged rats relative to young adult rats. Thus, collateral narrowing occurs more quickly in aged rats than young adult rats, and only young adults compensate for increased vascular resistance with an increase in flow velocity. In addition to changes in the diameter and velocity of flow in pial arterioles, a progressive reduction in perfused vessels on and below the cortical surface was apparent in both aged and young adult rats, but was more severe in aged rats. While potential fading of fluorescence and a slight reduction in the quality of the optics through the cranial window could potentially contribute to reduced density of flowing vessels over time, the consistency of the LSCI and TPLSM images and the progressive reductions in arteriole flux suggest that this reflects an impairment in microvascular perfusion due to failing collateral flow. The more severe reductions in collateral and microvascular flow apparent in aged rats likely accounts for the significantly greater volumes of ischemic damage relative to young adult rats 6 h after ischemic onset.

Notably, the native pial collateral circulation (number and size) varies greatly among humans and among rodents from different genetic background, even within a species [20,203,204]. Pial collaterals formation begins primarily between embryonic day 13.5 and 14.5 and their maturation continues through the first three weeks after birth [16,205,206]. Gene expression of *Vegfa* and *CLIC4* shape the development of collateral vessels [16,205,207,208]. However, it is not known how these genetic factors influence collaterals across the lifespan, and if changes in gene expression contribute to accelerate collateral failure. Recent studies of isolated collateral vessels in after filament MCAO in rats suggest that the elevation of intracranial pressure (ICP) may be responsible for collateral failure after stroke [209]. While ICP was not monitored in our study, dynamic difference in ICP may occur during acute between aged and young rats and may contribute to accelerated collateral failure observed here. Notably, Beard et al [209–211] stated that changes in collateral flow post-stroke appear to be primarily driven by the pressure drop across the collateral vessel, and were not due to changes in vessel diameter. That is, as ICP increases, cerebral perfusion pressure is reduced and collateral flow declines, providing a possible explanation for collateral failure. In our study, aged rats showed a more rapid narrowing of collateral vessels that was associated with a rapid and sustained decrease in collateral flow. Young adult rats had a slower decline in pial vessel diameter, though diameters at the final endpoint were comparable between groups. However, in young adult rats blood flow velocity and flux remained relatively stable over time, perhaps implicating a more severe increase in ICP in aged rats that reduces cerebral perfusion pressure as mechanisms of impaired collaterals in the aged. Strategies to reduce ICP may therefore be effective to maintain collateral flow in the aged. Metabolic risk factors, like metabolic syndrome and hyperuricemia, are known to contribute in poor leptomeningeal collateral status of patients with acute ischemic stroke [212]. Menon et al [212] hypothesized that endothelial dysfunction results from metabolic syndrome and hyperuricemia and leads to pial collateral deterioration [212]. In addition, Faber et al [18] also postulated that endothelial dysfunction could lead to a reduction in the density of cerebral native collaterals in mice. However, the effect of endothelial dysfunction in regulating hemodynamic of pial collaterals post stroke is still unknown, and the degree to which age contributes to this dysfunction remains to be confirmed.

Our finding of rapid failure of collaterals in aged rats may help partially explain worst clinical outcome in elderly relative to young patients. Moreover, our data may help explain results of completed Safety and efficacy of NeuroFlo Technology in Ischemic Stroke (SENTIS) trial [117]. Notably, the SENTIS trial showed that transient aortic occlusion (TAO) with the NeuroFlo catheter is safe in stroke patients and could improve outcome through augment cerebral blood flow after stroke onset in a subgroup of patients older than 70 years of age [117]. Enhanced efficacy in the elderly may reflect amelioration of ischemia to cerebral collateral collapse earlier after ischemic onset in the aged. Accelerated collateral failure as demonstrated here therefore reinforces the importance of early recanalization in the elderly, and suggests that the development of collateral therapeutics to preserve collateral flow might be particularly important for aged patients [117]. Notably, our study did not include reperfusion, and future studies could address the importance of collateral flow prior to recanalization in aged and young rats by incorporating a transient model of MCAo to model stroke with recanalization. Incorporation of approaches to reduce ICP in these studies could highlight the potentially important role of ICP in collateral failure and its potential as a target for collateral therapeutics.

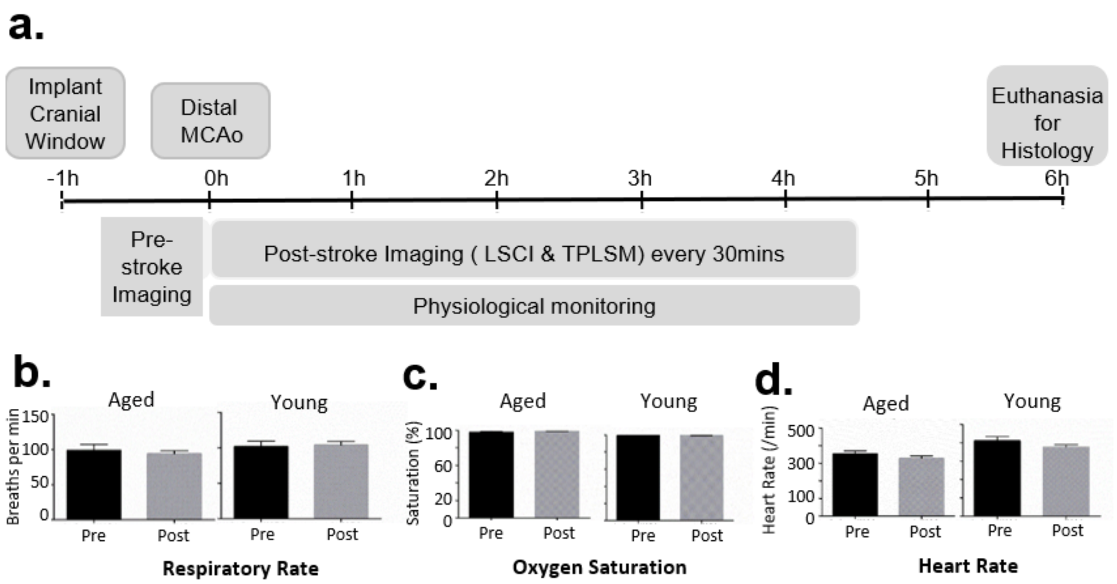

Figure 2-1 Experimental design & Average of physiological parameters of young and aged rats during the entire post-stroke imaging period

(**a**)Experimental timeline. (**b-d**) Average of physiological parameters of young and aged rats during the entire post-stroke imaging period.

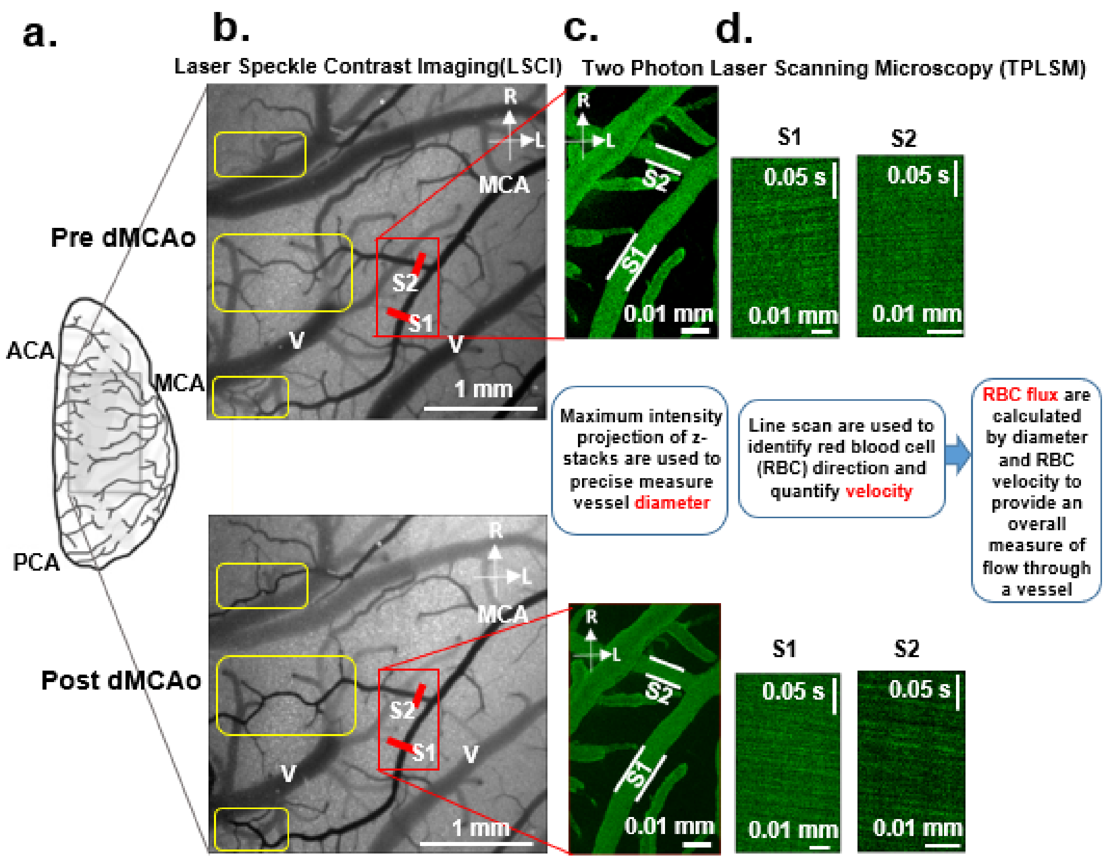

Figure 2- 2 Representative cortical surface pial collateral blood flow imaging before and after dMCAo using LSCI and TPLSM

LSCI and TPLSM were used to create high-spatiotemporal resolution maps of blood flow in pial vessels in the region of ischemia. A cranial window was placed over the cortex at the distal ends of the vascular territories of the ACA and MCA (**a**). Red dotted lines and shading show the approximate locations of ACA-MCA anastomose. This window placement allows visualization of changes in collateral flow after distal MCAO. (**b**) LSCI data clearly demonstrate that pial collaterals become patent immediately after ligation of distal MCA (see yellow boxes in **b**), representing retrograde flow from the distal branches of the ACA into the MCA territory.

(**c,d**) TPLSM was used to map the angioarchitecture of anastomoses and distal MCA segments. Maximum intensity projections of pial vessels located within a depth of 100-150 µm from the surface of the region demarcated by the red box in (**b**), including distal MCA segments S1 and S2, are shown in (**c**) to illustrate analyses of vessel diameter. (**d**) Center line RBC velocity was measured in vessel segments measured for diameter, allowing determination of velocity and direction of blood flow. The reversed direction of blood flow in collaterals after MCAO is apparent in both segments (see reversed slope of dashed lines in **d**). Figure 2-2a modified with permission from Winship et al. [11]. Scale bar, 100µm

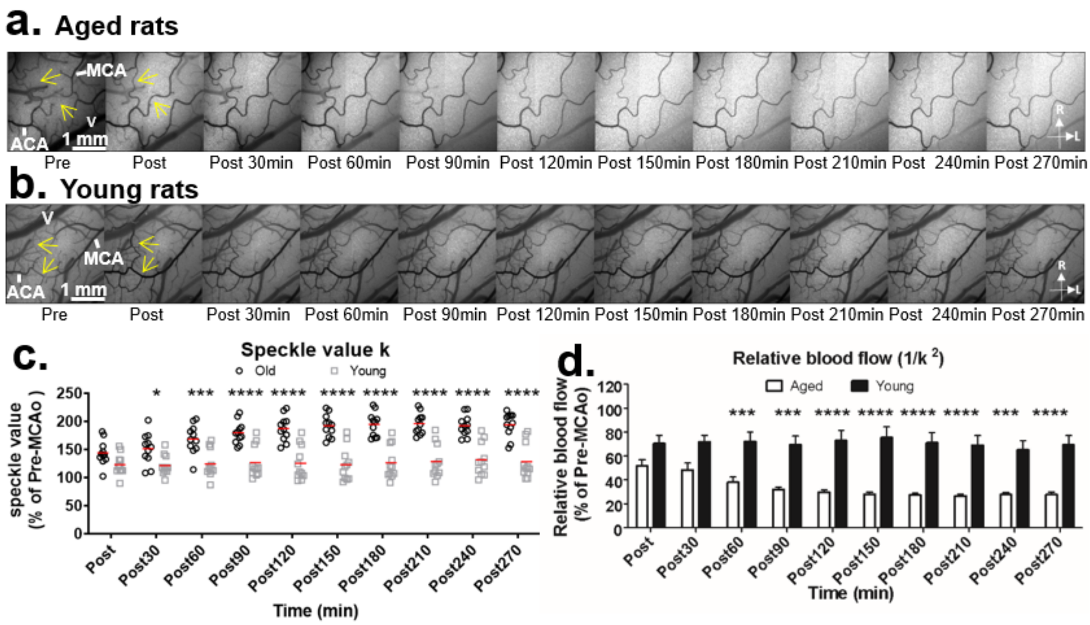

Figure 2- 3 Representative LSCI derived image sequences showing flow on the cortical surface of aged and young adult rats & Speckle contrast (*K*) and relatively blood flow (1/*K*^{2}) for aged and young adult rats

(**a,b**) Representative LSCI derived image sequences of speckle contrast showing flow on the cortical surface before and after dMCAo. Images showing flow changes over 270min (4.5h) post are illustrated for aged (**a**) and young adult rats (**b**). Immediately after dMCAo, robust anastomotic connections between distal segments of the ACA and MCA become visible in both groups (see yellow arrowheads showing absent or low flow in distal ACA-MCA anastomoses before stroke (left-most panel) and enhanced flow after dMCAo in next panel). Pial collaterals were more robust and persistent in young adult rats (n=11) relative to aged rats (n=11). Note the consistent increase in speckle contrast during the imaging period in the aged rats (**a**), which reflects decreasing flow over time, and relatively few visible pial vessels. Contrasting this decreased flow in aged rats, speckle contrast remains relatively stable during imaging after stroke in young adult rats (**b**). Speckle contrast (K) and relatively blood flow ($1/K^2$) for aged and young adult rats are shown in (**c**) and (**d**), respectively. Two-way ANOVA on K and $1/K^2$ identified significant main effects of age and Time X Age interactions (all $P<.0001$), and posthoc comparisons identified significantly group differences at all time points 60 minutes or more after ischemic onset in both measures. * $P<.05$, ***$P<.001$, **** $P<.0001$.

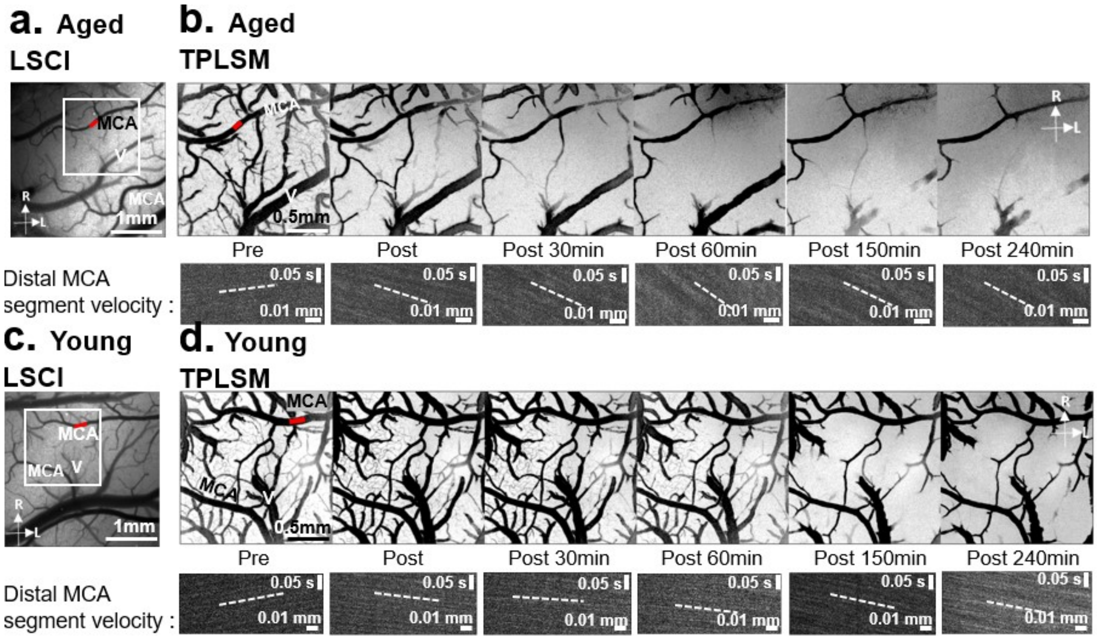

Figure 2- 4 Representative TPLSM derived image sequences showing pial collateral of aged and young adult rats

Representative TPLSM data before and after dMCAo. The rectangular box in the LSCI images from an aged rat (**a**) and young adult rat (**c**) demonstrate the location of the representative TPLSM images in (**b**) and (**d**). Scale bar, 1 mm. (**b**) and (**d**) show maximum intensity projections from region demarcated in (**a**) and (**c**). TPLSM revealed reduced flow in pial arteriole and diameter over time after dMCAo in both groups, though it was more severe in aged rats. Representative line scans show reduced RBC velocity in the MCA segment highlighted with a red line from the aged rat (**b**) and the young adult rat (**d**). Reversal in the direction of flow is apparent in both groups. Increasing slope in the aged rats shows reduced RBC velocity in this segment, as compared to more stable RBC velocity (and faster, indicated by a lower slope) in the young adult animal. Scale bar, 500 um.

R, rostral; L, lateral

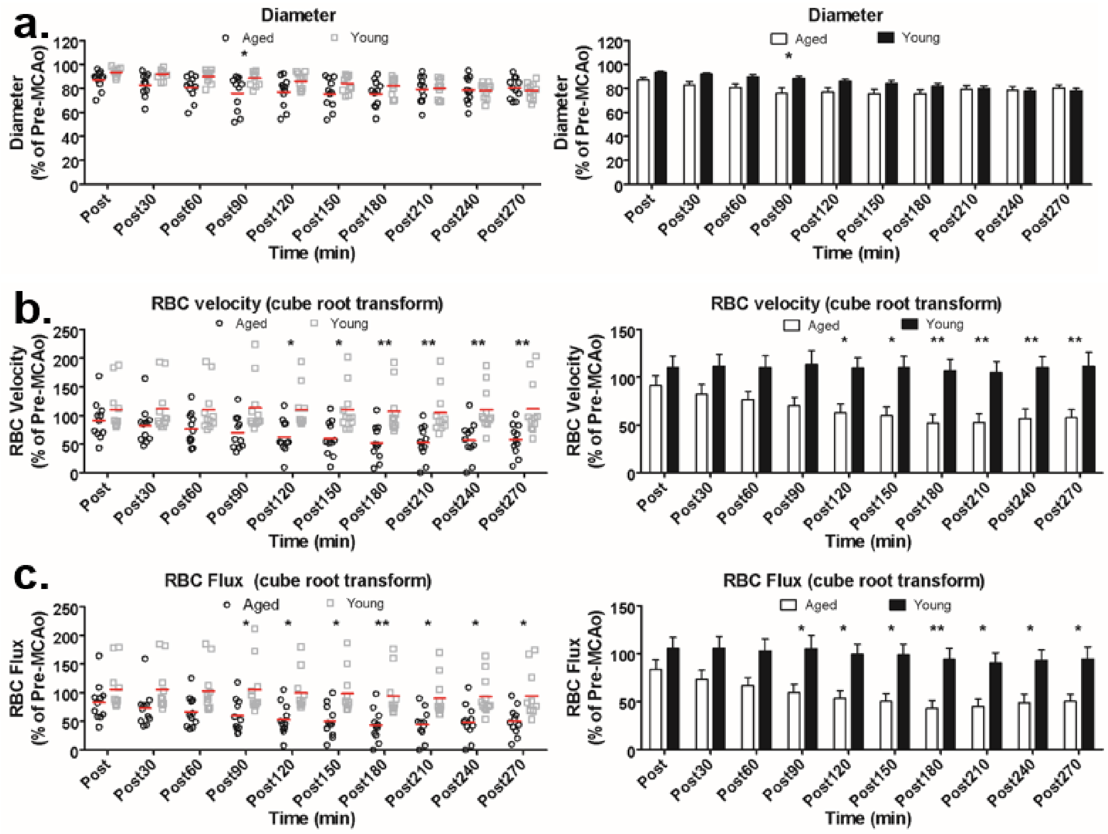

Figure 2- 5 Quantification of the mean diameter, RBC velocity, and RBC flux in aged rats and young rats after distal MCAO

Quantification of the mean diameter (**a**), RBC velocity (**b**), and RBC flux (**c**) in aged rats (n=11) and young rats (n=11) after distal MCAO. (**a**) Aged rats exhibited a more rapid narrowing of pial arterioles relative to young adult rats, though diameters at the completion of imaging were not different between aged and young rats. Two-way ANOVA confirmed a significant Time X Age interaction in pial arteriole diameter ($P < 0.0001$). (**b**) A greater reduction of RBC velocity over time after dMCAo was apparent in aged rats relative to young adult rats, and Two-way ANOVA confirmed a significant main effect of Time and Age ($P<0.0001$ and $P=0.0061$, respectively) and a significant Age x Time interaction ($P=0.0002$).

(**c**) Mean RBC flux for MCA segments downstream of collateral anastomoses was significantly reduced in aged rats relative to young rats. Two-way ANOVA revealed a significant main effect of Time ($P<0.0001$) and Age ($P=0.0057$), and a significant Age X Time interaction ($P=0.0159$). * $P<.05$, ** $P<.01$.

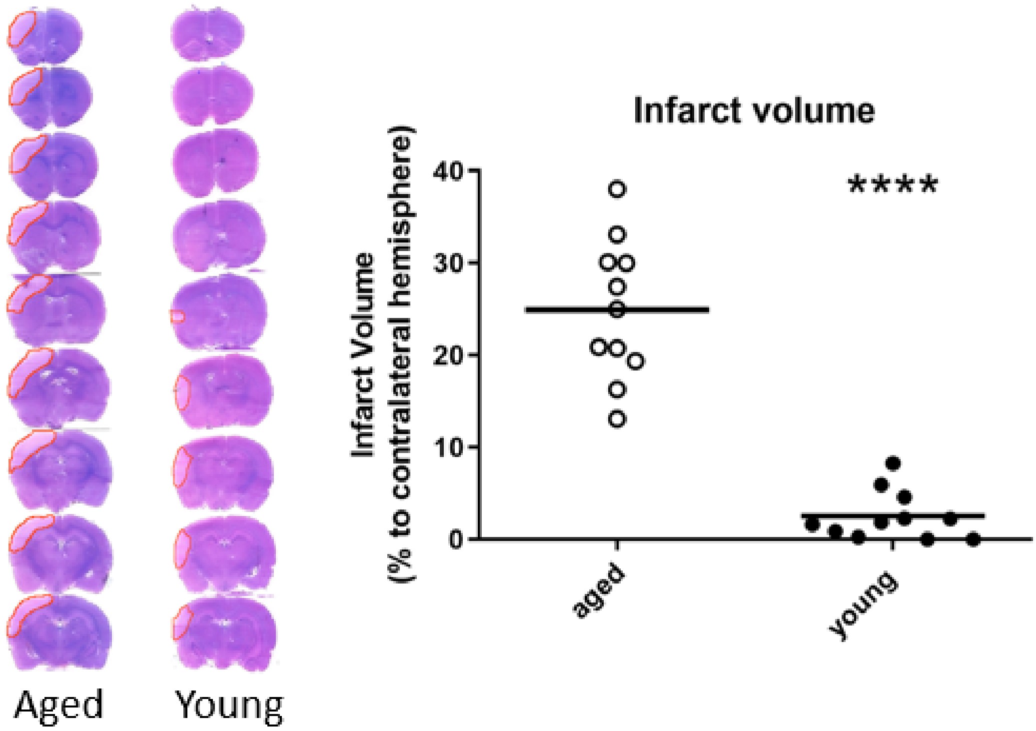

Figure 2- 6 Early ischemic damage measurements

H&E staining was used to visualize early ischemic damage in aged (n=11) and young adult (n=11) rats. A significantly larger volume of early ischemic damage was found in aged rats relative to young rats (P <0.001). Means of the infarct volumes are presented as percentage of their corresponding contralateral sides.

Chapter 3

Prevention of the collapse of pial collaterals by remote ischemic perconditioning during acute ischemic stroke

3.1. Introduction

Flow through cerebral collaterals is increasingly recognized as a key variable in determining outcome after acute ischemic stroke. The cerebral collaterals are auxiliary vascular pathways that can partially maintain blood flow to ischemic tissue when primary vascular routes are blocked [213–216]. The circulatory anastomoses that constitute the Circle of Willis are classified as “primary” collaterals [217],while the “secondary” collaterals include the pial or leptomeningeal collaterals [218]. Pial collaterals are anastomotic connections located on the cortical surface which connect distal branches of the anterior, middle, and posterior cerebral arteries (ACA, MCA, and PCA). Blood flow through pial collaterals after occlusion of the principal supplying artery (e.g. the MCA) allows retrograde filling of vessels in the ischemic penumbra. Good collateral flow is associated with reduced infarct core, improved prognosis, and better response to recanalization therapy [24,219–221]. Therapies that can augment collateral flow may therefore protect penumbral tissue and augment recanalization [222].

Ischemic conditioning was introduced in the 1980s [134] as a treatment to induce a tissues' endogenous protection against ischemic injury by the application of repetitive, brief ischemic periods before or after more severe ischemic insults (referred to as local pre- and post-conditioning, respectively). A significant breakthrough in the study of ischemic conditioning as a protective therapy was the discovery that ischemic conditioning induced at an organ remote to the site of severe ischemia (termed “remote ischemic conditioning”), such as the limb in the case of cerebral ischemia, can also protect target tissue [135]. Crucially, remote ischemic conditioning can be applied prior to stroke (termed remote ischemic preconditioning), after the onset of ischemia (termed remote ischemic per-conditioning (RIPerC), or at the time of reperfusion (termed remote ischemic post-conditioning) (Figure 3-1(a)) [136]. RIPerC has promise as an acute ischemic stroke treatment that can be applied during the ischemic period whether patients receive reperfusion treatment (e.g. rt-PA) or not [135]. Preliminary preclinical and clinical data suggest that RIPerC may be neuroprotective [8,137–140,142,144,223,224]. However, relatively little is known about the underlying protective mechanisms of RIPerC. Recent data suggest that RIPerC may increase cerebral blood flow [139,225], but its ability to augment collateral circulation has not been assessed. The objective of this study was to use advanced in vivo imaging to define changes in pial collateral flow during RIPerC. Here, high resolution in vivo laser speckle contrast imaging (LSCI) and two photon laser scanning microscopy (TPLSM) were used to map dynamic changes in pial collaterals during RIPerC after distal middle cerebral artery occlusion (MCAo) in rats. Our findings demonstrate that RIPerC induced by bilateral femoral artery occlusion (BFO) augments blood flow through pial collaterals by preventing their collapse or constriction over time.

3.2. Materials and Methods

Male Sprague–Dawley rats (2–5 months of age, n = 47) were used. Prior to experimental procedures, animals were housed in pairs on a 12-h day/night cycle and had access to food and water ad libitum. Procedures conformed to guidelines established by the Canadian Council on Animal Care, were approved by the Health Sciences Animal Care and Use Committee at the University of Alberta, and are reported in a manner consistent with the ARRIVE (Animal Research: Reporting in Vivo Experiments) guidelines. The experimental timeline is illustrated in Figure 3-1(b). Sample sizes estimates were based on variability in data from previous LSCI and TPLSM experiments in our laboratory.

3.2.1. Anesthesia and Monitoring

For LSCI experiments, anesthesia was induced with 4–5% isoflurane and maintained at ~1.0–1.5% isoflurane (in 70% nitrous oxide and 30% oxygen). Rats (n = 11 for each of the RIPerC and control groups) remained under isoflurane until completion of the imaging experiments, at which point they were removed from anesthetic until euthanasia 6 h after MCAo onset. While isoflurane allows stable and reliable anesthesia, it is a volatile inhalant anesthetic, has been associated with vasodilation or impaired vasoreactivity, and may mask neuroprotection during cerebral ischemia [226–230]. Nonetheless, published studies of collateral therapeutics from our group and others suggest that augmented collateral flow and/or neuroprotection is apparent with isoflurane anesthesia as well as alternative anesthetics (e.g. urethane or sodium pentobarbital) [72,213,231,232]. Nonetheless, our quantitative analyses of pial arteriole diameter using TPLSM were performed under urethane anesthesia to allow a comparison of vascular effects and degree of neuroprotection observed under isoflurane against a different anesthetic paradigm. While wakefulness and depth of anesthesia alter hemodynamics, the mechanisms of action for urethane spare many pathways involved in neurovascular coupling and recent studies support its use in studies of cerebral hemodynamics [233–236]. Therefore, for TPLSM experiments, rats (n = 8 for each of the RIPerC and control groups) were anaesthetized with urethane (i.p. 1.25 g/kg, divided into four doses delivered at 30-min intervals), then remained anaesthetized until euthanasia. During all surgery and imaging, temperature was maintained at 36.5 – 37.5℃ with a thermostatically controlled warming pad and heart rate, oxygen saturation, and breath rate were monitored using a pulse oximeter (MouseOx, STARR Life Sciences). In a separate cohort of isoflurane anesthetized rats (n = 6 RIPerC and 3 controls rats), blood pressure monitoring was performed via catheter in the ventral tail artery after MCAo and throughout RIPerC or sham treatment using a PressureMAT monitor (PendoTECH).

3.2.2. Cranial Windows

LSCI and TPLSM were performed through cranial windows using a thin skull preparation or a craniotomy, respectively [169,237]. For thin skull imaging, a midline incision was made on the scalp to expose the surface of the skull (Figure 3-1(d)). A ~6 × 4-mm section of the skull over the distal regions of the right MCA territory was thinned until translucent using a dental drill (frequently flushing with saline to dissipate heat). The outer skull layer and subjacent spongy bone were cleaned and smoothed by round scalpel, allowing surface vessels to be visualized through the remaining thin layer of bone. A layer of mineral oil was applied to the window and sealed with a cover slip.

Procedures for cranial windows via craniotomy were identical, except the skull over the right MCA territory was thinned until translucent using a dental drill and then gently removed. The cranial window was covered with a thin layer of 1.3% low-melt agarose, and sealed with a coverslip [169,213].

3.2.3. RIPerC via BFO

Femoral arteries were dissected from accompanying veins and nerves below the groin ligaments. RIPerC was initiated 60-min post-MCAo by occluding and releasing the femoral arteries bilaterally with vascular clamps for 3 cycles (each 15 min ON/OFF). Control rats received a sham surgery with equivalent anesthesia and arterial isolation but did not receive BFO.

3.2.4. LSCI

LSCI measures real time changes in cerebral blood flow with high spatial and temporal resolution in a two-dimensional, wide field of view [172,173,238]. By recording laser speckle on the surface of the cerebral cortex using a CCD camera with fixed exposure time, speckle blurring can be quantified to determine speckle contrast *K*. To collect LSCI data, rats were secured in ear bars on a custom-built stereotaxic plate under a video macroscope with a tandem lens configuration (× 1.7 magnification) and a Dalsa 1M60 Pantera camera [169,213,237]. A Thorlabs LDM 785S laser (20 mW, wavelength of 785 nm) was used to illuminate the rat cortex at about 30 ° incidence. Stacks of 100 sequential images (1024 × 1024 pixels) were acquired at 20 Hz (5 ms exposure time) during each imaging session. LSCI was performed before MCAo, 60-min post-MCAo (before RIPerC or sham treatment), and continued during 90 min of RIPerC (or sham) at 15-min intervals. All processing and analysis of laser speckle images were performed using ImageJ software (NIH) by a blinded experimenter. Maps of speckle contrast were made from the collected images of raw speckling by determining the speckle contrast factor K for each pixel in an image. K is calculated as the ratio of the standard deviation to the mean intensity ($K = \sigma_s/I$) in a small (5 × 5 pixels) region of the speckle image [172,173,238]. K ranges from 0 to 1. When the scattering particles (blood cells) are moving very fast, the speckle K will be very close to 0. Plots of K therefore show maps of blood flow with darker vessels illustrating faster blood flow velocity. To measure blood flow velocity within identified arteriole segments within or downstream of anastomoses (referred to as MCA segments or pial arterioles in the results section), speckle contrast profiles (Figure 3-3(a)) along multiple cross-sections of the anastomoses joining the distal ACA and MCA segments as well as segments of the MCA downstream of ACA anastomoses were extracted. The value of K at the center of these profiles (i.e. the speckle contrast K at the minima of the profile, Figure 3-3(a)) represents the vessel midline blood flow velocity. A better estimate of relative changes in blood flow velocity through these collateral channels was then attained by converting these centerline K values to correlation times (τ_c) using the equation

$$K^2=\tau_c/2T\{1-exp(-2T/\tau_c)\}$$

where T is the exposure time of the camera. τc values are approximately inversely proportional to the speed of the blood flow (i.e. $1/\tau_c$ is considered proportional to the blood flow velocity) [213,239]. Because anastomoses were generally not well-resolved prior to MCAo, analysis was performed on changes in vessel flow relative to post-MCAo measures (i.e. measurements recorded 60 min after MCAo onset). Blood flow velocity changes relative to 60-min post-MCAo (pre-treatment) are therefore illustrated as $\tau_{PostMCAo}/\tau_c$.

Diameter was determined for ACA-MCA anastomoses and MCA segments downstream of using an ImageJ plug-in that uses a full-width at half-maximum algorithm to estimate the inner vessel diameter using the same vessel profiles used to determine velocity (Figure 3-3(a)) [72,179,213,216].Vessel conformation and orientation can change between baseline imaging and post-MCAo image collection due to subtle difference in placement in the head holder and due to swelling and edema that may shift brain tissue under the cranial window following induction of MCAo. Moreover, anastomotic sections are typically not visible prior to ischemic onset, as the diameter and/or velocity of flow may be below resolution for LSCI. For these reasons, intravessel velocity and diameter measurements are presented as relative changes (percent change) from values measured 60 min after induction of MCAo (i.e. post-MCAo but pre-treatment). After this time point, vascular anatomy remains consistent in LSCI data and repeated measurements are not an issue.

To estimate changes in blood flow using a measure that incorporates changes in vessel midline blood flow velocity and diameter, relQ1 was calculated using the formula

$$relQ = \pi r^2{}_n(\tau_{PostMCAo}/\tau_c)$$

where r_n is the mean radius of the MCA segments in a given animal normalized to the radius at 60-min post-MCAo for that animal (i.e. Post-MCAo (pre-treatment) $r_n = 1$ and $\tau_{PostMCAo}/\tau_c = 1$, such that Post-MCAo relQ = π).

3.2.5. TPLSM

After implantation of the cranial window, fluorescein isothiocyanate–dextran (70,000 MW, Sigma-Aldrich) was injected via the lateral tail vein (0.3 ml, 5% (w/v) in saline). In vivo microscopy was then performed using a Leica SP5 MP TPLSM and Coherent Chameleon Vision II pulse laser tuned to 800 nm. Z-stacks through the first 200 μm of cortical tissue were acquired through the cranial window using a 10 × water dipping objective (Leica HCX APO L10×/0.3 W) and vessel diameter measurements were made from maximum intensity projections of these stacks using the same ImageJ plug-in (full-width at half-maximum algorithm) used in LSCI experiments [179]. While the repeated imaging schedule (15-min intervals) did not allow a comprehensive analysis of blood flow velocity with these regions of interest, red blood cell (RBC) velocity was measured in three to five vessels per region. For analysis of blood flow velocity, line scans were conducted on identifiable arterioles (>10-μm diameter). Blood flow velocity measurements were determined from line scan images by calculating the inverse slope of the linear streaks made by RBCs [73,81].

3.2.6. Distal MCAo

Cerebral ischemia was induced by distal MCA ligation (Figure 3-1(c)) in conjunction with bilateral common carotid artery (CCA) ligation [170]. This model is relevant to the most common type, location, and outcome of human stroke (distal MCAo with cortical infarct). By blocking the proximal cortical branch of MCA, this model generates well-defined ischemia in the MCA cortical territory and allows for a consistent blood flow reduction and infarct with rapidly developing neurological impairment. Distal MCA ligation and imaging protocols were performed by different individuals, and surgeons inducing ischemia were blind to the experimental group for each rat. CCAs were accessed through ventral midline cervical incisions and ligated with 4–0 prolene sutures below the carotid bifurcation. A temporal incision was then made and the right temporalis muscle was gently separated from the bone. A burr hole of 1.5 mm in diameter was made through the squamosal bone, the dura was removed, and the cortical MCA was visualized. The exposed distal MCA was isolated and ligated with a square knot by atraumatic 9–0 prolene suture above the rhinal fissure (Figure 3-1(c)).

3.2.7. Triphenyl Tetrazolium Chloride Staining

All rats were euthanized 6 h after induction of the MCAo. The brains were rapidly removed and sliced into seven coronal, 2 mm sections using a brain matrix, then incubated in 2% 2,3,5-triphenyltetrazolium chloride (TTC) solution at 37 ℃ for assessment of mitochondrial dehydrogenase activity. Tissue damage was assessed in digital images of TTC-stained tissue by a blinded experimenter using ImageJ (NIH) software. Volume of tissues showing early ischemic damage is expressed as a percentage of hemisphere. These measures were calculated for each tissue slice using the indirect method [180,181] to control for tissue distortion due to edema using the following equation

$$\text{Volume of ischemic damage (\%hemisphere)} = \mathbf{[\Sigma(A_C\text{-}A_{NI})/\ \Sigma(A_C)]*100}$$

where A_C is the area of the hemisphere contralateral to stroke in a given tissue slice and A_{NI} is the area of the non-injured tissue (i.e. non-ischemic tissue that stains red using TTC) in the ipsilateral (stroke affected) hemisphere of the same slice.

3.2.8. Statistics

Graphpad Prism was used for all statistical analyses. Two-way repeated measures ANOVAs were used to compare effects of RIPerC or sham treatment on vessel diameter, blood flow velocity, and RelQ. Post hoc comparisons were performed using Sidak's multiple comparisons test. Volumes of ischemic tissue damage (% hemisphere) were compared using an unpaired Student's t-test. Linear regression analyses were performed to determine to what extent the proportion of variance in the volume of tissue damage could be accounted for by variance in measures of MCA (pial arteriole) diameter or blood flow velocity in ischemic regions.

3.3. Results

3.3.1. LSCI of Collateral Blood Flow

LSCI produced high-resolution images of collateral flow from the ACA into the distal segments of the MCA (Figure 3-2(a)). LSCI maps of blood flow were acquired prior to MCAo, 60 min after MCAo but prior to RIPerC (or sham surgery), and during each 15-min cycle of BFO or release (3 cycles, Figure 3-1(b)). Figure3- 2(a) and (b) illustrates representative LSCI data from RIPerC and control rats, respectively. Panels (from left to right) show surface flow before MCAo, 60 min after distal MCAo, during the 3rd cycle of BFO or sham treatment (60–75-min post-stroke), and during the 3rd cycle of release or sham treatment (75–90-min post-stroke), respectively. In both groups, anastomoses join the distal segments of the ACA and MCA after MCAo. Neither RIPerC rats nor controls exhibited dramatically altered patterns of pial collateral blood flow following treatment. However, a reduction in speckle contrast (increased flow) in LSCI maps from RIPerC-treated rats contrasts with an apparent increase in speckle contrast over time in controls. Notably, this apparent increase in blood flow could not be explained by central hemodynamic effects, as there was no significant main effect of Treatment or a significant Treatment × Time interaction ($P > .05$) on arterial blood pressure (Figure 3-2(b)), oxygen saturation (Figure 3-2(c)), heart rate (Figure 3-2(d)), or breath rate (Figure 3-2(e))

3.3.1.1. Changes in Pial Arteriole Diameter and Blood Flow

Changes in diameter, blood flow velocity, and an overall flow (RelQ) during RIPerC or sham treatment were determined for distal branches of the MCA adjacent or downstream of collateral anastomoses with the ACA (Figure 3-3(a)). Mean LSCI data ($n = 11$ per treatment group) are shown in Figure 3-3(b) to (d). Diameter of ACA-MCA anastomoses and downstream MCA segments (mean ± s.e.m., 83.4 ± 4.7 μm) (Figure 3-3(b)) exhibited a significant main effect of Treatment group ($F_{(1, 20)} = 17.75$, $P = 0.0004$). Sidak's post hoc comparisons revealed that RIPerC-treated rats had significantly larger MCA segment diameters at all-time points (C1 = 1st cycle of clamp, R1 = 1st cycle of release…) during treatment relative to controls (left panel). Notably, MCA segments dilate following MCAo, so these differences reflect further dilation in RIPerC-treated animals contrasted with a gradual narrowing of these vessels in controls. Notably, single sample t-tests shows that the dilation due to RIPerC and the narrowing in control rats represents significant changes relative to post-MCAo values ($P = .006$ and .040, respectively, against a hypothetical post-MCAo of 100%). Figure 3-3(c) shows mean changes in blood flow velocity (correlation times, τc) relative to post-MCAo. No significant main effect or interaction was observed ($P > .05$). Overall, flow in MCA segments was estimated by calculating RelQ (Figure 3-3(d)). A significant main effect of Treatment on RelQ was observed ($F_{(1, 20)} = 4.686$, $P = 0.0427$), with

Sidak's comparisons suggesting the greatest difference in flow during the 1st cycle of BFO release.

3.3.2. Diameter Measurement using TPLSM

LSCI data suggest increased flow through collateral vessels after MCAo primarily due to a difference in the diameter of MCA segments between treatment groups. While LSCI measurements of diameter have been previously validated [213], they are an indirect measure of luminal diameter based on the speckle contrast. Additionally, LSCI experiments were performed under isoflurane anesthesia, which may itself induce vasodilation and partially mask treatment effects. TPLSM was therefore performed to directly assess the luminal diameter of anastomoses and pial MCA segments during RIPerC or sham treatment after distal MCAo in urethane anaesthetized rats (Figure 3-4, n = 8 per treatment group). Moreover, TPLSM allowed measurement of luminal diameter in smaller pial collaterals (mean ± s.e.m., 40.2 ± 3.1 μm) that could not always be reliably measured with wide field LSCI. Figure 3-4(b) shows maximum intensity projections of pial vessels from the region demarcated (white box) in the cranial window shown in Figure 3-4(a) from a control rat. Pial vessels were imaged 60 min after MCAo and again at 15-min intervals during the following 90 min (Figure 3-4(b)). Narrowing of MCA segments over time after MCAo was apparent in controls (Figure 3-4(b) and (d)) but did not occur in RIPerC-treated animals (Figure 3-4(f) and (h)). A significant main effect of treatment group on MCA segment diameter and a significant interaction between Treatment and Time was observed (Figure 3-4(c); Treatment, $F_{(1,}$

$_{14)} = 12.$, $P = 0.0031$; Time, $F_{(5,\ 70)} = 12.$, $P = 0.0031$; Interaction, $F_{(5,\ 70)} = 6.586$, $P < .0001$). Sidak's post hoc comparisons revealed that RIPerC-treated rats had significantly larger diameters at all-time points after the initial BFO clamp. Mean diameters (in μm) for MCA segments in RIPerC and control rats are shown in Figure 3-4(e) and (g), respectively. In the RIPerC groups, diameters did not change significantly over time (Repeated measures ANOVA, $P > .05$). However, a significant main effect of Time was observed in the control rats ($F_{(6, 42)} = 9.347$, $P < 0.0001$) and Sidak post hoc comparisons confirmed significantly smaller diameters relative to baseline during imaging at R1, C2, R2, C3, and R3 (all $P < .001$). No main effect of Treatment or significant interaction between Time and Treatment was detected for measures of RBC velocity in vessels within these regions ($P > .05$).

3.3.3. Early Ischemic Damage

TTC staining revealed a significant reduction in the volume of tissue showing early ischemic damage in rats treated with RIPerC (Figure 3-5, right panel, Student's t-test, $P = .0001$). Regression analyses were performed to examine volume of tissue damage as a function of LSCI- and TPLSM-derived measures of pial arteriole diameter and blood flow velocity (Figure 3-6). To examine if narrowing of MCA segments over time after MCAo was associated with increased ischemic damage, a regression analysis of the volume of early ischemic damage (from TTC-stained tissue) as a function of arteriole diameter at the final imaging time point was performed. Figure 3-6(a) shows a plot of damage (% of hemisphere) as a function of vessel diameter for all rats from both LSCI and TPLSM studies (n = 38, collapsing 19 rats each from RIPerC and control groups onto a single plot). A significant linear relationship between damaged tissue volume and vessel diameter was observed ($R^2 = 0.13$, $P = .024$), with increased narrowing from post-MCAo values being associated with greater infarct volume. The statistical relationship was strengthened when regression analyses were confined to more quantitative measurements of MCA segments from TPLSM experiments (Figure 3-6(b), $R^2 = 0.36$, $P = .014$).

To examine if tissue damage was associated with changes in regional blood flow velocity relative to baseline (pre-MCAo) values, a second regression analysis was performed. For this regression analysis, relative flow changes from baseline (pre-MCAo) were measured in a contiguous ROI consisting of a 500 × 500 pixel square positioned to include the distal MCA and ACA segments. Such regional measures of speckle contrast correlate highly with other measures of regional cerebral blood flow such as laser Doppler flowmetry [240], and allowed inclusion of pre-MCAo baseline values (whereas diameter and velocity measurements can be difficult to attain from anastomoses that are not well-resolved prior to ischemia). Mean correlations times normalized to baseline (pre-MCAo, τBaseline/τc) values are illustrated for the post-MCAo (pre-treatment) time point in Figure 3-6(c). Additionally, the mean τBaseline/τc measured during the treatment period is illustrated (i.e. this mean τBaseline/τc was calculated by determining the average of the six values measured during the 3 cycles of clamp and release). Consistent with intravessel measures from MCA segments (Figure

3-3(c)), multivariate analysis did not reveal a significant main effect of Treatment or a significant Time × Treatment interaction on τBaseline/τc calculated from the regional ROI. In Figure 3-6(d), volume of tissue showing signs of early ischemic damage is plotted as a function of regional flow velocity (τBaseline/τc) for all animals in LSCI and TPLSM studies. A significant linear relationship between damaged tissue volume and regional blood flow was observed ($R^2 = 0.30$, $P = .008$) with higher τBaseline/τc values being associated with smaller volumes of tissue damage.

3.4. Discussion

Using LSCI and TPLSM in rats with a distal MCAo, our data demonstrate that RIPerC induces a significant increase in blood flow through pial collaterals. Notably, this increase is due to continued dilation (from post-MCAo, pre-treatment values) of pial collaterals and MCA segments adjacent or downstream to ACA-MCA connections in treated animals, contrasting with progressive constriction of these same vessels in control rats. This prevention of "collateral collapse" was associated with a significant reduction in early ischemic damage 6 h after stroke.

3.4.1. Cerebral Blood Flow and Neuroprotection after RIPerC

Previous preclinical studies in mice suggest that RIPerC can improve regional cerebral blood flow after embolic MCAo [139,223]. The major finding of this study is that RIPerC improves blood flow through collateral vasculature by preventing the narrowing of these vessels over time after ischemic onset (as observed in control rats). This maintenance of post-stroke vasodilation in treated rats and narrowing of MCA segments over time in untreated rats was also observed in previous preclinical studies of transient aortic occlusion as a collateral therapeutic. As transient aortic occlusion also involves ligation of a femoral artery (to allow advancement of the dilation catheter to the descending aorta) and thus results in ischemia peripheral to the brain, this raises the interesting possibility that the vasodilation induced by transient aortic occlusion may share common humoral mediators with RIPerC. Notably, transient aortic occlusion had both dilatatory effects but also induced a significant increase in blood pressure in the carotid artery that manifests as significantly increased blood flow velocity. Here, RIPerC maintained or augmented pial arteriole diameter but was not associated with increased flow velocity or an increase in systemic blood pressure, suggesting that these two mechanisms of enhanced flow after aortic occlusion may have different origins (with vasodilation resulting from humoral factors released by peripheral ischemia and increased flow velocity due to blood flow diversion from the periphery to the head that increases blood pressure above the aortic occlusion and therefore increases cerebral perfusion pressure). Neuroprotection due to transient aortic occlusion reduces infarct by ~43% (24 h after ischemic onset) [114], comparable to our reduction in early ischemic damage using 3 cycles of RIPerC (~39% reduction at 6 h post). As such, increases in flow due to diameter changes alone may be sufficient to protect vulnerable tissue (without large increases in perfusion pressure).

In preclinical studies, RIPerC improves the efficacy of neuroprotection with minocycline, recanalization with tPA, and has been associated with a reduction of infarct and neurological deficits 24 and 48 h after stroke [135,138–140,142,223,241]. Moreover, RIPerC may reduce autophagy and protect the blood–brain barrier (reducing extravasation and hemorrhagic transformation) [224]. While several randomized clinical have shown RIPerC reduces myocardial infarct size in patients, clinical data in cerebral ischemia are limited [242,243]. In a recent randomized trial, investigators studied the effect of RIPerC as adjunctive therapy to intravenous rt-PA for acute ischemic stroke and assessed the feasibility of RIPerC performed during transport to hospital. The approach was found feasible, and 247 acute stroke patients received RIPerC as an adjuvant to rt-PA (196 patients received standard treatment) [144]. Although the study reported neutral results on follow-up measures, a tissue survival analysis suggested that prehospital RIPerC was neuroprotective.

Our data also suggest that RIPerC significantly reduces early ischemic damage. Notably, tissue damage was significantly dependent on the diameter of the pial arterioles, as increased narrowing of the pial arterioles (from post-MCAo measures) was associated with increased volume of ischemic damage (Figure 3-6(a) and (b)). However, it is important to note that these diameter measures are relative to values post-MCAo but prior to treatment (i.e. at a time point when arterioles are likely dilated relative to pre-stroke baseline), and we do not have measures of how dilated each vessel was relative to baseline. Consequently, an even stronger statistical relationship may be determined by studies that measure narrowing relative pre-stroke values. Interestingly, while RIPerC did not have a significant effect on blood flow velocity in LSCI or TPLSM studies (whether measuring within arterioles or using a regional measure), early ischemic damage did vary as a function of regional blood flow (Figure 3-6(d)). Given that regional measures of speckle contrast are highly correlated with other measures of regional cerebral blood flow such as laser Doppler flowmetry49 that reflect overall tissue flow and have previously been shown to be predictive of degree of ischemia, this relationship is not surprising. Combined, our data show that overall blood flow predicts tissue fate and identify prevention of cerebral arteriole narrowing as a protective effect of RIPerC treatment. This neuroprotective effect likely results from both increases in blood flow that shift penumbral flow beyond critical values for tissue viability, from maintenance of the integrity of the blood–brain barrier in ischemic regions, and from the release of humoral factors at the site of peripheral ischemia that confer neuroprotection in the brain [135,224].

3.4.2. Summary

Our data define collateral flow augmentation via prevention of collateral collapse as an important neuroprotective mechanism during RIPerC. Further preclinical and clinical study is required to allow for optimal clinical translation.

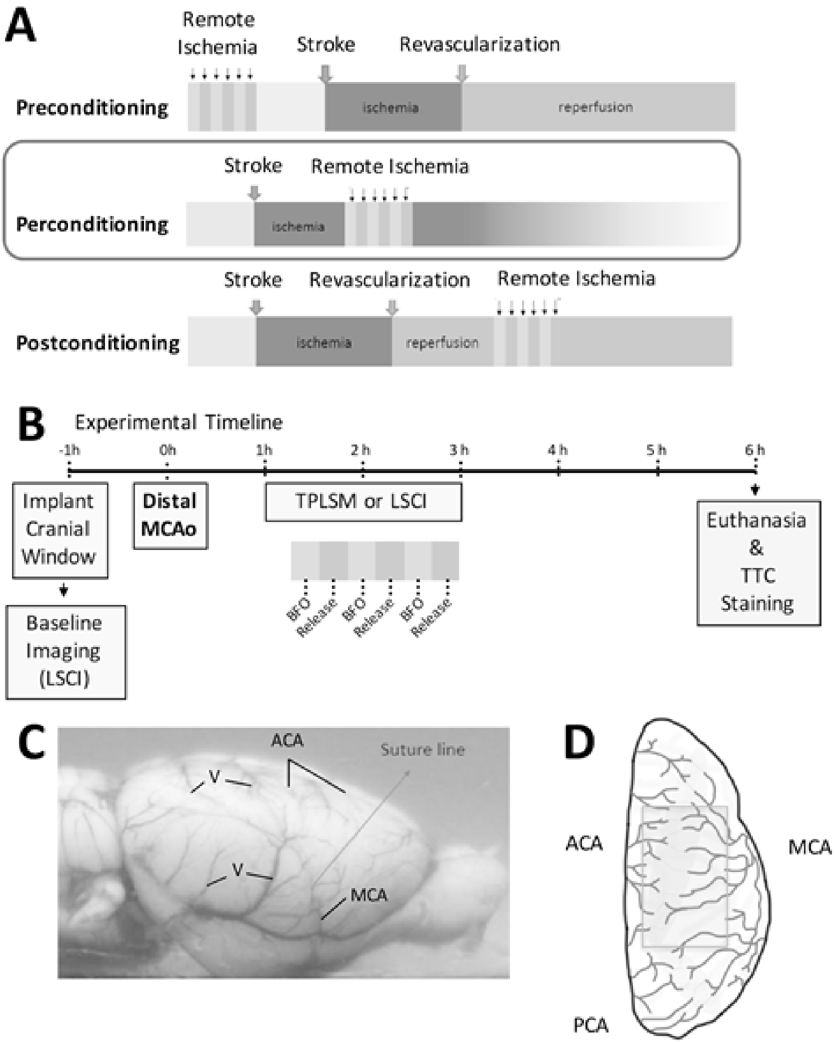

Figure 3-1 Remote ischemic conditioning & Experimental design & Lateral view of the rat brain showing the location of ligation of the right middle cerebral artery (MCA) & Schematic view of the dorsal surface of the rat cortex illustrating the placement of cranial imaging window

(**a**) Remote ischemic conditioning can be applied prior to stroke, after the onset of ischemia, or at the time of reperfusion (termed remote ischemic pre-, per-, or post-conditioning, respectively) (**b**) Experiment timeline. (**c**) A lateral view of the rat brain showing the location of ligation of the right middle cerebral artery (MCA) above the rhinal fissure that was used to induce distal occlusion of the MCA (MCAo). (**d**) A schematic of the dorsal surface of the rat cortex illustrating the placement of cranial imaging window over the distal territories of anterior cerebral artery (ACA) and MCA (modified with permission from Winship et al.1). TPLSM: two photon laser scanning microscopy; LSCI: laser speckle contrast imaging; TTC: 2,3,5-triphenyltetrazolium chloride staining; V: surface vein.

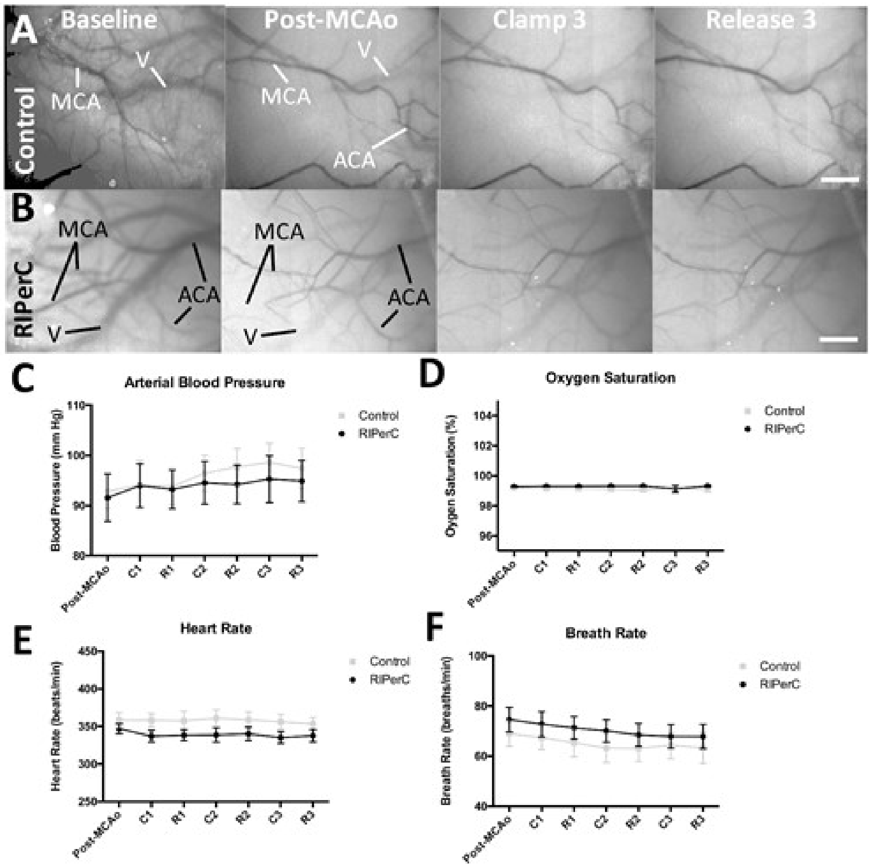

Figure 3- 2 Representative LSCI maps of collateral flow in RIPerC treated and control rat & Effects of RIPerC on systemic hemodynamics and physiological parameters

(**a, b**) Representative LSCI maps of collateral flow in a RIPerC treated and control rat. Panels (from left to right) show surface flow before middle cerebral artery occlusion (MCAo), 60 min after distal MCAo, during the third cycle of bilateral femoral occlusion (BFO) or sham treatment (60–75-min post-stroke), and during the third cycle of release or sham (75–90-min post-stroke), respectively. Overall, darkening of LSCI maps (from post-MCAo until final imaging) in RIPerC-treated animals suggests RIPerC is associated with an increase in flow in the imaging window. Scale bar, 1 mm. (**c–f**)

RIPerC was not associated with central hemodynamic effects as arterial blood pressure (n = 6 RIPerC rats and 3 controls), oxygen saturation (n = 10 RIPerC and 8 controls), heart rate (n = 10 RIPerC and 8 controls), and breath rate (n = 10 RIPerC and 8 controls) were unchanged by treatment relative to controls. Graphs show mean ± s.e.m. MCA: middle cerebral artery; ACA: anterior cerebral artery; V: surface vein; C1: 1st cycle of clamp; R1: 1st cycle of release; C2: 2nd cycle of clamp; R2: 2nd cycle of release; C3: 3rd cycle of clamp; R3: 3rd cycle of release.

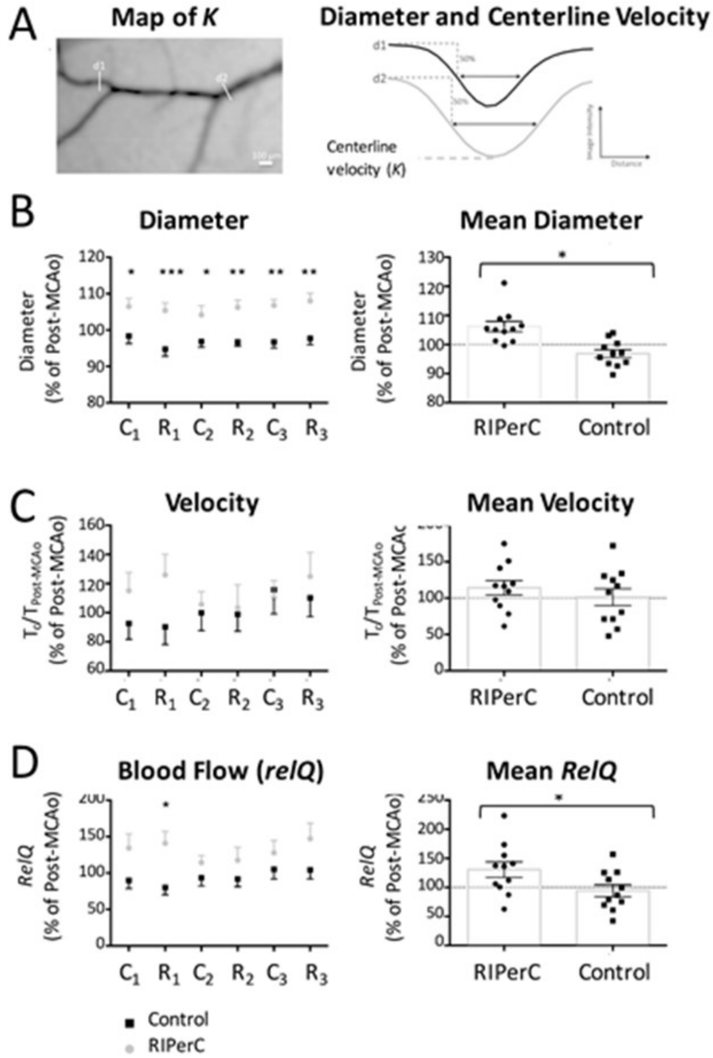

Figure 3- 3 Effects of RIPerC on pial vessel diameter, RBC velocity, and RBC blood flow after middle cerebral artery occlusion (MCAo) with LSCI

(**a**) Diameter and centerline blood flow velocity measures could be derived from profiles of speckle contrast spanning middle cerebral artery (MCA) segments. LSCI was used to determine relative changes in diameter (**b**) and blood flow velocity (**c**) in anterior cerebral artery (ACA)-MCA anastomoses and distal MCA segments. (**b**)

RIPerC-treated rats ($n = 11$) had significantly larger diameters at all-time points during treatment relative to controls ($n = 11$) (left panel, mean changes in diameter during the complete treatment period are illustrated at right). (**c**) Shows mean changes in correlation times (τc) relative to post-MCAo values. No significant main effect of Treatment was observed. (**d**) Overall flow in these pial arterioles was estimated by calculating RelQ. A significant main effect of Treatment on RelQ was observed, suggesting the greatest difference in flow during the 1st cycle of BFO release. $^{*}P < 0.05$; $^{**}P < 0.01$; $^{***}P < 0.001$. Graphs show mean ± s.e.m. MCAo: middle cerebral artery occlusion; C1: 1st cycle of clamp; R1: 1st cycle of release; C2: 2nd cycle of clamp; R2: 2nd cycle of release; C3: 3rd cycle of clamp; R3: 3rd cycle of release.

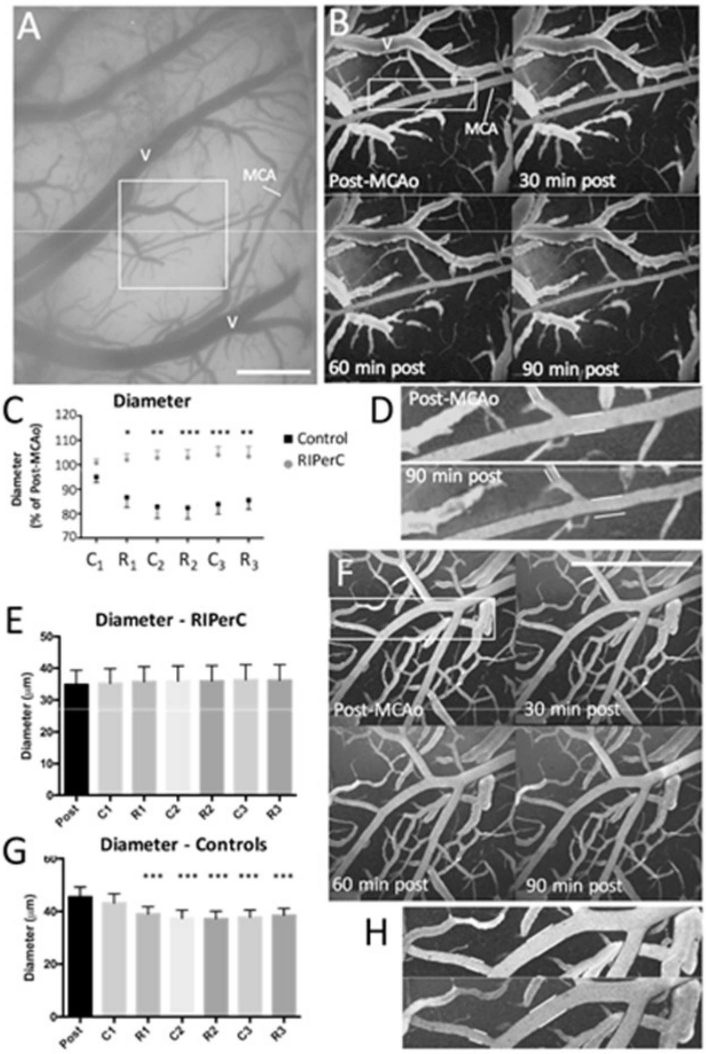

Figure 3- 4 Representative TPLSM maps of collaterals in RIPerC treated and control rat & Effects of RIPerC on pial vessel diameter, after middle cerebral artery occlusion (MCAo) with TPLSM

(**a**) Cranial window for two photon laser scanning microscopy (TPLSM) performed in a control rat. Scale bar, 0.5 mm. (**b**) Shows maximum intensity projections acquired during TPLSM of pial vessels from the region demarcated (white box) in (**a**).

Narrowing of pial collaterals and distal MCA segments over time after MCA occlusion (MCAo) was apparent in controls ($n = 8$) (**b, d**) but did not occur in RIPerC-treated animals ($n = 8$) (**f, h**). Scale bar in F, 0.5 mm. (**c**) Mean arteriole diameter over time after MCAo. Sidak's post hoc comparisons revealed that RIPerC-treated rats had significantly larger diameters at all-time points after the initial BFO clamp. (**e, g**) Repeated measures analyses confirmed that a significant reduction in arteriole diameter occurred in control rats (**g**) but not in RIPerC rats (**e**). Post hoc comparisons confirmed significant narrowing of vessels at R1, C2, R2, C3, and R3 ($P < .001$). Graphs show mean ± s.e.m. *$P < 0.05$; **$P < 0.01$; ***$P < 0.001$. MCA: middle cerebral artery; V: surface vein; C1: 1st cycle of clamp; R1: 1st cycle of release; C2: 2nd cycle of clamp; R2: 2nd cycle of release; C3: 3rd cycle of clamp; R3: 3rd cycle of release.

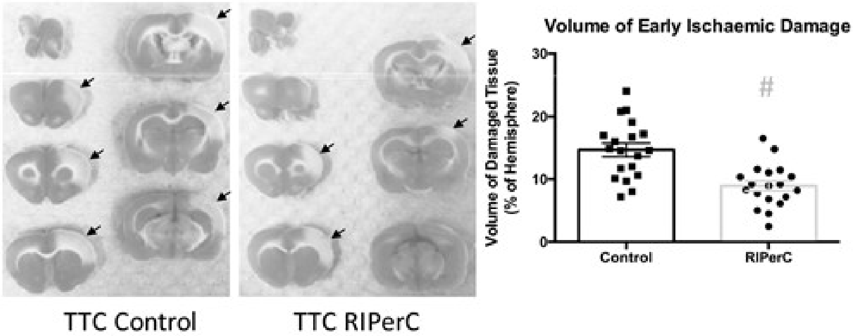

Figure 3- 5 Early ischemic damage measurements

Infarct volume at 6-h post-MCAo (percentage of hemisphere). A significant reduction in infarct volume was observed in RIPerC-treated animals (n = 19) compared to controls (n = 19) #P = 0.0001. TTC, 2,3,5-triphenyltetrazolium chloride staining.

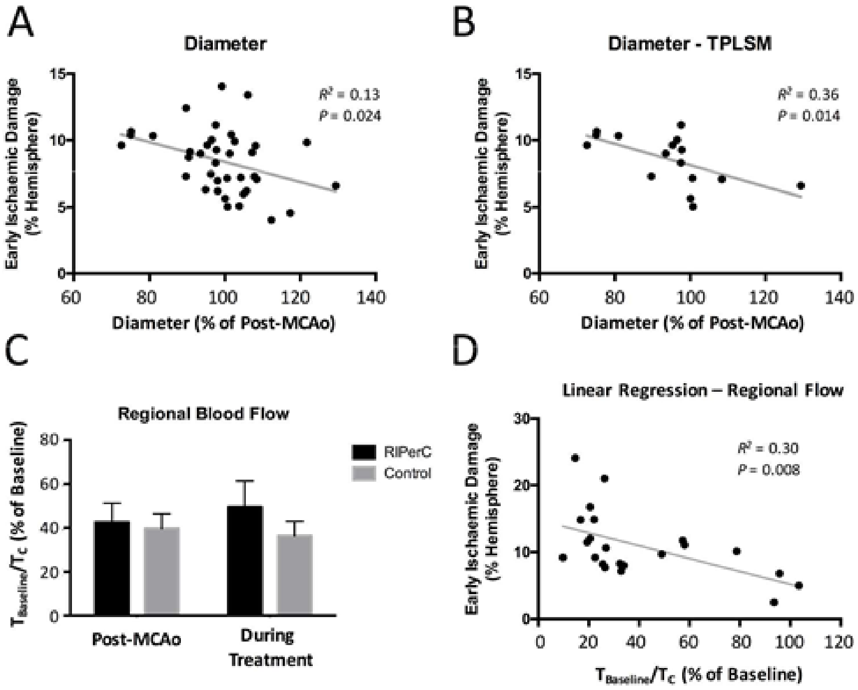

Figure 3- 6. Relationship between damaged tissue volume and regional blood flow

(**a**) The relationship between the diameter of the distal middle cerebral artery segments during the final imaging session (90 min after RIPerC or sham treatment onset) relative to the measurement at 60 min after middle cerebral artery occlusion (MCAo). When volume of tissue damage was examined as a function of arteriole diameter (relative to post-MCAo, collapsing all animals (n = 38) from both experimental groups in both laser speckle contrast imaging (LSCI) and two photon laser scanning microscopy (TPLSM) experiments into a single plot), a significant linear relationship was observed, and animals in which arterioles showed greater narrowing relative to post-MCAo measures tended to have larger volumes of ischemic damage. (**b**) The linear relationship was strengthened when only data from TPLSM experiments were included in the regression analysis. (**c, d**) The relationship between regional blood flow within the cranial window and the volume of early ischemic damage. (**c**) Blood flow in the region of interest in the penumbral region of the MCAo was reduced to 40% of pre-MCAo baseline prior to treatment (60 min after MCAo onset). Bars to the right of post-MCAo measures show the mean blood flow measures in the region of interest during the treatment period (i.e. the average of the τBaseline/τC values derived from the six time points during RIPerC or sham treatment). There was no main effect of RIPerC on regional flow ($P > .05$). (**d**) However, regional flow was predictive of ischemic damage, as a linear relationship between regional flow and volume of early tissue damage (again collapsing all animals from LSCI and TPLSM studies onto a single plot) was observed, with volume of damage increasing with reducing regional flow.

Chapter 4

Improved collateral flow and reduced damage after remote ischemic perconditioning in aged rats with distal middle cerebral artery occlusion

4.1. Introduction

Ischemic stroke is a devastating cerebral disease that occurs when arteries supplying the brain are obstructed. Ischemia leads to insufficient nutrient and oxygen supply to meet metabolic demand of the brain, thus inducing the damage or death of brain cells. Cerebral collaterals are subsidiary vascular channels in the cerebral circulation which can sustain blood flow to ischemic tissue when principal vascular routes fail [11–14]. Therefore, collateral circulation is a primary determinant of the degree of ischemia in the penumbra. Cerebral collaterals can be classified as primary or secondary collaterals. The primary collaterals refer to the circle of Willis, which allows blood flow exchange between anterior and posterior circulation and between hemispheres [15]. Secondary collaterals include the pial collaterals, which are also called leptomeningeal collaterals [16]. Pial collaterals are anastomotic connections located on the cortical surface which connect distal branches of adjacent arterial network, e.g. anterior cerebral artery (ACA)-middle cerebral artery (MCA); middle cerebral artery (MCA)-posterior cerebral artery (PCA) ACA-MCA; MCA-PCA [16,17]. When MCA occlusion occurs, pial collaterals become patent and provide compensatory blood flow from ACA and/or PCA to the ischemic penumbra of MCA [16]. However, collaterals are thought to be time limited and can fail over time [26–28]. The dropout of collaterals during stroke is related to the progression of the penumbra to irreversible ischemic infarct and impaired response to treatment [26–28]. Intravenous recombinant tissue plasminogen activator (IV r-tPA) is the only FDA approved medical treatment of ischemic stroke, but requires administration within 4.5h of symptom onset [137,244]. Although proven effective when administered within this therapeutic window, approximately half of patients treated with intravenous r-tPA still lack of histological and neurologic benefit, suffering subsequent disabilities and need help in daily living [137]. Strategies that can augment collaterals blood flow to reduce expansion of the infarct core before recanalization treatment are attractive and as they may expand time window for late reperfusion interventions to allow more patients to benefit [145].

Aging is one of the primary risk factors for ischemic stroke and it is known that the brain of the elderly has reduced ischemic tolerance [149–152]. Preclinical studies have reported that increasing age is associated with rarefaction of cerebral collaterals, leading to insufficient ability to maintain blood flow during ischemia [18,19]. As we have shown in Chapter 2, the hemodynamic evolution of the pial collateral circulation is also influenced by aging. Aged rats exhibited rapid and more severe failure of pial collaterals comparing to young rats, thus showing significantly greater volumes of ischemic damage at 6 h after ischemic onset.

Remote ischemic conditioning is a process induced by series of repetitive, transient episodes of ischemia/reperfusion on a non-vital remote organ such as limb to provide endogenous protection to ischemia in vital organs like the heart or brain [26,135]. Remote ischemic conditioning can be performed before vital organ ischemia (termed remote ischemic preconditioning), after the onset of vital organ ischemia but before reperfusion (termed remote ischemic per-conditioning (RIPerC), or at the time of reperfusion (termed remote ischemic post-conditioning) [26,136]. We demonstrated in Chapter 3 that RIPerC induced by BFO within 1 hour post dMCAo is effective in preventing collateral collapse and reducing early ischemic damage in young adult rats [26]. However, given the more severe impairment in collateral flow observed in the aged (Chapter 2), it remains unclear if such an effect of RIPerC would be observed in aged rats. Demonstration of a benefit of remote ischemia as a collateral therapeutic in the aged is important, as human stroke occurs predominantly in the elderly [148,245]. Therefore, in order to provide further evidence to support bench to bedside translation of RIPerC, we examined hemodynamic changes in pial collateral flow with RIPerC treatment in aged rats in this chapter. Here, high resolution in vivo laser speckle contrast imaging (LSCI) and two photon laser scanning microscopy (TPLSM) were combined to map dynamic changes in pial collaterals during RIPerC after distal middle cerebral artery occlusion (dMCAo) in aged rats. Our findings demonstrated that RIPerC induced by BFO within 1 hour post dMCAo is effective in reducing early ischemic damage and improves collateral blood flow in aged animals.

4.2. Materials and Methods:

Aged Male Sprague–Dawley rats (16-18 months of age) were used (sham treatment: n=8; RIPerC: n=9). Prior to experimental procedures, animals were housed in pairs on a 12-h day/night cycle and had access to food and water ad libitum. Procedures conformed to guidelines established by the Canadian Council on Animal Care and were approved by the Health Sciences Animal Care and Use Committee at the University of

Alberta. Procedures and results reporting is consistent with the ARRIVE guidelines.[168] The experimental timeline is illustrated in Figure 4-1(a).

4.2.1. Anesthesia and Monitoring

Light anesthesia was induced using an induction chamber with 4–5% isoflurane (in 70% nitrogen and 30% oxygen) prior to intraperitoneal injections of urethane (i.p. 1.25 g/kg, divided into four doses delivered at 30-min intervals). Isoflurane was discontinued after the first urethane injection, and rats remained anaesthetized until euthanasia. During all surgery and imaging, temperature was maintained at 36.5–37.5C with a thermostatically controlled warming pad and heart rate, oxygen saturation, and breath rate were monitored using a pulse oximeter (MouseOx, STARR Life Sciences).

4.2.2. Cranial Window

LSCI and TPLSM were performed through cranial windows implanted after craniotomy. A midline incision was made on the scalp to expose the surface of the skull. A 5*5 mm section of the skull over the distal regions of the right MCA territory was thinned until translucent using a dental drill (frequently flushing with saline to dissipate heat) and then gently removed. The dura matter was removed, then the cranial window was covered with a thin layer of 1.3% low melt agarose and sealed with a glass coverslip as previously described [11,27].

4.2.3. dMCAo

Cerebral ischemia was induced by bilateral common carotid artery (CCA) ligation in addition with distal MCA ligation [26,170]. Distal MCA ligation and imaging protocols were performed by different individuals, and surgeons inducing ischemia were blind to the experimental group for each rat. CCAs were accessed through ventral midline cervical incisions and ligated with 4–0 prolene sutures below the carotid bifurcation. A temporal incision was then made and the right temporalis muscle was gently separated from the bone. A burr hole of 1.5 mm in diameter was made through the squamosal bone, the dura was removed, and the cortical MCA was visualized. The exposed distal MCA was isolated with a loose square knot by atraumatic 9–0 prolene suture above the rhinal fissure before stroke. After pre-stroke imaging, the knot was ligated to induce permanent dMCAo.

4.2.4. LSCI

LSCI measures real time changes in cerebral blood flow with high spatial and temporal resolution over a wide field of view [171–173]. To collect LSCI data, rats were secured in ear bars on a custom-built stereotaxic plate under a Leica SP5 MP laser scanning microscope. A Thorlabs LDM 785S laser (20 mW, wavelength of 785 nm) was used to illuminate the rat cortex at approximately 30 ° incidence. Stacks of 101 sequential images (1024 × 1024 pixels) were acquired at 20 Hz (5 ms exposure time) during each imaging session. All processing and analysis of laser speckle images were performed using ImageJ software (NIH) by a blinded experimenter. Maps of speckle contrast were made from the collected images of raw speckling by determining the speckle contrast factor K for each pixel in an image. K is calculated as the ratio of the standard deviation to the mean intensity ($K = \sigma_s/I$) in a small (5 × 5 pixels) region of the speckle image [171–173]. Plots of K show maps of blood flow with darker vessels illustrating faster blood flow velocity [174,175]. For quantification of penumbral flow, K was measured in a contiguous ROI consisting of an 800 × 800 pixel square positioned to include the distal MCA and ACA segments. Because cerebral blood flow (CBF) velocity in selected region of interest was inversely proportional to the square of speckle contrast value K [176,177].

$$v \propto \frac{1}{K^2}$$

Therefore, $1/K^2$ is also used to illustrate CBF velocity change in LSCI figures.[174,178]

4.2.5. TPLSM

TPLSM was performed using a Leica SP5 MP TPLSM and Coherent Chameleon Vision II pulse laser tuned to 800 nm. Blood plasma was labelled with fluorescein isothiocyanate–dextran (70,000 MW, Sigma-Aldrich) injected (0.3 mL (5% (w/v) in saline, 0.2 mL supplements as required) via the tail vein [73,81]. Z-stacks through the first 0.15mm of cortical tissue were acquired through the cranial window using a 10 × water dipping objective (Leica HCX APO L10×/0.3 W) and vessel diameter measurements were made from maximum intensity projections of these stacks using ImageJ plug-in (full-width at half-maximum algorithm) [179]. For acquisition of red blood cell (RBC) velocity, line scans were performed in the lumen of arterioles over a length of 50-100 pixels at scan rates of 1200Hz. While the repeated imaging schedule (30-min intervals) did not allow a comprehensive analysis of blood flow velocity in all vessels within these regions of interest, RBC velocity was via line scans in three identifiable arterioles (>0.05mm diameter) per region. RBC velocity was determined from line scan images by calculating the slope of streaks [73,81]. RBC flux, which provides an overall measure of flow through each vessel, was calculated using the following equation:

$$\text{Flux}=(\pi/8)(d^2)(v)$$

where v is the RBC velocity along the central axis of the vessel, and d is the vessel diameter.

4.2.6. RIPerC via BFO

Femoral arteries were dissected from accompanying veins and nerves below the groin ligaments. RIPerC was initiated 60-min post-dMCAo by occluding and releasing the femoral arteries bilaterally with vascular clamps for 3 cycles (each occlusion or release lasted for 15 min). Control rats received a sham surgery with equivalent anesthesia and arterial isolation but did not receive BFO.

4.2.7. Triphenyl Tetrazolium Chloride Staining

All rats were euthanized 6 h after induction of the dMCAo. The brains were rapidly removed and sliced into seven coronal, 2 mm sections using a brain matrix, then incubated in 2% 2,3,5-triphenyltetrazolium chloride (TTC) solution at 37 ℃ for assessment of mitochondrial dehydrogenase activity. Tissue damage was assessed in digital images of TTC-stained tissue by a blinded experimenter using ImageJ (NIH) software. Volume of tissues showing early ischemic damage is expressed as a percentage of hemisphere. These measures were calculated for each tissue slice using the indirect method [180,181] to control for tissue distortion due to edema using the following equation

$$\text{Volume of ischemic damage (\%hemisphere)} = \left[\boldsymbol{\Sigma(A_C - A_{NI}) / \Sigma(A_C)}\right]\boldsymbol{*100}$$

where A_C is the area of the hemisphere contralateral to stroke in a given tissue slice and A_{NI} is the area of the non-injured tissue (i.e. non-ischemic tissue that stains red using TTC) in the ipsilateral (stroke affected) hemisphere of the same slice.

4.2.8. Statistical Analysis

Statistical analyses were performed using Graph Pad Prism (GraphPad software, San Diego, CA, US). RBC velocity and RBC flux data exhibited a right skewed distribution, so a cubed root transformation was applied. Two-way analysis of variance (ANOVA) with repeated measures were used to compare effects of RIPerC and sham treatment on aged rats with LSCI measures (speckle value, relative blood flow) and TPLSM measures (vessel diameter, RBC velocity, and RBC flux). Post hoc comparisons were performed using Holm-Sidak's multiple comparisons test. Volumes of ischemic tissue infarct (% of contralateral hemisphere) and physiological parameters (pulse, respiratory rate and oxygen saturation) were compared using an unpaired Student's t-test. Values are expressed as mean ± S.D. Sample sizes estimates were based on variability in data from previous LSCI and TPLSM experiments in our laboratory.

4.3. Results:

LSCI and TPLSM were used to assess changes of pial collateral flow immediately before and for 4.5h after dMCAo (at intervals of 30 mins, Figure 4-1(a)). Physiological parameters remained stable throughout imaging (Figure 4-1(b-d)). LSCI and TPLSM were used to create high-spatiotemporal resolution maps of blood flow in pial vessels in the region of ischemia, including measures of regional flow (LSCI, Figure 4-2) as well as pial vessel diameter, RBC velocity, and RBC flux (TPLSM, Figure 4-3) [11].

4.3.1. LSCI Reveals Cortical Blood Flow in Aged Control and Aged RIPerC Treatment Rats

Figure 4-2 shows LSCI derived maps of speckle contrast showing flow changes over 270 min (4.5 h) post stroke in Aged control rats and Aged RIPerC treated rats. Immediately after dMCAo, robust anastomotic connections join the distal segments of MCA from ACA in both groups (arrows). In aged controls, penumbral flow decreased during the imaging period (as indicated by a consistent reduction in visible pial vessels and increase in speckle contrast brightness during the imaging period (Figure 4-2(a)). Qualitatively, this reduction in flow (increased speckle) appeared less severe in RIPerC treated rats (Figure 4-2(b)).

Mean speckle contrast values (*K*) are shown in Figure 4-2(c). Two-way ANOVA revealed a significant main effect of Time ($F_{(10,150)}$ =35.67, $P<0.0001$), as well as a significant Time X Treatment interaction (($F_{(10,150)}$ =1.959, P =0.0416); Treatment, n.s., $F_{(1,15)}$ =0.9625, P =0.3421). A more proportional measure of blood flow can be attained by determining the inverse square of the speckle contrast values. Relative blood flow ($1/K^2$) normalized to pre dMCAo values is shown in Figure 4-2(d).[174,178] Flow in both groups dropped gradually to less than 50% and remained low throughout imaging. Again, a two-way ANOVA revealed a significant main effect of Time ($F_{(9,135)}$ =13.42, P <0.0001) on relative blood flow ($1/K^2$), but there was no statistically significant main effect of Treatment ($F_{(1,15)}$ =1.256, P =0.2801) and no interaction of Time and Treatment ($F_{(9,135)}$ =0.5807, P =0.8111).

4.3.2. TPLSM Reveals Dynamic Changes in Pial Arteriole Diameter, RBC Velocity, and Flux after dMCAo

TPLSM was performed to directly assess the luminal diameter, RBC velocity and RBC flux of distal branches of the MCA adjacent or downstream of collateral anastomoses with the ACA during RIPerC (Figure 4-3(a)) or sham treatment (Figure 4-3(b)) after distal dMCAo. Panels (from left to right) show LSCI maps before dMCAo, before dMCAo, 60 min after distal dMCAo, 150 min after dMCAo (during the 3rd cycle of BFO releasing or sham treatment), and 270min dMCAo, respectively. Obvious narrowing of distal MCA segments over time after dMCAo was apparent in Aged controls but were less apparent in RIPerC-treated animals (representative images in Figure 4-3(a-b), group quantification in Figure 4-3(c-d)). Figure 4-3(c) shows pial diameter data normalized to pre dMCAo values. Two-way ANOVA demonstrated a significant main effect of Time ($F_{(1.484, 22.27)}$ =10.28, P =0.0016) and Treatment ($F_{(1,15)}$ =7.416, P =0.0157) on pial arteriole diameter, as well as a significant Time X Treatment interaction ($F_{(9,135)}$ =3.696, P =0.0004). However, post hoc comparisons did not identify any significant differences between treatment groups at individual time-points. To compensate for potential variation in blood flow after dMCAo but prior to treatment, Figure 4-3(d) shows diameters normalized to values measured 60 minutes after ischemic onset. Two-Way ANOVA revealed a significant main effect of Treatment ($F_{(1,15)}$ =13.05, P =0.0026) and Time ($F_{(3,45)}$ =2.894, P =0.0455), but no Time X Treatment interaction ($F_{(6,90)}$ =0.6786, P=0.6673) . Holm-Sidak's post hoc comparisons revealed that RIPerC-treated rats had significantly larger diameters ($P < 0.05$) at all-time points after the initiation of the first BFO clamp, with the exception of 120 min post dMCAo. Thus, consistent with findings in younger adult rats [26], rats, RIPerC protected against collateral narrowing in aged rats.

Figure 4-4(a-b) show mean changes in red blood cell (RBC) velocity relative to pre-dMCAo and relative to 60min post dMCAo (i.e. post-ischemia but pre-treatment), respectively. A significant main effect of Time ($F_{(1.077,16.16)}$ =7.727, P =0.0120) was found for RBC velocity when normalized to pre dMCAo values. However, no main effect of Treatment ($F_{(1,15)}$ =1.216, P =0.2875) or significant Time X Treatment interactions ($F_{(9,135)}$ =0.8977, P =0.5293) were detected for measures of RBC whether data was normalized to pre-dMCAo value or to velocity 60 min post dMCAo.

Mean RBC flux for arteriole segments downstream of collateral anastomoses in RIPerC treated and control rats are shown in Figure 4-5(c). RBC flux is a critical measure of perfusion, as it is proportional to the oxygen and nutrient carrying capacities of a blood vessel.[75,182] Analysis of RBC flux between groups revealed a significant main effect of Time ($F_{(1.079,16.18)}$ =12.35, P=0.0024), but no effect of Treatment and Age x Time interaction ($F_{(9,135)}$ =1.748, P=0.0841) when normalized to pre-dMCAo value. When normalized to post-dMCAo but pretreatment values (i.e. 60 min post-dMCAo), however, a significant main effect of RIPerC Treatment on RBC flux was found ($F_{(1,15)}$ =4.59, P =0.049). Thus, when normalized to flux after dMCAo but prior to treatment, in order to better isolate a change in flux due to treatment itself, TPLSM data confirmed that RIPerC treatment increased RBC flux through collateral vessels, primarily due to increased diameter of the MCA segments due to RIPerC treatment.

4.3.3. Early Ischemic Damage

All rats were euthanized at 6 h post dMCAo and stained with TTC to demarcate regions with early ischemic damage. As illustrated in Figure 4-5, a significantly smaller volume of early ischemic damage was found in RIPerC rats relative to sham treated rats (P =0.0241).

4.4. Discussion:

In Chapter 2, we demonstrated that pial collateral blood flow collapsed over time in aged rats after dMCAo. This collapse of pial collateral blood flow exacerbates the insufficient perfusion of the penumbra and leads to greater ischemic damage. Clinically, collateral therapeutics that can preserve collateral flow may be able "freeze" penumbra before recanalization via thrombolysis or thrombectomy and thereby reduce stroke severity. Maintaining collateral flow prior to recanalization may be particularly important in aging populations with impaired collateral dynamics

Several reports suggest that RIPerC can enhance cerebral blood flow in preclinical models of stroke. While they did not directly assess cerebral collateral flow, Hoda et al. studied CBF after RIPerC using laser Doppler flowmetry and LSCI in an autologus thromboembolic MCA occlusion mouse model [139,140,223]. These studies demonstrated that RIPerC is effective not only alone but also in combination with i.v. r-tPA in enhancing cerebral blood flow near ischemic areas in young male, ovarectomized females and aged male mice (12 months old) [139,140,146,147,223]. In agreement with this, the data in Chapter 3 demonstrated with LSCI and TPLSM that RIPerC could augment pial collateral flow by preventing collateral collapse in young rats after dMCAo.

According to Stroke Therapy Academic Industry Roundtable (STAIR) recommendations, which were established in an attempt to improve translation of preclinical stroke therapies, preclinical studies of therapies like RIPerC should be performed in aged animals that better approximate human stroke patients [246]. While the data in Chapter 3 show collateral flow enhancement in young adult rats, to date no *in vivo* studies have directly investigated the effects on cerebral blood flow through pial collaterals after RIPerC in aged rats. Here, the combination of TPLSM and LSCI in aged rats provided both wide field assessment of penumbral blood flow as well as precise quantification of the diameter of pial vessels and the direction and velocity of blood flow within individual collateral segments [26].

The relative blood flow measured with LSCI (Figure 4-2) in the wide field imaging suggested enhancement of blood flow in RIPerC treated rats, but the data were not definitive when normalized to post-stroke values. Using 2PLSM (Fig.4-3 & Fig.4-4), we found that pial collaterals of aged control rats continuously constrict after dMCAo, reaching approximately 83% of prestroke baseline diameter by 4.5h after stroke onset. However, this collateral failure was not as severe in the RIPerC treated group, as the diameter of pial collaterals in RIPerC treated group remained above 93% of pre stroke baseline measurement throughout imaging. When diameter measurements of post RIPerC (sham) treatment are normalized to measurement immediately prior to treatment (60min post-stroke), a significant effect of treatment on preventing diameter collapse in RIPerC group was observed. Post hoc analysis demonstrated a significant difference between treatment groups at 90min post and all time points after 150 min post dMCAo onset. RIPerC maintained pial diameter was approximately 97% of pre-treatment measurement at the final imaging session 4.5h hour post stroke. No significant main effect of RIPerC treatment on RBC velocity was observed. However, a significant main effect of Treatment on RBC flux, the overall measurement of blood flow through each vessel segment, was confirmed when flux values were normalized to post-dMCAo values. This greater flow of RBCs per second through individual pial collaterals from the ACA that supply penumbral regions induced by dMCAo was associated with significantly smaller volumes of early ischemic damage at 6 hour post dMCAo. Thus, our findings of RIPerC in aged rats provide further scientific rationale for exploring translation of RIPerC treatment from bench to bedside. The first randomized trial to examine adjunctive neuroprotective effects of RIPerC to r-tPA treatment in acute stroke patients in the prehospital setting has been conducted in Denmark [135,137,144]. It found the approach was safe and no intolerable discomfort or adverse events caused by RIPerC were reported [144,146]. After adjustment for baseline severity of hypo-perfusion, there was evidence of tissue protection by RIPerC in post hoc MRI data analysis using a voxel based logistic regression method [144–146]. Thus, RIPerC is a promising to be an adjunctive therapy to spare functionally intact brain tissues before thrombolysis and thrombectomy treatment.

There remain several issues that need to be addressed before RIPerC can be optimally translated to clinical settings. First, while most preclinical studies of RIPerC including ours are performed on rodent hind limbs via femoral ligation [135,138–140,142,223–225,247], such an invasive RIPerC technique is not practical in clinical settings owing to increased complexity and risk of complications [248,249]. Therefore, clinical studies generally involve upper limb ischemia via inflation of a blood pressure cuff [137,144]. Blood pressure cuff inflation/deflation instead of BFO should therefore be used in future collateral flow studies to simulate clinical application. Secondly, the time of application of RIPerC, the number of RIPerC cycles, and the ischemic duration in each cycle of RIPerC vary between different published papers [135,138–140,142,223–225,247]. To allow sufficient time for TPLSM imaging scanning and processing to quantify individual pial collateral during RIPerC, 15 min occlusion / reperfusion periods were used in our study. However, such long duration of limb ischemia may not the best practice in the clinical situation and could increase risk of limb necrosis. While no consensus about the most appropriate RIRerC protocol exist in either preclinical or clinical study, four cycles of 5 min of ischemia followed by 5 min of reperfusion are commonly used in humans [146]. Differences in the hemodynamic and neuroprotective effects of different paradigms of remote ischemia need to be systematically assessed not only in preclinical studies but also on clinical trials [26]. Thirdly, pial collateral collapse prevention by RIPerC on both young adult and aged rats is promising but the signal pathway underlying this effect is still unknown and the mechanisms remain to be determined. It is known that nitric oxide plays important role in regulating vascular tone, causing vasodilation [250]. Nitric oxide has been shown to be associated with remote ischemic conditioning (RIC) protection in liver and cardio ischemia [251–253]. Notably, mice treated with remote ischemic pre conditioning have elevated microvascular blood flow in the liver and are protected from liver ischemia. Nitrite and nitrate are considered as stable physiological reservoirs and storage pools for nitric oxide [254–256], and treated mice have elevated nitrite and nitrate levels in the blood and liver. Moreover, liver protection was abolished with nitric oxide scavengers and in eNOS knockouts models

[147,251,252]. In a study of remote ischemic pre conditioning for cardio protection, Rassaf et al [253] reported that remote ischemic preconditioning RIC could increase nitrite level not only in plasma but also in the heart of mice. Again, cardio protection with remote ischemic pre conditioning was lost in eNOS knockouts mice. Notably, plasma nitrite levels also increase after remote ischemic conditioning in healthy human volunteers [147,253]. However, the evidence for the role of nitric oxide in protection due to remote ischemic conditioning are mostly acquired from remote ischemic preconditioning and healthy remote ischemic conditioning studies. There remains a lack of sufficient and strong published evidence to support the role of nitric oxide in RIPerC treatment induced cerebral blood flow reservation. However, Hoda et al. found that the mRNA expression of endothelial nitric oxide synthase at the site of limb conditioning resulted in a 10 folds enhancement in blood vessels, leading to increased concentrations of nitric oxide in plasma [257]. Based on these findings, it is reasonable to hypothesize that nitric oxide maybe also serve as mediator in preventing collateral collapse in our RIPerC study. However, more experiments are needed to prove this hypothesis. Nitric oxide scavengers and eNOS knockout models could be used in the future with in vivo imaging to evaluate effect RIPerC treatment on pial collaterals.

In conclusion, data in this Chapter showed that the neuroprotective effect of RIPerC may occur at least in part due to the prevention of pial collateral collapse in aged rats. Using TPLSM individual vessel imaging, we showed that RIPerC enhanced penumbral microcirculation by maintaining retrograde blood flow from ACA to distal MCA segments during MCA occlusion. This confirmation of the collateral therapeutic effects of RIPerC have broad implications for its use as a stand-alone or adjuvant acute stroke therapy.

Figures

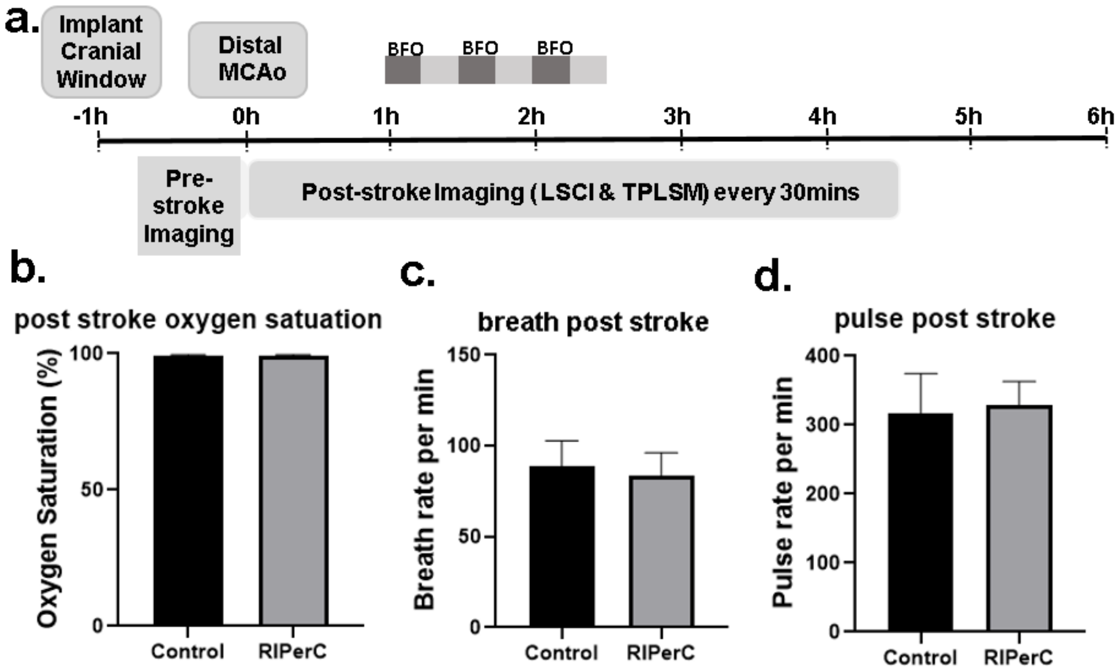

Figure 4- 1 Experimental design & Physiological parameters of aged RIPerC and aged sham treatment rats during imaging of post dMCAo

Experimental timeline (**a**). Physiological parameters of RIPerC and Sham treatment rats during imaging of post dMCAo (**b-d**).

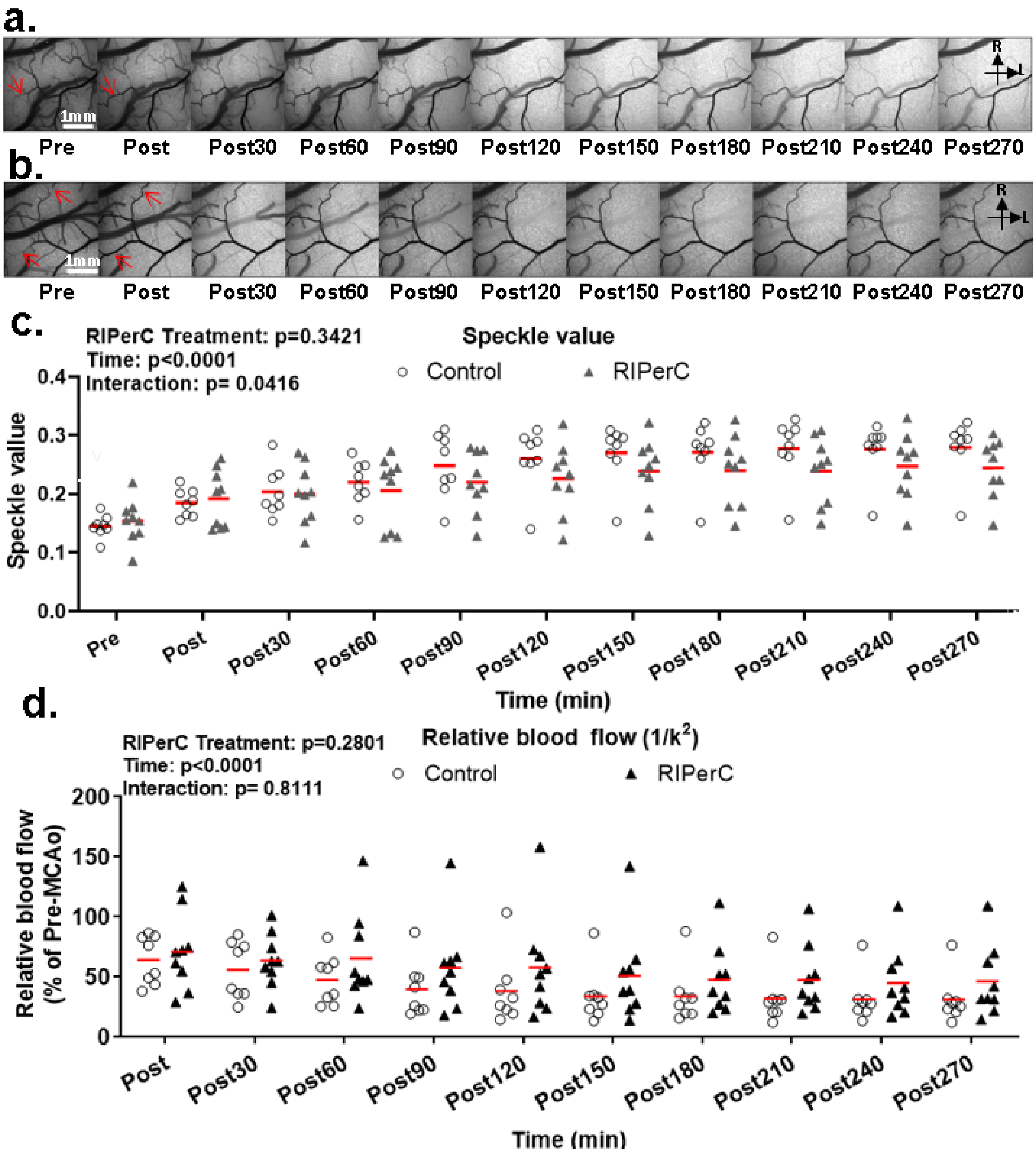

Figure 4- 2 Representative LSCI derived image sequences showing flow on the cortical surface of aged RIPerC and aged sham treatment rats & speckle contrast (*K*) and relatively blood flow ($1/K^2$) for aged RIPerC and aged sham treatment rats

Representative LSCI derived image sequences of speckle contrast showing flow on the cortical surface before and after dMCAo. Images showing flow changes over 270min (4.5h) post are illustrated for control (**a**) and RIPerC rats (**b**). Immediately after dMCAo, robust anastomotic connections between distal segments of the ACA and MCA were observed in both groups. LSCI revealed an increase of speckle contrast value (c) and reducing relative blood flow (d) after dMCAo in both control and RIPerC treated group. Mean speckle contrast values (*K*) are shown in (**c**). Two-way ANOVA revealed a significant main effect of Time ($F_{(10,150)}$ =35.67, P<0.0001), as well as a significant Time X Treatment interaction (($F_{(10,150)}$ =1.959, P =0.0416); Treatment, n.s., $F_{(1,15)}$ =0.9625, P =0.3421). A more proportional measure of blood flow can be attained by determining the inverse square of the speckle contrast values. Relative blood flow ($1/K^2$) normalized to pre dMCAo values is shown in (**d**). Flow in both groups dropped gradually to less than 50% and remained low throughout imaging. Again, a two-way ANOVA revealed a significant main effect of Time ($F_{(9,135)}$ =13.42, P <0.0001) on relative blood flow ($1/K^2$), but there was no statistically significant main effect of Treatment ($F_{(1,15)}$ =1.256, P =0.2801) and no interaction of Time and Treatment ($F_{(9,135)}$ =0.5807, P =0.8111).

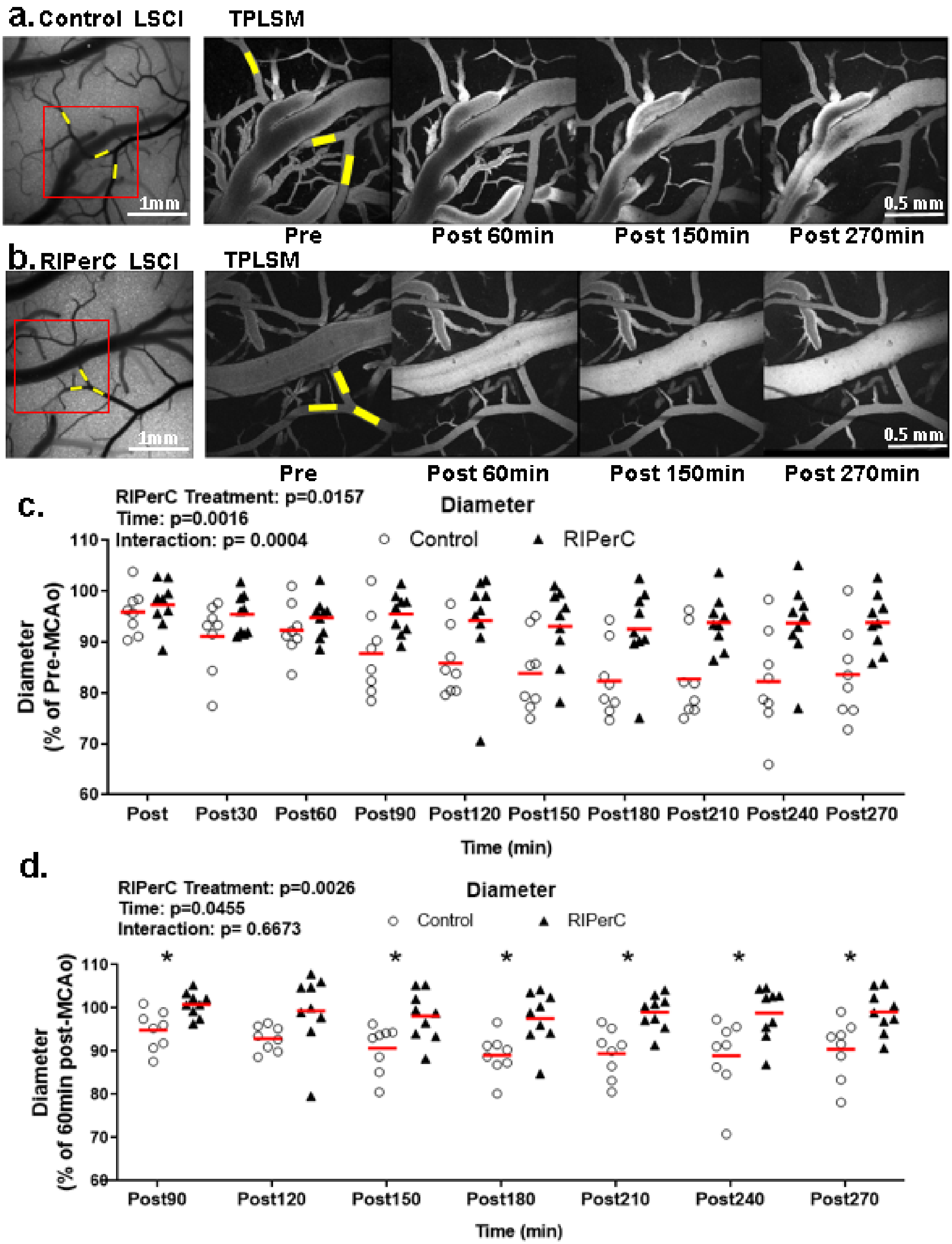

Figure 4- 3 Representative TPLSM derived image of aged RIPerC and aged sham treatment rats & Quantification of mean diameter in aged RIPerC and aged sham treatment rats relative to pre-dMCAo and pre-treatment (60min post dMCAo)

Representative images of control rat (a) and RIPerC rat (b). Panels of TPLSM images on the right show maximum intensity projections from region demarcated with rectangular box in LSCI images. Scale bar, 1 mm.

(**c**) shows pial diameter data normalized to pre dMCAo values. Two-way ANOVA demonstrated a significant main effect of Time ($F_{(1.484,\ 22.27)}$ =10.28, P=0.0016) and Treatment ($F_{(1,15)}$ =7.416, P=0.0157) on pial arteriole diameter, as well as a significant Time X Treatment interaction ($F_{(9,135)}$ =3.696, P =0.0004). However, post hoc comparisons did not identify any significant differences between treatment groups at individual time-points. To compensate for potential variation in blood flow after dMCAo but prior to treatment, (**d**) shows diameters normalized to values measured 60 minutes after ischemic onset. Two-Way ANOVA revealed a significant main effect of Treatment ($F_{(1,15)}$ =13.05, P =0.0026) and Time ($F_{(3,45)}$ =2.894, P=0.0455), but no Time X Treatment interaction ($F_{(6,90)}$=0.6786, P=0.6673). Holm-Sidak's post hoc comparisons revealed that RIPerC-treated rats had significantly larger diameters ($P < 0.05$) at all-time points after the initiation of the first BFO clamp, with the exception of 120 min post dMCAo.

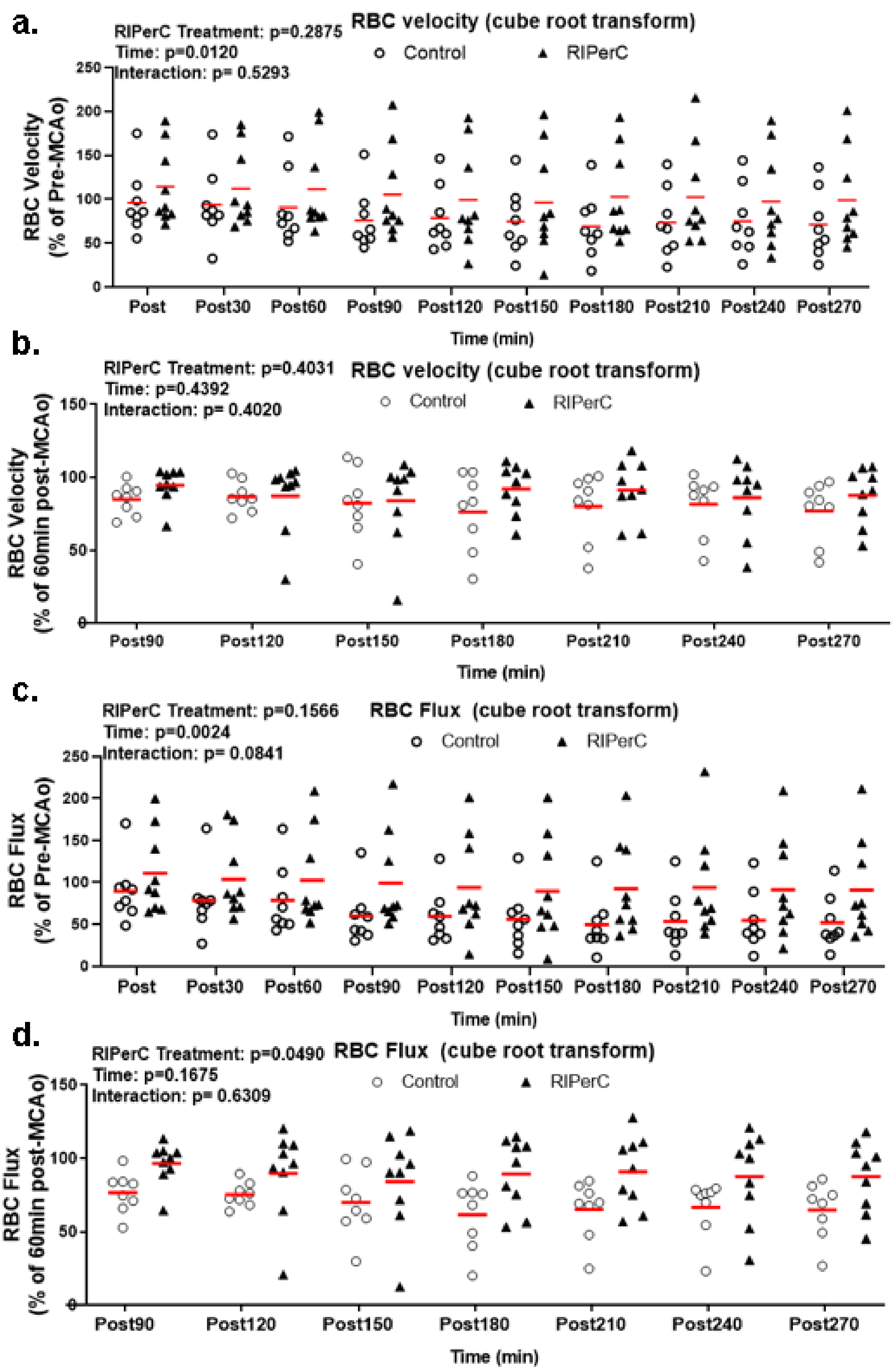

Figure 4- 4. Quantification of mean RBC velocity, and RBC flux in aged RIPerC and aged sham treatment rats relative to pre-dMCAo and pre-treatment (60min

post dMCAo). (**a-b**) show mean changes in red blood cell (RBC) velocity relative to pre-dMCAo and relative to 60min post dMCAo (i.e. post-ischemia but pre-treatment), respectively. A significant main effect of Time ($F_{(1.077,16.16)}$ =7.727, P =0.0120) was found for RBC velocity when normalized to pre dMCAo values. However, no main effect of Treatment ($F_{(1,15)}$ =1.216, P =0.2875) or significant Time X Treatment interactions ($F_{(9,135)}$ =0.8977, P =0.5293) were detected for measures of RBC whether data was normalized to pre-dMCAo value or to velocity 60 min post dMCAo. Mean RBC flux for arteriole segments downstream of collateral anastomoses in RIPerC treated and control rats are shown in (**c**). Analysis of RBC flux between groups revealed a significant main effect of Time ($F_{(1.079,16.18)}$ =12.35, P=0.0024), but no effect of Treatment and Age x Time interaction ($F_{(9,135)}$ =1.748, P=0.0841) when normalized to pre-dMCAo value. When normalized to post-dMCAo but pretreatment values (i.e. 60 min post-dMCAo), however, a significant main effect of RIPerC Treatment on RBC flux was found ($F_{(1,15)}$ =4.59, P =0.049). Thus, when normalized to flux after dMCAo but prior to treatment, in order to better isolate a change in flux due to treatment itself, TPLSM data confirmed that RIPerC treatment increased RBC flux through collateral vessels, primarily due to increased diameter of the MCA segments due to RIPerC treatment.

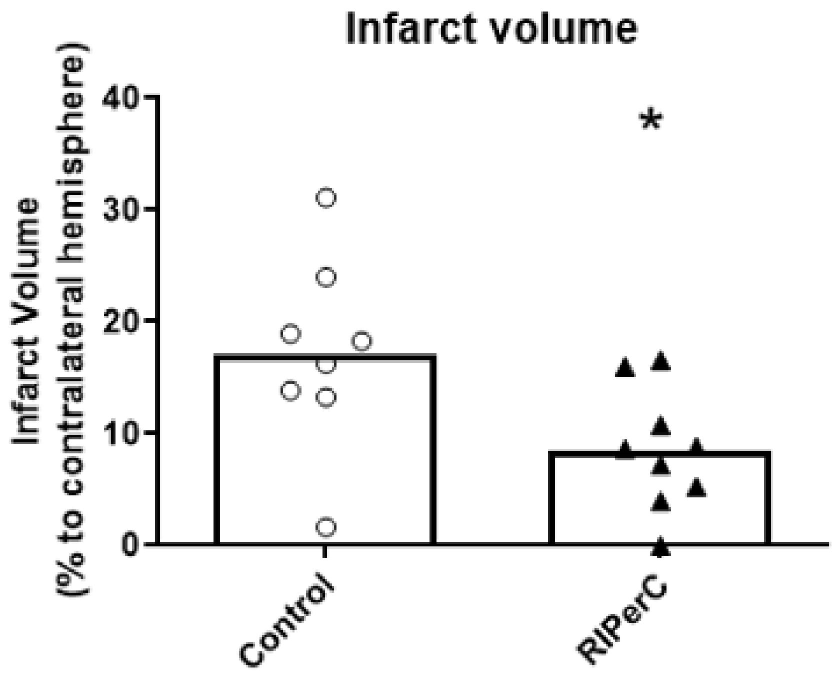

Figure 4- 5 Early ischemic damage measurements

A significantly larger volume of early ischemic damage was found in control rats relative to RIPerC treated rats (P =0.0241). Means of the infarct volumes are calculated as percent of their corresponding contralateral sides.

Chapter 5

Acute and sustained milrinone therapy as a collateral therapeutic for ischemic stroke

5.1. Introduction

Ischemic stroke is a devastating cerebral vascular disease that occurs when arteries supplying the the brain are obstructed. Cerebral collaterals are alternative vascular channels in the cerebral circulation which can provide blood flow to hypo-perfused brain tissues when principal vascular routes fail [11–14]. Therefore, collateral circulation plays an important role in determining the degree of ischemia in the penumbra. Cerebral collaterals can be classified as primary or secondary collaterals. The circle of Willis, referred as the primary collaterals, allows blood flow exchange between anterior and posterior circulation and between hemispheres [15]. Pial collaterals, also known as leptomeningeal collaterals, are considered as secondary collaterals [16]. Pial collaterals are anastomotic connections located on the cortical surface which connect distal branches of adjacent arterial network [16,17]. When artery distal to circle of Willis, like MCA, is obstructed, pial collaterals become patent and provide compensatory blood flow from ACA and/or PCA to the ischemic penumbra of MCA [16]. Therefore, strategies that can augment collaterals blood flow to reduce expansion of the infarct core are attractive in ischemic stroke therapy [145].

Over the last several decades, numerous studies have examined the role of phosphodiesterases and their inhibitors in a number of cardiovascular and cerebrovascular disorders. The phosphodiesterases (PDE) are a family of enzymes containing 11 subgroups with more than 30 different isozymes of enzymes [258,259]. This family of enzymes is responsible for the degradation of cyclic nucleotides [260–262]. Cyclic nucleotides, including adenosine 3, 5-cyclic monophosphate (cAMP) and cyclic guanosine monophosphate (cGMP) have long been recognized as intracellular second messengers [263,264]. Cyclic nucleotides are produced by enzymes located on the interior to the cell membrane in response to extracellular signals [265,266]. Cyclic nucleotides interact with molecules in the cytosol and/or nucleus, participating in a variety of intracellular biological actions, including receptor-effector coupling, protein-kinase cascades, cell signal transduction and function regulation [267]. PDEs hydrolyze the 3'phosphoester bond of cyclic nucleotides thereby terminating their signaling [261].

Phosphodiesterase 3 (PDE3) is one of the most pivotal AMP degrading phosphodiesterases in arterial tissues [268]. PDE3 is primarily expressed in vascular smooth muscle cells and cardiac myocytes, and plays a significant role in modulating vascular smooth muscle cell proliferation and vascular tone regulation and cardiac contractility [269,270]. Milrinone is a potent selective PDE3 inhibitor and can inhibit cAMP specific PDE3 in both cardiac myocytes and vascular smooth muscle cells [153]. Milrinone has been shown to be safe and is widely administered to treat patients with acute and chronic heart failure due to its inotropic and vasodilatory effects, leading to cardiac contractility enhancement and systemic vascular resistance reduction, respectively [159,271–274]. The inotropic effect of milrinone is largely attribute to PDE3 inhibition, leading to intracellular cyclic AMP accumulation and an increase of cyclic AMP dependent protein kinase A (PKA). PKA not only phosphorylates the myofilament proteins which can promote action of myosin and actin, but also phosphorylates calcium channels causing trans-sarcolemmal calcium influx. Both of these lead to cardiac contractility enhancement and cardiac output augmentation [154–156]. The vasodilatation effect of milrinone is mediated by increasing cAMP in vascular smooth muscle which stimulates calcium uptake into the sarcoplasmic reticulum, reducing the affinity of troponin C to calcium available for contraction, and thus relaxing vascular tone [272,275].

Based on PDE3 localization in cerebral arteries smooth muscle cells [272,273], PDE3 inhibitors may result in potent cerebral vasodilatory effects with augmentation of cardiac output (inotropic effect) and may thereby drive greater cerebral blood flow. Drexler et al [276] examined the hemodynamics and cerebral vascular profile following intravenous milrinone in normal conscious rats. Radioactive microspheres were used for blood flow measurement. Intravenous milrinone with dose of 3ug/kg/min for 15mins increased cerebral blood flow significantly (25% enhancement relative to before infusion) without affecting heart rate, blood pressure or systemic vascular resistance. When the dose of milrinone were raised to 6ug/kg/min for another 15mins on the same rat, significant cerebral blood flow enhancement was still observed (40% enhancement relative to before infusion), but was accompanied with a systemic vascular resistance reduction. Iida et al [277] used rabbits to study the effect of milrinone on cerebral microcirculation. A closed transparent cranial window was used for observation of cerebral pial circulation. The diameters of pial arterioles and pial venules were measured with video micrometer. Three different dose of intravenous milrinone

(0.5, 5, 20ug/kg/min) were used. A dose dependent effects of intravenous milrinone on the dilation of pial arterioles and venules of normal rabbits was observed. To examine whether blood brain barrier disruption, a pathophysiological process engaged in many cerebral vascular disease, could change the effect of i.v. milrinone on pial vessels, a solution of 25% mannitol was infused at a rate sufficient to disrupt BBB without causing serious immediate neurotoxicity. The dose of 0.5 and 5 ug/kg/min milrinone still effectively dilated pial arterioles. In a clinical prospective study, Sulek et al [278] reported that intravenous milrinone could increase middle cerebral artery blood flow velocity of patients after cardiopulmonary bypass surgery.

The efficacy of milrinone in treating cerebral vasospasm after subarachnoid hemorrhage has also been investigated. In a study by Nishiguchi et al [272], milrinone was given intra-arterially via the vertebral artery 7 days after subarachnoid hemorrhage in a canine model. Angiography showed that milrinone could effectively relax vasospasm in basilar arteries. The dogs were euthanized after angiography and complementary histologic experiments were performed. Nishiguchi et al [272] found that milrinone increased cAMP within the vessel wall and reduced corrugation of the elastic lamina and decreased vessel thickness. Since late 1990s, milrinone has been used in different hospitals across the world as a therapeutic option for SAH patients to serve as a vasorelaxant, which can prevent or treat the delay cerebral ischemia that can follow SAH [273,275,279–284]. In 2012, it was reported that milrinone had become the second most common drug used to treat symptomatic cerebral vasospasm after SAH in a European survey [285]. However, no randomized controlled trial of milrinone has been conducted so far and the route of milrinone administration, the timing, dose as well as co-interventions still varied among different reports [273,275,279–284].

The effects of milrinone on pial vessels dilation and cerebral blood flow enhancement indicates it may be useful for ischemic stroke as well. To provide preclinical evidence demonstrating the treatment effect of milrinone in cerebral ischemic stroke, two set of experiments were performed. Experiment I used laser speckle contrast imaging (LSCI) to define whether acute systemic collateral pharmacotherapy with milrinone lactate is effective for augmenting pial collateral flow and the most effective dose. Experiment II assessed whether supplementing acute milrinone infusion with continuous subacute administration after distal MCAo has a significant effect on physiological parameters (blood pressure, heart rate, activity) and assessed if this prolonged milrinone lactate treatment could reduce ischemic stroke damage.

5.2. Materials and Methods:

Male Sprague–Dawley rats (4-8 months of age, 400-650g of weight) were used. Prior to experimental procedures, animals were housed in pairs on a 12-h day/night cycle and had access to food and water ad libitum. Procedures conformed to guidelines established by the Canadian Council on Animal Care and were approved by the Health Sciences Animal Care and Use Committee at the University of Alberta. Procedures and results reporting is consistent with the ARRIVE guidelines [168].

5.2.1. Experiment I

The experimental timeline is illustrated in Figure 5-1(a) LSCI was used to measure pial collateral blood flow during and post-acute ischemic stroke. A lateral tail vein was catheterized (for intravenous infusion, see 5.2.1.2). Blood pressure monitoring was performed via a catheter in the ventral tail artery (5.2.1.2). A thin cranial window was made as described in §5.2.1.3. Baseline LSCI (5.2.1.5) was performed to define cerebral blood flow prior to stroke. Stroke was generated using the permanent distal MCAo model(5.2.1.4) [26,170,286]. Commercial milrinone lactate solution (1mg/ml) purchased from Fresenius Kabi Canada Ltd was used and diluted with normal saline to get different doses (3ug/kg/min, 6ug/kg/min, and 12ug/kg/min) of infusion solution. To determine the most effective dose of milrinone during MCAo, rats were divided into 4 groups (control, n=12; 3ug/kg/min, n=9; 6ug/kg/min, n=9; 12ug/kg/min, n=9;), each receiving a 60-minute infusion of milrinone lactate (or vehicle control) via the femoral vein starting 1h after ischemic onset.

5.2.1.1. Anesthesia and Monitoring

Light anesthesia was induced using an induction chamber with 4–5% isoflurane (in 70% N_2 and 30% O_2) prior to intraperitoneal injections of urethane (i. p. 1.25 g/kg, divided into four doses delivered at 30-min intervals). Isoflurane was discontinued after the first urethane injection, and rats remained anaesthetized until euthanasia. During all surgery and imaging, temperature was maintained at 36.5–37.5C with a thermostatically controlled warming pad and heart rate, oxygen saturation, and breath rate were monitored using a pulse oximeter (MouseOx, STARR Life Sciences).

5.2.1.2. Tail Artery and Tail Vein Cannulation

The tail vein and the ventral tail artery were cannulated with a silicone catheter for drug infusion and blood pressure monitoring, respectively (tail artery catheters contained 500 IU/ml heparinized saline).

5.2.1.3. Cranial Window

LSCI was performed through a cranial window using a thin skull preparation. A midline incision was made on the scalp to expose the surface of the skull. A 5x5 mm section of the skull over the distal regions of the right MCA territory was thinned until translucent using a dental drill (frequently flushing with saline to dissipate heat). The outer skull layer and subjacent spongy bone were cleaned and smoothed by round scalpel, allowing surface vessels to be visualized through the remaining thin layer of bone. A thin layer of 1.3% low melt agarose was applied to the window and sealed with a glass coverslip.

5.2.1.4. dMCAo

Cerebral ischemia was induced by bilateral common carotid artery (CCA) ligation in addition with distal MCA ligation [26,170,286]. Distal MCA ligation and imaging protocols were performed by different individuals, and surgeons inducing ischemia were blind to the experimental group for each rat. CCAs were accessed through ventral midline cervical incisions and ligated with 4–0 prolene sutures below the carotid bifurcation. A temporal incision was then made and the right temporalis muscle was gently separated from the bone. A burr hole of 1.5 mm in diameter was made through the squamosal bone, the dura was removed, and the cortical MCA was visualized. The exposed distal MCA was isolated with a loose square knot by atraumatic 9–0 prolene suture above the rhinal fissure before stroke. After pre-stroke imaging, the knot was ligated to induce permanent dMCAo. All the incisions were sewed using surgical suture.

5.2.1.5. LSCI

LSCI measures real time changes in cerebral blood flow with high spatial and temporal resolution over a wide field of view [171–173]. To collect LSCI data, rats were secured in ear bars on a custom-built stereotaxic plate under a Leica SP5 MP laser scanning microscope. A Thorlabs LDM 785S laser (20 mW, wavelength of 785 nm) was used to illuminate the rat cortex at approximately 30 ° incidence. Stacks of 101 sequential images (1024 × 1024 pixels) were acquired at 20 Hz (5 ms exposure time) during each imaging session. All processing and analysis of laser speckle images were performed using ImageJ software (NIH) by a blinded experimenter. Maps of speckle contrast were made from the collected images of raw speckling by determining the speckle contrast factor K for each pixel in an image. K is calculated as the ratio of the standard deviation to the mean intensity ($K = \sigma_s/I$) in a small (5 × 5 pixels) region of the speckle image.[171–173] Plots of K show maps of blood flow with darker vessels illustrating faster blood flow velocity. [174,175] For quantification of penumbral flow, K was measured in a contiguous

ROI consisting of an 650×650 pixel square positioned to include the distal MCA and ACA segments. Because cerebral blood flow (CBF) velocity in selected region of interest was inversely proportional to the square of speckle contrast value K.[176,177]

$$v \propto \frac{1}{K^2}$$

Therefore, $1/K^2$ is also used to illustrate CBF velocity change in LSCI figures.[174,178]

5.2.1.6. Triphenyl Tetrazolium Chloride Staining

Rats in the acute imaging study were euthanized 3 h after induction of the MCAo. The brains were rapidly removed and sliced into seven coronal, 2 mm sections using a brain matrix, then incubated in 2% 2,3,5-triphenyltetrazolium chloride (TTC) solution at 37℃ for assessment of mitochondrial dehydrogenase activity. However, owing to the early euthanasia following ischemic onset, no reliable tissue damage was observed in any treatment group and analyses of ischemic damage could not be performed.

5.2.2. Experiment II

In the second experiment, to assess whether prolonged milrinone treatment can reduce ischemic stroke damage, rats were randomly divided into 2 groups, a milrinone lactate treatment group (n=12) and vehicle treatment group (n=12). 5 rats from each group were used to determine milrinone's effect on physiological parameters. Experimental timelines are defined in Figure 5-1(b). Isoflurane anesthesia was used during surgery and infusion (5.2.2.1). Briefly, 5 days before inducing stroke, rats were implanted with telemetry probe (5.2.2.2) to monitor physiology status (activity, BP, HR).

After inducing stroke (5.2.2.3), milrinone lactate was given at a dose of 6ug/kg/min for 60 mins through tail vein infusion (5.2.2.4). An Alzet osmotic mini pump with a dose of 3ug/kg/min (5.2.2.5) was implanted subcutaneously (5.2.2.6) for long term subcutaneous milrinone administration. After intravenous infusion, rats were sent back to cage for continuous monitoring of physiology parameters for 5 days (5.2.2.7) via telemetry. Rats were euthanized and brains were stained with cresyl violect to identify infarct size on the 5th day post stroke.

5.2.2.1. Anesthesia and Monitoring

3% isoflurane (in 70% N_2, 30 %O_2) was used for anesthesia induction and 2% isoflurane for maintenance during surgery. Rectal temperature was maintained at 36.5 C during surgery with use of a temperature regulated heating pad.

5.2.2.2. Telemetry Probe Implantation and Monitoring

The battery operated telemetry probe (TA11PA-C20) probes were calibrated using the calibrating data provided by the manufacturer for each probe. The zero levels were checked before each implantation. On the day before surgery, telemetry probes were sterilized by an immersion soak in 2% glutaraldehyde overnight. The probe was implanted at the left groin area with its tip inserted into the left femoral artery. After implantation, the telemetry probes were magnetically activated to check for proper function, then turned off until the day prior t stroke surgery when the probes were activated again. After surgery, rats were housed individually in cages at room temperature and allowed free access to food and water. The activity, blood pressure and heart rate of rats were continuously recorded real time using biotelemetry system for 24 hours and served as baseline. Data from the probe were transmitted via radio frequency signals to receiver placed below cages every 30 seconds. The activity recorded by the probe does not indicate an exact distance rats travelled but provides a relative measure based on signal strength [287]. Simple head movements, such as grooming and chewing, are not recorded by the system as activity. The Dataquest ART system (Data Science International) counted whole body movement as activity which guaranteed the accuracy of activity recording [287]. The telemetry method is precise and has the advantage of being non-stressful as rats are monitored in their home cage without extensive human interaction [288].

5.2.2.3. dMCAo

Permanent distal MCAO model (bilateral carotid arteries occlusion in conjunction with right middle cerebral artery ligation) was used for inducing stroke [26,170,286]. Common carotid arteries (CCAs) were accessed through ventral midline cervical incisions and ligated with 4-0 prolene sutures below the carotid bifurcation. To access to right middle cerebral artery (rMCA), a scalp incision was done at the area between the right external auditory canal and the right eye. After the scalp was opened, the right temporalis muscle was gently separated and retracted from the bone. A burr hole of 1.5 mm in diameter were drilled through the squamosal bone. After removing the bone piece carefully, a small syringe needle was used to make a small incision and remove the dura mater for visual inspection of rMCA. The distal rMCA was ligated with a square knot by atraumatic 9-0 prolene suture above the rhinal fissure. All the incisions were sewed using surgical suture.

5.2.2.4. Infusion

For milrinone lactate treatment group rats, one hour after inducing stroke on rats, a loading dose of milrinone lactate dissolved in 0.6 ml 0.9% saline was administered by intravenous infusion (6ug/kg/min) through a catheter inserted into the tail vein over a 60 minute period. Rats in sham treatment group were given 0.6 ml normal saline infusion.

5.2.2.5. Milrinone Lactate Solution

In order to give a rat weighted 0.6kg milrinone lactate administration with a dose of 3ug/kg/min for 5 days, 21.6mg of milrinone lactate should be dissolved and be filled into the 2ml Alzet osmotic mini pump. Commercial milrinone lactate solution used in Experiment I could not reach such a concentration, therefore milrinone lactate powder bought from ARK Pharm, Inc. was used for preparing solution to fill in Alzet osmotic mini pump. Based on the weight of rats (0.45-0.6kg), 16-22mg of milrinone lactate were dissolved in to 0.2ml DMSO, then diluted with 1.8ml PEG 300 to prepare the solution for Alzet osmotic mini pump.

5.2.2.6. Alzet Mini Pumps Implantation

Chronic administration of the milrinone was performed by using Alzet osmotic mini pumps (model 2ML1, 2ml, 10 ul/h) implanted subcutaneously on the back. Alzet mini pumps were filled and primed by incubation at 37°C for overnight in a tube containing sterile saline 2 day before surgery. The Alzet mini pump implantation surgery was started while the rats received tail vein infusion. Briefly, the incision area (mid-scapular) was shaved and sterilized and a 1.5cm horizontal incision was made on skin. After that, a hemostat were inserted into the incision to create a pocket for pump by spreading subcutaneous tissues. The pump was inserted into the pocket then the wound was closed with sutures. The chronic daily rate of milrinone was 3ug/kg/min for 5 days. For the sham treatment group, Alzet osmotic mini pumps were filled with the vehicle without milrinone lactate (1.8ml PEG 300+0.2ml DMSO).

5.2.2.7. Post Stroke Monitoring and Infarction Measurement

After recovery from anesthesia, rats were sent back to home cage housed individually, the telemetry probes were turned on, and activity, blood pressure and heart rate were monitored for 5 days. On the 5th day of Experiment II, animals were euthanized and transcardially perfused with 0.9% saline, followed by 4% paraformaldehyde. Forty micron thick sections were cut throughout the entire forebrain and stained with cresyl violet for assessment of infarct size. Slices were scanned and the amount of infarct damage was measured using ImageJ software (NIH).

5.2.3. Statistics

Graphpad Prism (GraphPad software, San Diego, CA, US) was used for all statistical analyses. Two-way analysis of variance (ANOVA) with repeated measures were used to compare effects of milrinone lactate or sham treatment on relative blood flow with LSCI measures. Post hoc comparisons were performed using Holm-Sidak's multiple comparisons test. Volumes of ischemic tissue damage (% hemisphere) and physiological parameters (blood pressure, heart rate and activity) were compared using an unpaired Student's t-test. Values are expressed as mean ± S.E.M.

5.3. Results:

5.3.1. Experiment I

5.3.1.1. LSCI Reveals Increased Penumbral Blood Flow in Milrinone Treated Rats relative to Vehicle Control Rats

Representative LSCI derived maps of speckle contrast showing flow changes over 3 hours post stroke for sham and milrinone treated rats are shown in Figure 5-2(a). Qualitatively, LSCI derived maps of blood flow suggested increased blood flow relative to vehicle controls after infusion of milrinone (note a consistent increase in brightness in saline controls that is not apparent in milrinone treated animals). Notably, there was no significant effect of milrinone treatment on systemic blood pressure ($F_{(3,35)}$ =0.9331, P= 0.4350) (Figure 5-2(b)). Relative blood flow normalized to values before dMCAO and to values measured 60 minutes after dMCAO (to control for different levels of ischemia between rats) are illustrated for sham controls and animals treated with three doses of milrinone are illustrated in Figure 5-3(a) and 3(b), respectively. In both cases, two-way ANOVA did not identify a significant main effect of Time (Normalized to pre-dMCAo: $F_{(3,105)}$ =0.2925, P= 0.8307; Normalized to 60 minutes after dMCAo: $F_{(2,70)}$ =0.6550, P= 0.5226) or Treatment (Normalized to pre-dMCAo: $F_{(9,105)}$ =1.702, P= 0.0976; Normalized to 60 minutes after dMCAo: $F_{(6,70)}$ =0.7726, P= 0.5941), and no significant interaction of Time and Treatment (Normalized to pre-dMCAo: $F_{(3,35)}$ =0.5461, P= 0.6540; Normalized to 60 minutes after dMCAo:$F_{(3,35)}$ =2.210, P= 0.1153). However, statistical analysis of milrinone groups only (removing vehicle controls) via two-way ANOVA did not identify a main effect of milrinone dose (Normalized to pre-dMCAo: $F_{(2,24)}$ =0.8340, P= 0.4465; Normalized to 60 minutes after dMCAo: $F_{(2,24)}$ =0.4107, P= 0.6678) or a Dose x Time interaction (Normalized to pre-dMCAo: $F_{(6,72)}$ =0.3975, P= 0.8783; Normalized to 60 minutes after dMCAo: $F_{(4,48)}$ =1.020, P= 0.4064). As milrinone dose had no effect, Figure 5-3(c) shows relative blood flow normalized to 60 minutes post-dMCAO (or sham surgery) in sham controls and pooled milrinone treated animals. Two-way ANOVA on pooled data identified a significant main effect of milrinone Treatment ($F_{(1,37)}$ =5.690, P= 0.0223). While the blood flow of saline group rats remained around 90% of baseline (pre-treatment) during all imaging sessions, flow in the milrinone treated rats increased within the first half hour of infusion to 115% of post dMCAO values and remained stable throughout imaging.

5.3.2. Experiment II

The results in Experiment I suggested that acute administration of milrinone could enhance penumbral blood flow after dMCAo, although no dose response was observed. However, the effect of milrinone on infarction could not be assessed with recovery only to 3 h after ischemic onset. Milrinone has been used to treat myocardial failure and cerebral vasospasm in SAH for a period of days [280,283]. Therefore, Experiment II was performed to see whether prolonged subcutaneous milrinone would be neuroprotective after dMCAo.

5.3.2.1. Prolonged Milrinone Treatment does not Influence Physiological Parameters or Significantly Reduce Infarct

Figure 5-4 shows physiological variables assessed using telemetry throughout recovery. Two way ANOVA revealed a significant effect of Time (blood pressure: ($F_{(8,64)}$=86.25, P<0.0001; heart rate: ($F_{(8,64)}$=6.036, P<0.0001;activity: ($F_{(6,48)}$=9.474, P<0.0001;), but no effect of Treatment (blood pressure: ($F_{(1,8)}$=0.8305, P=0.3888; heart rate: ($F_{(1,8)}$=1.252, P=0.2956; activity: ($F_{(1,8)}$=0.07777, P=0.7874;) or Time*Treatment interaction (blood pressure: ($F_{(8,64)}$=1.387, P=0.2195; heart rate: ($F_{(8,64)}$=0.7348, P=0.6604; activity: ($F_{(6,48)}$=1.411, P=0.2300;) for blood pressure (Figure 5-4(a)), heart rate (Figure 5-4(b)), and activity (Figure 5-4(c)). In Figure 5-5, Cresyl Violet staining was used to identify infarct at 5 days after treatment. Notably, milrinone did not significantly reduce infarct volume relative to sham controls (control: 12.89%± 1.922%; milrinone: 8.901%±1.509%; unpaired Student's t-test, P = 0.1170).

5.4. Discussion:

Collateral circulation refers to subsidiary vascular networks that provide residual blood flow to the affected brain tissues during acute ischemic stroke. Collaterals are a key variable in determining ischemic stroke prognosis because the drop out of collaterals is associated with progression of penumbra to irreversible ischemic infarct. Therefore, therapeutics which can enhancing cerebral pial collateral blood flow may be helpful in maintaining penumbral viability. PDE3 is reported to be expressed in both cardiac myocytes and cerebral arteries smooth muscle cells. Therefore, milrinone, a PDE3 inhibitor, has a potent combination of inotropic effects (augmentation of cardiac output) and cerebral vasodilatory effects and may have impact in regulating cerebral pial collateral blood flow during ischemic stroke.

In Experiment I, we assessed collateral flow augmentation after dMCAo and treatment with intravenous milrinone. While not conclusive, the data provided support for further study of milrinone as a collateral therapeutic. Notably, we did not observe a dose response, suggesting that we may not have identified the optimal drug dose. However, when blood flow measurements from all three doses of milrinone were pooled, a statistically significant effect of Treatment was observed, with blood flow in the penumbral regions (measured by LSCI) at approximately 115% of pre-treatment baseline during infusion and for at least one hour after infusion. In contrast, blood flow in the saline controls was approximately 90% of pre-treatment baseline. This improved collateral flow is consistent with Drexler and Iida' findings [276,277]. Both Drexler and Iida studied the effect of milrinone on cerebral blood flow in normal non-ischemic animals (rats by Drexler & rabbits by Iida). Drexler et al [276] demonstrated that 15min of 3ug/kg/min and 6ug/kg/min milrinone infusion could enhance cerebral blood flow relative to before infusion by 25% and 40%, respectively. Similarly, Iida et al [277] observed dose dependent effects of intravenous milrinone (0.5, 5, 20ug/kg/min for 30min each) on dilation of pial arterioles. We are the first to demonstrate the persistent improvement of penumbral flow due to milrinone infusion during acute ischemic stroke in rats. Early milrinone may therefore be useful to maintain cerebral blood flow and improve cerebral perfusion and thereby maintain tissue viability prior to thrombolytic or endovascular treatment.

The pathophysiology of cerebral ischemia evolves over hours and days after ischemic onset [9,289], suggesting that a transient increase in flow might not have permanent benefit (merely delaying cell death). Thus, a chronic administration paradigm that ensures plasma concentrations of milrinone in the optimal range throughout the acute and subacute periods may have greater benefit. Such administration paradigms (continuous infusion of PDE inhibitors over several days) have been validated in patients' treatment for chronic heart failure, SAH, and secondary stroke prevention [273,290–292]. Alzet osmotic mini pump can be implanted in animals and have the advantage of delivering drugs without frequent handling [293]. Schoemaker et al [294] used Alzet pump for prolonged milrinone therapy in rats with heart failure due to myocardial infarction. Two weeks of 150ug/kg/h (2.5ug/kg/min) milrinone were administered and restored cardiac function without alternating mean arterial pressure and heart rate. Therefore, Alzet osmotic mini pump were used in Experiments II for continuous milrinone lactate administration after ischemic stroke in non-restrained rats. During the 5 days period of treatment (intravenous infusion and subacute administration by Alzet osmotic mini pump), no significant change in physiological parameters (heart rate, blood pressure and activity) between milrinone treatment and vehicle control groups were observed. Rats were stable and tolerated the pump and milrinone (or vehicle) treatment well. Rats were euthanized at day 5 post stroke for infarct volume measurement. However, the difference in infarct volume between milrinone treated rats and controls did not reach statistical significance ($P=0.117$). A sample size calculation based on the mean for each group (control: 12.9%; milrinone: 8.9%) and the overall standard deviation (6.2%) with $\alpha=0.05$ and $\beta=0.8$ suggest that up to 38 rats would be required in each group prove statistical significance. Thus, while the data suggest that milrinone is well tolerated and potentially protective during the subacute period following ischemic stroke, the data are not conclusive and further studies are required.

In conclusion, we found that milrinone increases collateral flow acutely and continuous subacute administration of milrinone is well tolerated, but the efficacy in this model of stroke was not clear. Milrinone may be useful to serve as an adjunctive collateral therapy to enhance pial collateral flow before recanalization. However, the ischemic stroke model used in this chapter was a permanent occlusion model, and as such does not represent the increasingly common occurrence of recanalization in the patient population. Further study using treatment with milrinone during occlusion in a transient MCA occlusion (i.e. either a filament occlusion or thromboembolic occlusion followed intravenous r-tPA treatment) will be incorporated to determine if milrinone is effective as an adjunct treatment to maintain tissue viability prior to reperfusion. Moreover, determination of optimal doses and temporal profile, as well as potential risks for hemorrhagic transformation also remain to be studied. Since prolonged treatment of milrinone is safe but efficacy of neuroprotection did not reach statistical significance, its efficacy as a potential treatment for ischemic stroke patients not eligible for recanalization therapy is not clear. A preclinical experimental design that includes daily cerebral blood flow measurement and detailed functional outcome will be utilized in the future.

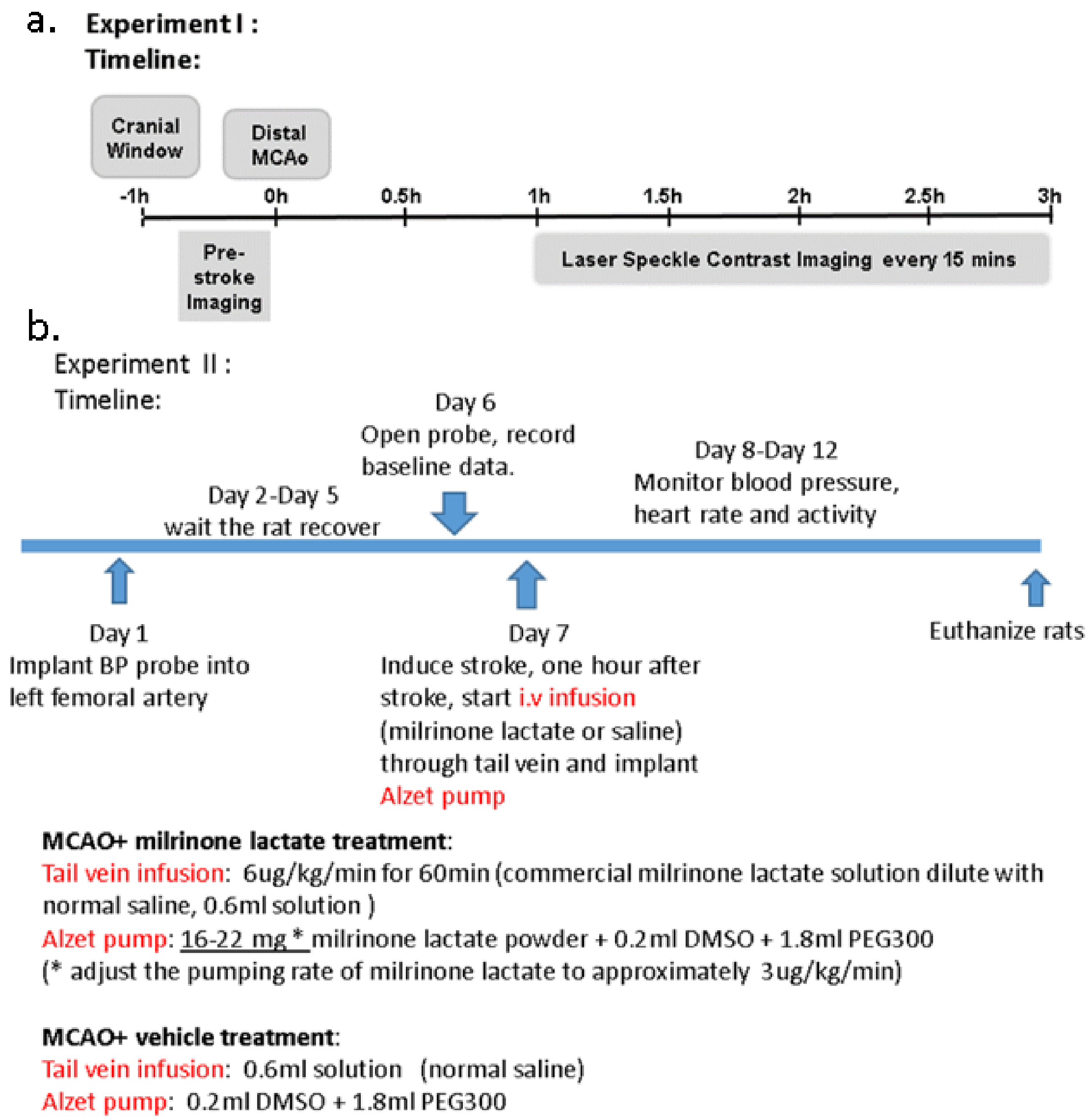

Figure 5- 1 Experimental design

(**a**) Experimental I timeline. (**b**) Experimental II timeline.

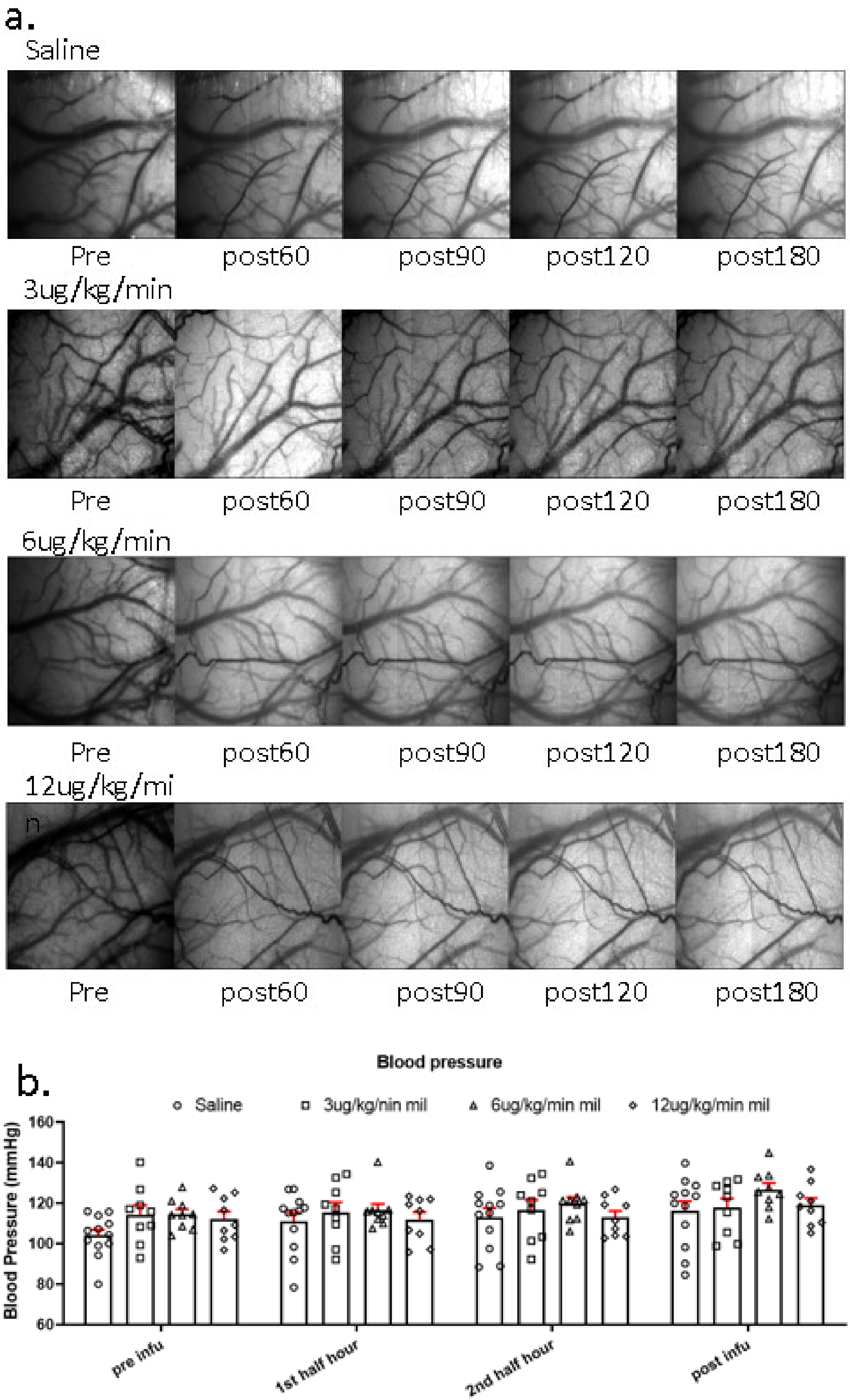
a.
Saline
Pre
post60
post90
post120
post180
3ug/kg/min
Pre
post60
post90
post120
post180
6ug/kg/min
Pre
post60
post90
post120
post180
12ug/kg/mi
n
Pre
post60
post90
post120
post180
b.
Blood pressure
Saline
3ug/kg/nin mil
6ug/kg/min mil
12ug/kg/min mil
Blood Pressure (mmHg)
160
140
120
100
80
60
pre infu
1st half hour
2nd half hour
post infu

Figure 5- 2 Representative LSCI derived maps of speckle contrast showing flow on the cortical surface over 3 hours post stroke for sham and 3 different dose of milrinone treated rats in Experimental I & Blood pressure of milrinone and sham treatment rats during imaging in Experimental I

Representative LSCI derived maps of speckle contrast showing flow changes over 3 hours post stroke for sham and milrinone treated rats are shown in (**a**). Qualitatively, LSCI derived maps of blood flow suggested increased blood flow relative to vehicle controls after infusion of milrinone (note a consistent increase in brightness in saline controls that is not apparent in milrinone treated animals). Notably, there was no significant effect of milrinone treatment on systemic blood pressure ($F_{(3,35)}$ =0.9331, P= 0.4350) (**b**).

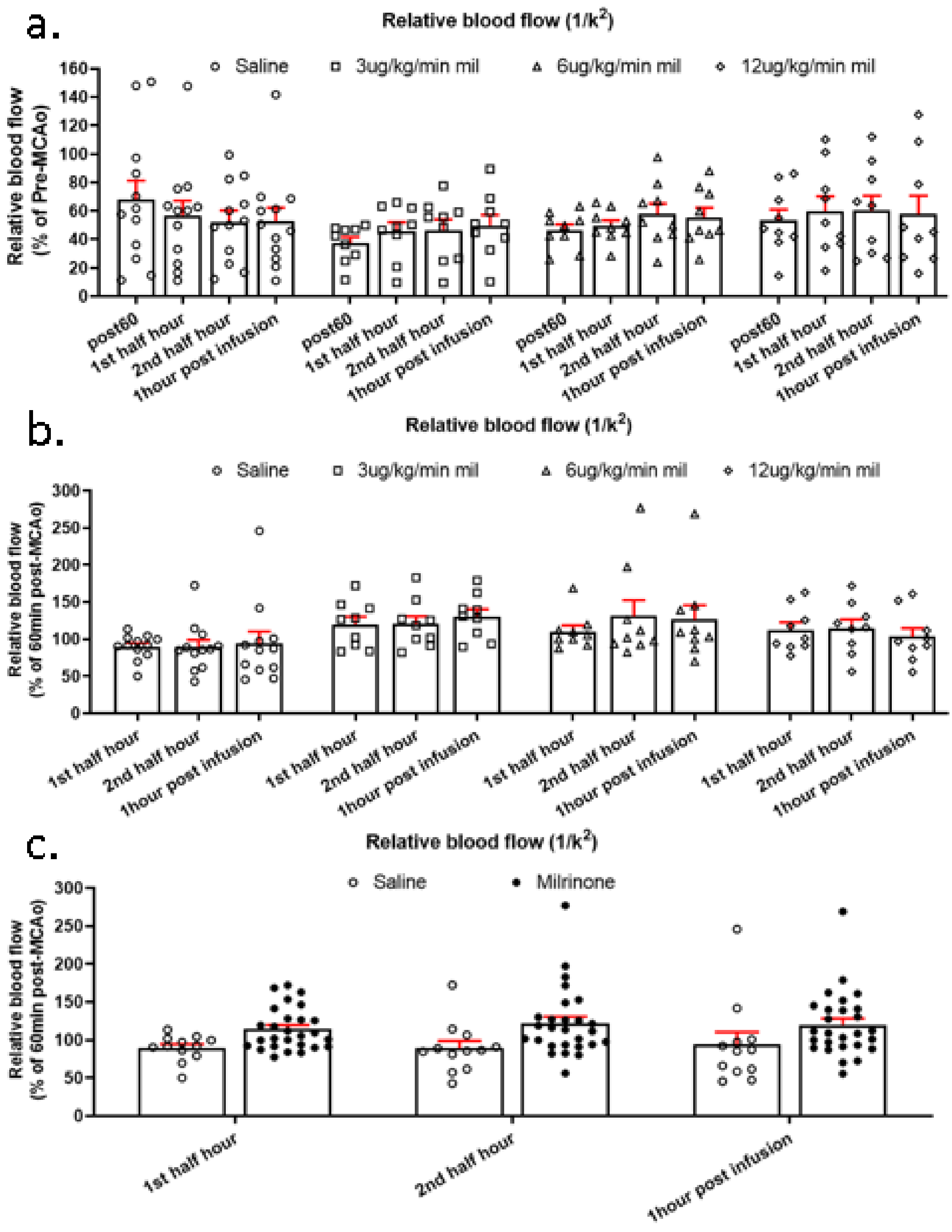

Figure 5- 3 Quantification of Relative blood flow for sham controls and animals treated with three different doses of milrinone

Relative blood flow normalized to values before dMCAO and to values measured 60 minutes after dMCAO (to control for different levels of ischemia between rats) are illustrated for sham controls and animals treated with three doses of milrinone are illustrated in (**a**) and (**b**), respectively. In both cases, two-way ANOVA did not identify a significant main effect of Time (Normalized to pre-dMCAo: $F_{(3,105)}$ =0.2925, P= 0.8307; Normalized to 60 minutes after dMCAo: $F_{(2,70)}$ =0.6550, P= 0.5226) or Treatment (Normalized to pre-dMCAo: $F_{(9,105)}$ =1.702, P= 0.0976; Normalized to 60 minutes after dMCAo: $F_{(6,70)}$ =0.7726, P= 0.5941), and no significant interaction of Time and Treatment (Normalized to pre-dMCAo: $F_{(3,35)}$ =0.5461, P= 0.6540; Normalized to 60 minutes after dMCAo:$F_{(3,35)}$ =2.210, P= 0.1153). However, statistical analysis of milrinone groups only (removing vehicle controls) via two-way ANOVA did not identify a main effect of milrinone dose (Normalized to pre-dMCAo: $F_{(2,24)}$ =0.8340, P= 0.4465; Normalized to 60 minutes after dMCAo: $F_{(2,24)}$ =0.4107, P= 0.6678) or a Dose x Time interaction (Normalized to pre-dMCAo: $F_{(6,72)}$ =0.3975, P= 0.8783; Normalized to 60 minutes after dMCAo: $F_{(4,48)}$ =1.020, P= 0.4064). As milrinone dose had no effect, (**c**) shows relative blood flow normalized to 60 minutes post-dMCAO (or sham surgery) in sham controls and pooled milrinone treated animals. Two-way ANOVA on pooled data identified a significant main effect of milrinone Treatment ($F_{(1,37)}$ =5.690, P= 0.0223). While the blood flow of saline group rats remained around 90% of baseline (pre-treatment) during all imaging sessions, flow in the milrinone treated rats increased within the first half hour of infusion to 115% of post dMCAO values and remained stable throughout imaging.

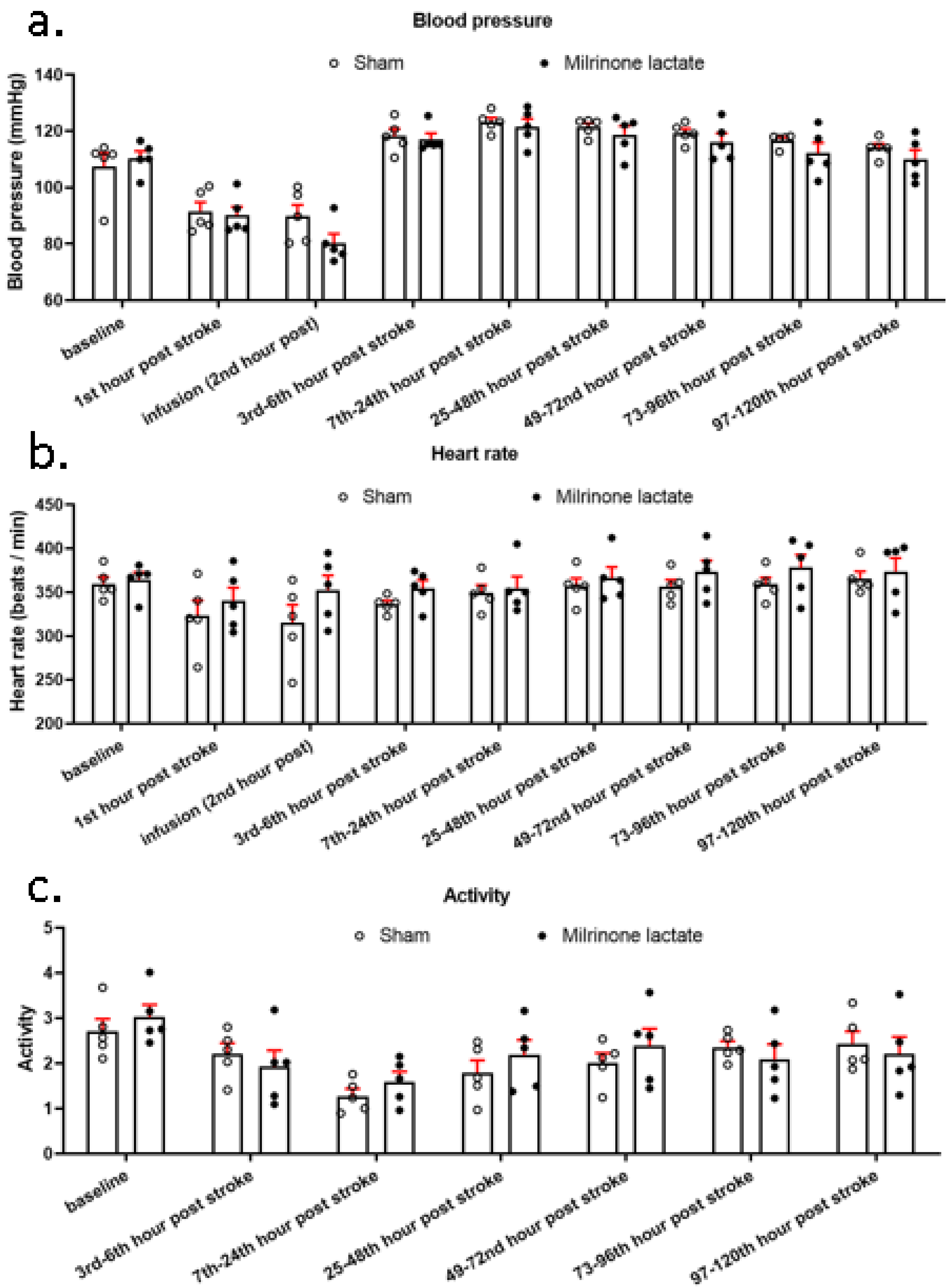

Figure 5- 4 Average of physiological parameters (blood pressure, heart rate and activity) of prolonged milrinone treated and sham treated rats during the entire post-stroke period in Experimental II

Two way ANOVA revealed a significant effect of Time (blood pressure: ($F_{(8,64)}$=86.25, P<0.0001; heart rate: ($F_{(8,64)}$=6.036, P<0.0001;activity: ($F_{(6,48)}$=9.474, P<0.0001;), but no effect of Treatment (blood pressure: ($F_{(1,8)}$=0.8305, P=0.3888; heart rate: ($F_{(1,8)}$=1.252, P=0.2956; activity: ($F_{(1,8)}$=0.07777, P=0.7874;) or Time*Treatment interaction (blood pressure: ($F_{(8,64)}$=1.387, P=0.2195; heart rate: ($F_{(8,64)}$=0.7348, P=0.6604; activity: ($F_{(6,48)}$=1.411, P=0.2300;) for blood pressure (Figure 5-4(**a**)), heart rate (Figure 5-4(**b**)), and activity (Figure 5-4(**c**)).

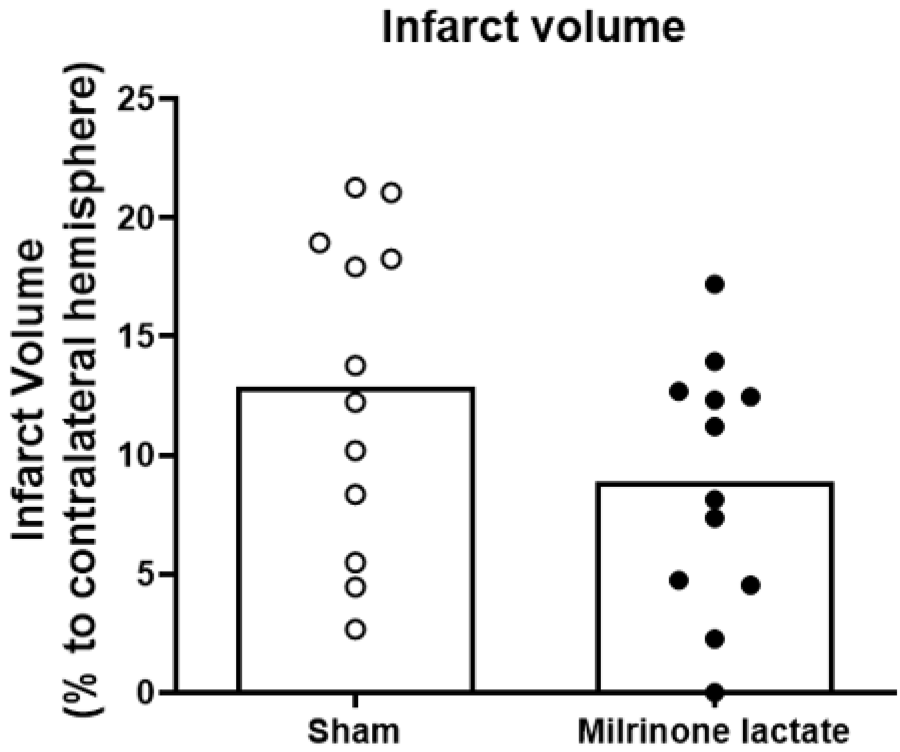

Figure 5- 5 Infarction volume measurements at 5th day post stroke

Cresyl Violet staining was used to identify infarct at 5th days after stroke. Notably, milrinone did not significantly reduce infarct volume relative to sham controls (control: 12.89%± 1.922%; milrinone: 8.901%±1.509%; unpaired Student's t-test, P = 0.1170).Means of the infarct volumes are presented as percentage of their corresponding contralateral sides.

Chapter 6

Summary of Findings & Future Directions

6.1. Summary of Findings

The main objective of this thesis was to use advance imaging techniques (LSCI and TPLSM) to further our understanding of the hemodynamic evolution of pial collaterals after stroke and provide preclinical evidence on a pair of pial collateral enhancement treatments (RIPerC and intravenous milrinone administration) to facilitate bench to bedside translation. Reviewed below, the results of our in vivo imaging studies provide novel insight on the dynamics the cerebral pial collateral circulation over time after stroke, suggesting that collaterals will fail over time and that techniques to improve collateral blood flow can reduce ischemic damage during acute stroke.

In Chapter 2, we confirmed clinical observations that suggest that cerebral pial collateral circulation is time limited and will fail over time. Notably, we are the first to use advanced imaging in animal models to demonstrate that collateral failure is more severe in aged rats. Aged rats exhibit significantly impaired pial collateral dynamics, including accelerated constriction of pial collateral diameters, reduced blood red blood cell velocity and impaired red blood cell flux relative to young adult rats. Such findings are relevant as aging is the primary risk factor for ischemic stroke and the brains of the elderly have reduced ischemic tolerance [149–152]. The dropout of collaterals during stroke is related to the progression of penumbra to irreversible ischemic infarct and impaired response to treatment [26–28]. Thus, impaired collateral dynamics or accelerated pial collateral failure would contribute to worse outcome in elderly patients. Enhancing cerebral pial collateral blood flow by mechanical or pharmacological means may therefore be particular helpful in stroke therapy for aged patients, especially before recanalization treatment in order to maintain tissue viability.

In Chapter 3, we showed that remote ischemic perconditioning (RIPerC), which involves inducing a series of repetitive, transient peripheral cycles of ischemia and reperfusion during cerebral ischemia, could prevent collateral collapse in young adult rats. This prevention of "collateral collapse" was associated with a significant reduction in early ischemic damage 6 h after stroke. RIPerC has been shown to be neuroprotective in animal models of cerebral ischemia, but there are few studies on its neuroprotective mechanisms [139,223,295,296]. Our data shows that the significant protective effect of RIPerC may be due to enhanced cerebral blood flow via collaterals.

According to the Stroke Therapy Academic Industry Roundtable (STAIR) recommendations, which were established in an attempt to improve quality of preclinical stroke therapy studies, preclinical studies of therapies like RIPerC should be performed in aged animals that better approximate human stroke patients [246]. In Chapter 4, in order to provide further evidence to support bench to bedside translation of RIPerC, we examine hemodynamic changes of pial collateral flow with RIPerC treatment in aged rats. Our findings demonstrated RIPerC could enhance penumbral circulation by maintaining pial collaterals that allow retrograde blood flow from ACA to distal MCA segments during MCA occlusion. Improved blood flow due to RIPerC persisted throughout imaging and was associated with reduce infarct volume.

In Chapter 5, we evaluated collateral blood flow modulation by systemic collateral pharmacotherapy with milrinone, a potent selective phosphodiesterase 3 (PDE3) inhibitor that exerts inotropic and vasodilatory effects [159,273]. We found that milrinone increased collateral flow acutely. However, the effect of acute milrinone on infarction was not determined. To assess whether prolonged milrinone treatment can further enhance collateral blood flow and reduce ischemic stroke damage, Alzet osmotic mini pump were used for continuous milrinone lactate administration after ischemic stroke in non-restrained rats. During the 5 days period of treatment (intravenous infusion and subacute administration by Alzet osmotic mini pump), rats were stable and tolerated the pump and milrinone (sham) treatment well. Thus, sustained milrinone was well tolerated, consistent with studies in humans (heart failure and SAH) and in animal models. However, the difference in infarct volume between milrinone treated rats and controls did not reach statistical significance (P=0.117).

There are several future studies that can address issues raised by our research.

6.2. Limitations and Future Directions for Study of Aging and Collateral Flow

Beard et al[210,211,297] recently reported that the elevation of intracranial pressure (ICP) may be the primarily cause of collateral failure after stroke. That is to say, as ICP increases, cerebral perfusion pressure is reduced and collateral flow declines, leading to collateral failure. We found pial collateral failure is more severe in aged rats relative to young adult rats. However, ICP was not monitored in our study and we were unable to relate any dynamic difference of ICP between aged and young stroke rats with pial collateral collapse at present. In order to demonstrate the effect of intracranial pressure (ICP) with pial collateral impairment, in future studies PA-C10 telemetric pressure probes (Data Sciences Int.) could be implanted in the epidural space for ICP measurement during LSCI and TPLSM imaging [298]. Head-down tilt, which promotes gravitational blood flow diversion from the lower body to the head, is associate with increases intracranial pressure (ICP) [299–301]. Simone et al. reported that 60 min of 15° head down tilt is effective in enhancing cerebral perfusion of acute ischemic stroke by laser Doppler measurement [300]. However, the influence of head-down tilt on ICP and pial collaterals were not studied. This interplay between collateral enhancement and ICP induced failure is worth investigating in the future, particularly in the aged.

Our data more clearly defined the effects of aging on the dynamics of collateral circulation. However, the mechanism behind the compensatory increase in flow velocity that is present in young adult rats and absent in aged rats is still undefined. Moreover, it is known that metabolic risk factors, like metabolic syndrome and hyperuricemia which can exacerbate endothelial dysfunction, contribute in poor leptomeningeal collateral status of patients with acute ischemic stroke [212,302]. A metabolic syndrome rat model [303,304] or the hyperuricemic rat model [305,306] could be used for in vivo pial collateral imaging in the future to better illuminate the relationship between collateral failure and risk factors beyond aging.

Faber et al [18] postulated that endothelial dysfunction is associated with reduced cerebral native collaterals density in mice. Of interest, it would be important to determine the effect of endothelial dysfunction in regulating hemodynamic of pial collaterals post stroke. Future studies should also determine the degree to which age contributes to this dysfunction. After in vivo imaging, cerebral micro vessels could be isolated based on Youhai's protocol [307] and the endothelial nitric oxide synthase (eNOS) and phosphorylated eNOS measured with western blots to study the aged related effect of eNOS signaling dysfunction in hemodynamic regulation of pial collaterals [308].

6.3. Limitations and Future Directions of RIPerC Studies

Our data demonstrated that RIPerC could prevent collapse of pial collateral, thus maintaining retrograde blood flow from ACA to distal MCA segments and reducing early ischemic damage after stroke. Including ours, most preclinical studies of RIPerC are performed invasively on rodent hind limbs via femoral artery ligation [135,138–140,142,143,223,225,247–249], Conversely, clinical studies generally involve upper limb ischemia via inflation of a blood pressure cuff [144,152]. However, a comparison of different methods and locations of peripheral ischemia has not been done. Nonetheless, to match clinical approaches, blood pressure cuff inflation/deflation on upper limbs instead of invasive femoral artery ligation should be used in our future collateral flow studies to simulate clinical application. Moreover, there is currently no consensus about the most appropriate RIRerC protocol in either preclinical or clinical studies. The time of application of RIPerC, the ischemic duration in each cycle of RIPerC and the number of RIPerC cycles vary between different preclinical RIPerC published papers [135,138–140,142,143,223,225,247–249]. In order to have sufficient time allowing TPLSM imaging scanning and processing to quantify individual pial collateral during RIPerC, 15 min occlusion/reperfusion periods were used in our study. Such long duration of limb ischemia could increase risk of limb necrosis and may not be appropriate to apply on stroke patients. Four cycles of 5 min of ischemia followed by 5 min of reperfusion are commonly used in past and ongoing clinical randomized control studies [146,309]. Refined imaging protocols and faster TPLSM imaging using technologies such as piezo-enabled objectives would potentially allow for replication of 5 min limb occlusion/reperfusion cycles to better evaluate their ability to prevent pail collateral collapse as described in Chapter 3 and Chapter 4.

The underlying mechanisms and signaling pathway involved in pial collateral collapse prevention by RIPerC is unknown for both young adult and aged rats. It is well known that nitric oxide can regulate vasodilation by modulating vascular tone [250]. Nitric oxide has been shown playing roles in remote ischemic conditioning protection of liver and cardio ischemia [251–253]. Nitric oxide is unstable , therefore it is reserve and storage as nitrite and nitrate inside human bodies [254–256]. In liver ischemia studies, Abu-Amara et al. found that remote ischemic pre conditioning elevated nitrite and nitrate levels in the blood, enhanced liver microcirculation, and thus contributes to liver protection. Such protective effects are abolished with nitric oxide scavenger and disappeared in eNOS knockouts models [147,251,252]. Rassaf et al [147,253] also reported in cardio ischemia protection study that mice treated with remote ischemic pre conditioning have elevated nitrite level not only in plasma but also in the heart. However, the remote ischemic pre conditioning induced cardio protection was lost in eNOS knockouts mice. Notably, since these nitric oxide data were based RIC initiated prior to ischemia (RIPreC) and investigated different target organ (liver, heart) protection, strong evidence to support the role of nitric oxide in RIPerC treatment induced pial collateral collapse prevention. Supporting evidence was found by Hoda et al [257], who observed that at the site of limb conditioning, the mRNA expression of endothelial nitric oxide synthase in the blood vessels had a 10 fold increase, leading to increased plasma nitric oxide concentration.Thus we hypothesize that nitric oxide likely plays a significant role in preventing collateral collapse during RIPerC. Further in vivo imaging experiments using NO scavengers and eNOS knockout mice will be pursued in future to investigate the role of nitric oxide in pial collateral collapse prevention by RIPerC.

Last but not least, since RIPerC works immediately in preventing pial collateral collapse and is easy to be applied to stroke patients during transportation, it was then take into consideration that whether RIPerC could serve as synergetic therapy to keep more penumbra alive before recanalization therapy. The recently published

DAWN and DEFUSE 3 trials reported significant benefit of endovascular treatment in ischemic stroke patients last known to be normal 6 to 24 hours (DAWN) and 6 to 16 hours (DEFUSE 3) before medical intervention [31,32]. Therefore, more and more patients will have chance for recanalization therapy. However, only comprehensive stroke center have DSA available for endovascular treatment, thus therapeutic treatments like RIPerC which emphasize freezing the penumbra during patient transportation are essential to be studied. Future in vivo pial collaterals imaging studies of RIPerC should incorporate a transient model of MCAo to model stroke with recanalization. Intraluminal filament middle cerebral artery occlusion (MCAO) stroke model [310,311] may be a good choice since it allows recanalization by filament withdrawn to mimic human stroke cases which have endovascular treatment.

6.4. Limitations and Future Directions of Milrinone Experiments

We found that milrinone increases collateral flow acutely post stroke in the dMCAo model, and that improved flow persisted after milrinone infusion ended. However, no dose response was observed, indicating that we may not have identified the optimal drug dose. The drug dose used in our study (3,6,12 ug/kg/min) were derived from Drexler and Iida' research [276,277]. Both Drexler and Iida studied the effect of milrinone on cerebral blood flow on healthy non-ischemic animals (rats and rabbits). Drexler et al. showed that15min of 3ug/kg/min and 6ug/kg/min could get cerebral blood flow enhancement relative to before infusion by 25% and 40%, respectively [276]. Iida et al. observed dose dependent effects of intravenous milrinone (0.5, 5, 20ug/kg/min for

30min each) on dilation of pial arterioles [277]. The pathophysiological difference between ischemic stroke and normal cerebral tissue may account for the lack of apparent dose effect, and an increased range could be studied in future experiments. Early milrinone infusion may be useful to serve as conjunctive therapy to maintain cerebral blood flow and improve cerebral perfusion before and during thrombolytic or endovascular treatment. To address this, future studies of early milrinone infusion should use transient model of MCAo to simulate stroke with recanalization. Secondly, milrinone infusion is simple to administer and could be performed during ambulance transportation after stroke onset. However, the symptoms of ischemic and hemorrhagic stroke are similar and the early diagnosis of ischemic vs. hemorrhagic stroke is difficult before imaging. It is important to determine if milrinone has any detrimental effects in intracerebral hemorrhagic stroke in the future.

Limited by the large sample requirement due to high infarct size variability, we did not acquire convincing proof that validates neuroprotection due to sustained milrinone treatment. More rats could be used in the future to determine the protective benefit (or lack thereof) of sustained milrinone administration. Additionally, determination of plasma concentration during sustained treatment is important, and High Performance Liquid Chromatography (HPLC) could be used to evaluate plasma milrinone concentration during subcutaneous milrinone administration by Alzet osmotic mini pump. Additional assessment of cerebral blood flow of stroke rats during sustained treatment is another important experimental addition. Functional assessments should also be used to evaluate the influence of blood flow enhancement by milrinone on ischemic stroke rats' functional outcome.

Milrinone is the first PDE inhibitors we selected to study as a collateral therapeutic. Many other related PDE inhibitors (e.g. cilostazol and ibudilast) are also available and can be explored for future study. Cilostazol is also a selective PDE3 inhibitor. It has been FDA approved for relieving symptoms of intermittent claudication, a peripheral arterial disease caused by obstruction of lower extremity arteries that reduces arterial flow during exercise and/or at rest [312]. Studies of cilostazol demonstrated that it cannot only increase cerebral blood flow after SAH, but also reduce incidence of secondary stroke by inhibiting platelet aggregation [292,313,314]. Ibudilast is a non-selective PDE4 inhibitor with additional selectivity for PDE3 [315,316]. PDE4 exhibited anti-inflammatory actions on immune cells [317]. Ibudilast may therefore augment collateral blood flow (PDE3 inhibition) while reducing inflammation (PDE4 inhibition) in ischemic tissue. Therefore, cilostazol and ibudilast are worth for study as acute collateral therapeutics [315,317].

Finally, only a single time point of treatment was explored (milrinone treatment started at 1hour post stroke), so the determination of a therapeutic window remains to be performed. Notably, the collapse of collaterals later after ischemic onset might suggest that a greater improvement might be observed with later administration. Further study will address the appropriate therapeutic window for milrinone infusion.

6.5. Conclusion

Preclinical in vivo imaging with LSCI and TPLSM is a powerful combination of imaging modalities that allow a researcher to directly study hemodynamic and compensatory aspects of cerebral pial collateral circulation during acute ischemic stroke. Our data show novel dynamics of collateral collapse in the aged and provide support for a pair of therapeutic interventions to modulate collateral flow. New therapeutic strategies like RIPerC and milrinone have potential to be an adjunctive therapy to spare functionally intact brain tissues before thrombolysis and thrombectomy.

Comprehensive bibliography

1. Dziennis S, Qin J, Shi L, Wang RK. Macro-to-micro cortical vascular imaging underlies regional differences in ischemic brain. *Sci. Rep.* 2015;5:10051.

2. Deng Z, Wang Z, Yang X, Luo Q, Gong H. In vivo imaging of hemodynamics and oxygen metabolism in acute focal cerebral ischemic rats with laser speckle imaging and functional photoacoustic microscopy. *J. Biomed. Opt.* 2012;17:0814151–0814159.

3. WHO | Stroke, Cerebrovascular accident [Internet]. WHO. [cited 2019 Feb 20];Available from: https://www.who.int/topics/cerebrovascular_accident/en/

4. Terpolilli NA, Kim S-W, Thal SC, Kataoka H, Zeisig V, Nitzsche B, et al. Inhalation of nitric oxide prevents ischemic brain damage in experimental stroke by selective dilatation of collateral arterioles. *Circ. Res.* 2012;110:727–738.

5. Chauhan A, Al Mamun A, Spiegel G, Harris N, Zhu L, McCullough LD. Splenectomy protects aged mice from injury after experimental stroke. *Neurobiol. Aging*. 2018;61:102–111.

6. Reeves MJ, Bushnell CD, Howard G, Gargano JW, Duncan PW, Lynch G, et al. Sex differences in stroke: epidemiology, clinical presentation, medical care, and outcomes. *Lancet Neurol.* 2008;7:915–926.

7. Rojas JI, Zurrú MC, Romano M, Patrucco L, Cristiano E. Acute ischemic stroke and transient ischemic attack in the very old – risk factor profile and stroke subtype between patients older than 80 years and patients aged less than 80 years.

Eur. J. Neurol. 2007;14:895–899.

8. Wang Y, Reis C, Applegate R, Stier G, Martin R, Zhang JH. Ischemic conditioning-induced endogenous brain protection: Applications Pre-, Per- or Post-Stroke. *Exp. Neurol.* 2015;272:26–40.

9. Moustafa RR, Baron J-C. Pathophysiology of ischaemic stroke: insights from imaging, and implications for therapy and drug discovery. *Br. J. Pharmacol.* 2008;153:S44–S54.

10. Stankowski JN, Gupta R. Therapeutic targets for neuroprotection in acute ischemic stroke: lost in translation? *Antioxid. Redox Signal.* 2011;14:1841–1851.

11. Winship IR, Armitage GA, Ramakrishnan G, Dong B, Todd KG, Shuaib A. Augmenting collateral blood flow during ischemic stroke via transient aortic occlusion. *J. Cereb. Blood Flow Metab.* 2014;34:61–71.

12. Liebeskind DS. Collateral Circulation. *Stroke*. 2003;34:2279–2284.

13. Ramakrishnan G, Armitage GA, Winship IR. Understanding and Augmenting Collateral Blood Flow During Ischemic Stroke. *Acute Ischemic Stroke* [Internet]. 2012 [cited 2019 Feb 20];Available from: https://www.intechopen.com/books/acute-ischemic-stroke/understanding-and-augmenting-collateral-blood-flow-during-ischemic-stroke

14. Shuaib A, Butcher K, Mohammad AA, Saqqur M, Liebeskind DS. Collateral

blood vessels in acute ischaemic stroke: a potential therapeutic target. *Lancet Neurol.* 2011;10:909–921.

15. Hendrikse J, van Raamt AF, van der Graaf Y, Mali WPTM, van der Grond J. Distribution of Cerebral Blood Flow in the Circle of Willis. *Radiology*. 2005;235:184–189.

16. Winship I. Cerebral collaterals and collateral therapeutics for acute ischemic stroke. *Microcirculation*. 2015;22(3):228–36.

17. Brozici M, Zwan A van der, Hillen B. Anatomy and Functionality of Leptomeningeal Anastomoses. *Stroke*. 2003;34:2750–2762.

18. Faber JE, Zhang H, Lassance-Soares RM, Prabhakar P, Najafi AH, Burnett MS, et al. Aging causes collateral rarefaction and increased severity of ischemic injury in multiple tissues. *Arterioscler. Thromb. Vasc. Biol.* 2011;31:1748–1756.

19. Sonntag WE, Lynch CD, Cooney PT, Hutchins PM. Decreases in cerebral microvasculature with age are associated with the decline in growth hormone and insulin-like growth factor 1. *Endocrinology*. 1997;138:3515–3520.

20. Zhang H, Prabhakar P, Sealock R, Faber JE. Wide genetic variation in the native pial collateral circulation is a major determinant of variation in severity of stroke. *J. Cereb. Blood Flow Metab. Off. J. Int. Soc. Cereb. Blood Flow Metab.* 2010;30:923–934.

21. Liebeskind DS. Collaterals in acute stroke: beyond the clot. *Neuroimaging Clin. N. Am.* 2005;15:553–573, x.

22. Liebeskind DS, Jahan R, Nogueira RG, Zaidat OO, Saver JL, SWIFT Investigators. Impact of collaterals on successful revascularization in Solitaire FR with the intention for thrombectomy. *Stroke*. 2014;45:2036–2040.

23. Lima FO, Furie KL, Silva GS, Lev MH, Camargo ECS, Singhal AB, et al. The pattern of leptomeningeal collaterals on CT angiography is a strong predictor of long-term functional outcome in stroke patients with large vessel intracranial occlusion. *Stroke*. 2010;41:2316–2322.

24. Bang OY, Saver JL, Kim SJ, Kim G-M, Chung C-S, Ovbiagele B, et al. Collateral flow predicts response to endovascular therapy for acute ischemic stroke. *Stroke*. 2011;42:693–699.

25. Iwasawa E, Ichijo M, Ishibashi S, Yokota T. Acute development of collateral circulation and therapeutic prospects in ischemic stroke. *Neural Regen. Res.* 2016;11:368–371.

26. Ma J, Ma Y, Dong B, Bandet MV, Shuaib A, Winship IR. Prevention of the collapse of pial collaterals by remote ischemic perconditioning during acute ischemic stroke. *J. Cereb. Blood Flow Metab.* 2016;0271678X16680636.

27. Armitage GA, Todd KG, Shuaib A, Winship IR. Laser Speckle Contrast Imaging of Collateral Blood Flow during Acute Ischemic Stroke. *J. Cereb. Blood Flow*

Metab. 2010;30:1432–1436.

28. Wang Z, Luo W, Zhou F, Li P, Luo Q. Dynamic change of collateral flow varying with distribution of regional blood flow in acute ischemic rat cortex. *J. Biomed. Opt.* 2012;17:125001.

29. Caplan LR, Hennerici M. Impaired Clearance of Emboli (Washout) Is an Important Link Between Hypoperfusion, Embolism, and Ischemic Stroke. *Arch. Neurol.* 1998;55:1475–1482.

30. Pham M, Bendszus M. Facing Time in Ischemic Stroke: An Alternative Hypothesis for Collateral Failure. *Clin. Neuroradiol.* 2016;26:141–151.

31. Albers GW, Marks MP, Kemp S, Christensen S, Tsai JP, Ortega-Gutierrez S, et al. Thrombectomy for Stroke at 6 to 16 Hours with Selection by Perfusion Imaging. *N. Engl. J. Med.* 2018;378:708–718.

32. Nogueira RG, Jadhav AP, Haussen DC, Bonafe A, Budzik RF, Bhuva P, et al. Thrombectomy 6 to 24 Hours after Stroke with a Mismatch between Deficit and Infarct. *N. Engl. J. Med.* 2018;378:11–21.

33. Albers GW. Late Window Paradox. *Stroke*. 2018;49:768–771.

34. Bang OY, Saver JL, Kim SJ, Kim G-M, Chung C-S, Ovbiagele B, et al. Collateral Flow Averts Hemorrhagic Transformation After Endovascular Therapy for Acute Ischemic Stroke. *Stroke*. 2011;42:2235–2239.

35. Christoforidis GA, Karakasis C, Mohammad Y, Caragine LP, Yang M, Slivka AP. Predictors of Hemorrhage Following Intra-Arterial Thrombolysis for Acute Ischemic Stroke: The Role of Pial Collateral Formation. *Am. J. Neuroradiol.* 2009;30:165–170.

36. Raymond SB, Schaefer PW. Imaging Brain Collaterals: Quantification, Scoring, and Potential Significance. *Top. Magn. Reson. Imaging TMRI*. 2017;26:67–75.

37. Cuccione E, Padovano G, Versace A, Ferrarese C, Beretta S. Cerebral collateral circulation in experimental ischemic stroke. *Exp. Transl. Stroke Med.* [Internet]. 2016 [cited 2017 Apr 11];8. Available from: http://www.ncbi.nlm.nih.gov/pmc/articles/PMC4772465/

38. Liu L, Ding J, Leng X, Pu Y, Huang L-A, Xu A, et al. Guidelines for evaluation and management of cerebral collateral circulation in ischaemic stroke 2017. *Stroke Vasc. Neurol.* 2018;3:117–130.

39. Heit JJ, Zaharchuk G, Wintermark M. Advanced Neuroimaging of Acute Ischemic Stroke: Penumbra and Collateral Assessment. *Neuroimaging Clin. N. Am.* 2018;28:585–597.

40. Willinsky RA, Taylor SM, TerBrugge K, Farb RI, Tomlinson G, Montanera W. Neurologic complications of cerebral angiography: prospective analysis of 2,899 procedures and review of the literature. *Radiology*. 2003;227:522–528.

41. Bang OY, Goyal M, Liebeskind DS. Collateral Circulation in Ischemic Stroke:

Assessment Tools and Therapeutic Strategies. *Stroke J. Cereb. Circ.* 2015;46:3302–3309.

42. Martinon E, Lefevre PH, Thouant P, Osseby GV, Ricolfi F, Chavent A. Collateral circulation in acute stroke: Assessing methods and impact: A literature review. *J. Neuroradiol.* 2014;41:97–107.

43. Ginsberg MD. Expanding the concept of neuroprotection for acute ischemic stroke: The pivotal roles of reperfusion and the collateral circulation. *Prog. Neurobiol.* 2016;145–146:46–77.

44. Han A, Yoon DY, Chang SK, Lim KJ, Cho B-M, Shin YC, et al. Accuracy of CT angiography in the assessment of the circle of Willis: comparison of volume-rendered images and digital subtraction angiography. *Acta Radiol. Stockh. Swed. 1987*. 2011;52:889–893.

45. Kaschka IN, Kloska SP, Struffert T, Engelhorn T, Gölitz P, Kurka N, et al. Clot Burden and Collaterals in Anterior Circulation Stroke: Differences Between Single-Phase CTA and Multi-phase 4D-CTA. *Clin. Neuroradiol.* 2016;26:309–315.

46. Menon BK, d'Esterre CD, Qazi EM, Almekhlafi M, Hahn L, Demchuk AM, et al. Multiphase CT Angiography: A New Tool for the Imaging Triage of Patients with Acute Ischemic Stroke. *Radiology*. 2015;275:510–520.

47. Smit EJ, Vonken E, van Seeters T, Dankbaar JW, van der Schaaf IC, Kappelle LJ,

et al. Timing-invariant imaging of collateral vessels in acute ischemic stroke. *Stroke*. 2013;44:2194–2199.

48. Konstas AA, Wintermark M, Lev MH. CT perfusion imaging in acute stroke. *Neuroimaging Clin. N. Am.* 2011;21:215–238, ix.

49. Hoeffner EG, Case I, Jain R, Gujar SK, Shah GV, Deveikis JP, et al. Cerebral perfusion CT: technique and clinical applications. *Radiology*. 2004;231:632–644.

50. Wintermark M, Sincic R, Sridhar D, Chien JD. Cerebral perfusion CT: Technique and clinical applications. *J. Neuroradiol.* 2008;35:253–260.

51. Donahue J, Wintermark M. Perfusion CT and acute stroke imaging: Foundations, applications, and literature review. *J. Neuroradiol.* 2015;42:21–29.

52. Barlinn K, Alexandrov AV. Vascular Imaging in Stroke: Comparative Analysis. *Neurotherapeutics*. 2011;8:340–348.

53. Liu L-P, Xu A-D, Wong LK, Wang DZ, Wang Y-J. Chinese Consensus Statement on the Evaluation and Intervention of Collateral Circulation for Ischemic Stroke. *CNS Neurosci. Ther.* 2014;20:202–208.

54. Hartung MP, Grist TM, François CJ. Magnetic resonance angiography: current status and future directions. *J. Cardiovasc. Magn. Reson.* 2011;13:19.

55. Song H-S, Kang C-K, Kim JS, Park C-A, Kim Y-B, Lee DH, et al. Assessment of pial branches using 7-tesla MRI in cerebral arterial disease. *Cerebrovasc. Dis.*

Basel Switz. 2010;29:410.

56. Weinreb JC, Abu-Alfa AK. Gadolinium-based contrast agents and nephrogenic systemic fibrosis: why did it happen and what have we learned? *J. Magn. Reson. Imaging JMRI*. 2009;30:1236–1239.

57. Nael K, Doshi A, De Leacy R, Puig J, Castellanos M, Bederson J, et al. MR Perfusion to Determine the Status of Collaterals in Patients with Acute Ischemic Stroke: A Look Beyond Time Maps. *AJNR Am. J. Neuroradiol.* 2018;39:219–225.

58. Potreck A, Seker F, Hoffmann A, Pfaff J, Nagel S, Bendszus M, et al. A novel method to assess pial collateralization from stroke perfusion MRI: subdividing Tmax into anatomical compartments. *Eur. Radiol.* 2017;27:618–626.

59. Lee MJ, Son JP, Kim SJ, Ryoo S, Woo S-Y, Cha J, et al. Predicting Collateral Status With Magnetic Resonance Perfusion Parameters: Probabilistic Approach With a Tmax-Derived Prediction Model. *Stroke*. 2015;46:2800–2807.

60. Galinovic I, Kochova E, Khalil A, Villringer K, Piper SK, Fiebach JB. The ratio between cerebral blood flow and Tmax predicts the quality of collaterals in acute ischemic stroke. *PloS One*. 2018;13:e0190811.

61. Lyu J, Ma N, Liebeskind DS, Wang DJJ, Ma L, Xu Y, et al. Arterial Spin Labeling Magnetic Resonance Imaging Estimation of Antegrade and Collateral Flow in Unilateral Middle Cerebral Artery Stenosis. *Stroke*. 2016;47:428–433.

62. Lou X, Yu S, Scalzo F, Starkman S, Ali LK, Kim D, et al. Multi-delay ASL can identify leptomeningeal collateral perfusion in endovascular therapy of ischemic stroke. *Oncotarget*. 2017;8:2437–2443.

63. de Havenon A, Haynor DR, Tirschwell DL, Majersik JJ, Smith G, Cohen W, et al. Association of Collateral Blood Vessels Detected by Arterial Spin Labeling Magnetic Resonance Imaging With Neurological Outcome After Ischemic Stroke. *JAMA Neurol.* 2017;74:453–458.

64. Wu B, Wang X, Guo J, Xie S, Wong EC, Zhang J, et al. Collateral circulation imaging: MR perfusion territory arterial spin-labeling at 3T. *AJNR Am. J. Neuroradiol.* 2008;29:1855–1860.

65. Hartkamp NS, van Osch MJP, Kappelle J, Bokkers RPH. Arterial spin labeling magnetic resonance perfusion imaging in cerebral ischemia. *Curr. Opin. Neurol.* 2014;27:42–53.

66. Christoforidis GA, Rink C, Kontzialis MS, Mohammad Y, Koch RM, Abduljalil AM, et al. An endovascular canine middle cerebral artery occlusion model for the study of leptomeningeal collateral recruitment. *Invest. Radiol.* 2011;46:34–40.

67. Senarathna J, Rege A, Li N, Thakor NV. Laser Speckle Contrast Imaging: theory, instrumentation and applications. *IEEE Rev. Biomed. Eng.* 2013;6:99–110.

68. Briers JD. Laser speckle contrast imaging for measuring blood flow. *Opt. Appl.*

2007;37:139.

69. Duncan DD, Kirkpatrick SJ. Can laser speckle flowmetry be made a quantitative tool? *J. Opt. Soc. Am. A Opt. Image Sci. Vis.* 2008;25:2088–2094.

70. Parthasarathy AB, Tom WJ, Gopal A, Zhang X, Dunn AK. Robust flow measurement with multi-exposure speckle imaging. *Opt. Express*. 2008;16:1975–1989.

71. Ayata C, Shin HK, Salomone S, Ozdemir-Gursoy Y, Boas DA, Dunn AK, et al. Pronounced Hypoperfusion during Spreading Depression in Mouse Cortex. *J. Cereb. Blood Flow Metab.* 2004;24:1172–1182.

72. Ramakrishnan G, Dong B, Todd KG, Shuaib A, Winship IR. Transient Aortic Occlusion Augments Collateral Blood Flow and Reduces Mortality During Severe Ischemia due to Proximal Middle Cerebral Artery Occlusion. *Transl. Stroke Res.* 2016;7:149–155.

73. Shih AY, Driscoll JD, Drew PJ, Nishimura N, Schaffer CB, Kleinfeld D. Two-photon microscopy as a tool to study blood flow and neurovascular coupling in the rodent brain. *J. Cereb. Blood Flow Metab.* 2012;32:1277–1309.

74. Zhang S, Murphy TH. Imaging the impact of cortical microcirculation on synaptic structure and sensory-evoked hemodynamic responses in vivo. *PLoS Biol.* 2007;5:e119.

75. Shih AY, Friedman B, Drew PJ, Tsai PS, Lyden PD, Kleinfeld D. Active dilation of penetrating arterioles restores red blood cell flux to penumbral neocortex after focal stroke. *J. Cereb. Blood Flow Metab. Off. J. Int. Soc. Cereb. Blood Flow Metab.* 2009;29:738–751.

76. Nishimura N, Rosidi NL, Iadecola C, Schaffer CB. Limitations of collateral flow after occlusion of a single cortical penetrating arteriole. *J. Cereb. Blood Flow Metab. Off. J. Int. Soc. Cereb. Blood Flow Metab.* 2010;30:1914–1927.

77. Mulligan S, A Macvicar B. Two-photon fluorescence microscopy: Basic principles, advantages and risks. *Mod Res Educ Top Microsc*. 2007;2.

78. Svoboda K, Denk W, Kleinfeld D, Tank DW. In vivo dendritic calcium dynamics in neocortical pyramidal neurons. *Nature*. 1997;385:161–165.

79. Kleinfeld D, Mitra PP, Helmchen F, Denk W. Fluctuations and stimulus-induced changes in blood flow observed in individual capillaries in layers 2 through 4 of rat neocortex. *Proc. Natl. Acad. Sci. U. S. A.* 1998;95:15741–15746.

80. Shih AY, Blinder P, Tsai PS, Friedman B, Stanley G, Lyden PD, et al. The smallest stroke: occlusion of one penetrating vessel leads to infarction and a cognitive deficit. *Nat. Neurosci.* 2013;16:55–63.

81. Tennant KA, Brown CE. Diabetes Augments In Vivo Microvascular Blood Flow Dynamics after Stroke. *J. Neurosci.* 2013;33:19194–19204.

82. Luo C, Liang F, Ren H, Yao X, Liu Q, Li M, et al. Collateral blood flow in different cerebrovascular hierarchy provides endogenous protection in cerebral ischemia. *Brain Pathol. Zurich Switz.* 2017;27:809–821.

83. Wang D, Wang Y. Tissue window, not the time window, will guide acute stroke treatment. *Stroke Vasc. Neurol.* 2019;4:1–2.

84. Vishnu VY, Srivastava MP. Innovations in acute stroke reperfusion strategies. *Ann. Indian Acad. Neurol.* 2019;22:6.

85. Nishijima Y, Akamatsu Y, Weinstein PR, Liu J. Collaterals: implications in cerebral ischemic diseases and therapeutic interventions. *Brain Res.* 2015;1623:18–29.

86. Liebeskind DS. Collateral lessons from recent acute ischemic stroke trials. *Neurol. Res.* 2014;36:397–402.

87. Eames PJ, Blake MJ, Dawson SL, Panerai RB, Potter JF. Dynamic cerebral autoregulation and beat to beat blood pressure control are impaired in acute ischaemic stroke. *J. Neurol. Neurosurg. Psychiatry*. 2002;72:467–472.

88. Vlcek M, Schillinger M, Lang W, Lalouschek W, Bur A, Hirschl MM. Association between course of blood pressure within the first 24 hours and functional recovery after acute ischemic stroke. *Ann. Emerg. Med.* 2003;42:619–626.

89. Larrue V, von Kummer R R, Müller A, Bluhmki E. Risk factors for severe hemorrhagic transformation in ischemic stroke patients treated with recombinant tissue plasminogen activator: a secondary analysis of the European-Australasian Acute Stroke Study (ECASS II). *Stroke*. 2001;32:438–441.

90. Tejima E, Katayama Y, Suzuki Y, Kano T, Lo EH. Hemorrhagic transformation after fibrinolysis with tissue plasminogen activator: evaluation of role of hypertension with rat thromboembolic stroke model. *Stroke*. 2001;32:1336–1340.

91. Selim M, Fink JN, Kumar S, Caplan LR, Horkan C, Chen Y, et al. Predictors of hemorrhagic transformation after intravenous recombinant tissue plasminogen activator: prognostic value of the initial apparent diffusion coefficient and diffusion-weighted lesion volume. *Stroke*. 2002;33:2047–2052.

92. Ko Y, Park JH, Yang MH, Ko S-B, Han M-K, Oh CW, et al. The significance of blood pressure variability for the development of hemorrhagic transformation in acute ischemic stroke. *Stroke*. 2010;41:2512–2518.

93. Jickling GC, Liu D, Stamova B, Ander BP, Zhan X, Lu A, et al. Hemorrhagic transformation after ischemic stroke in animals and humans. *J. Cereb. Blood Flow Metab.* 2014;34:185–199.

94. Ahmed Niaz, Wahlgren Nils, Brainin Michael, Castillo José, Ford Gary A., Kaste Markku, et al. Relationship of Blood Pressure, Antihypertensive Therapy, and Outcome in Ischemic Stroke Treated With Intravenous Thrombolysis. *Stroke*.

2009;40:2442–2449.

95. Powers WJ, Rabinstein AA, Ackerson T, Adeoye OM, Bambakidis NC, Becker K, et al. 2018 Guidelines for the Early Management of Patients With Acute Ischemic Stroke: A Guideline for Healthcare Professionals From the American Heart Association/American Stroke Association. *Stroke*. 2018;49:e46–e110.

96. Schwarz S, Georgiadis D, Aschoff A, Schwab S. Effects of induced hypertension on intracranial pressure and flow velocities of the middle cerebral arteries in patients with large hemispheric stroke. *Stroke*. 2002;33:998–1004.

97. Hillis AE, Ulatowski JA, Barker PB, Torbey M, Ziai W, Beauchamp NJ, et al. A pilot randomized trial of induced blood pressure elevation: effects on function and focal perfusion in acute and subacute stroke. *Cerebrovasc. Dis. Basel Switz.* 2003;16:236–246.

98. Wityk RJ. Blood pressure augmentation in acute ischemic stroke. *J. Neurol. Sci.* 2007;261:63–73.

99. Chileuitt L, Leber K, McCalden T, Weinstein PR. Induced hypertension during ischemia reduces infarct area after temporary middle cerebral artery occlusion in rats. *Surg. Neurol.* 1996;46:229–234.

100. Shin HK, Nishimura M, Jones PB, Ay H, Boas DA, Moskowitz MA, et al. Mild induced hypertension improves blood flow and oxygen metabolism in transient focal cerebral ischemia. *Stroke*. 2008;39:1548–1555.

101. Rordorf G, Koroshetz WJ, Ezzeddine MA, Segal AZ, Buonanno FS. A pilot study of drug-induced hypertension for treatment of acute stroke. *Neurology*. 2001;56:1210–1213.

102. Bogoslovsky T, Häppölä O, Salonen O, Lindsberg PJ. Induced hypertension for the treatment of acute MCA occlusion beyond the thrombolysis window: case report. *BMC Neurol.* 2006;6:46.

103. Oluigbo CO, Makonnen G, Narouze S, Rezai AR. Sphenopalatine ganglion interventions: technical aspects and application. *Prog. Neurol. Surg.* 2011;24:171–179.

104. Suzuki N, Hardebo JE, Kåhrström J, Owman C. Selective electrical stimulation of postganglionic cerebrovascular parasympathetic nerve fibers originating from the sphenopalatine ganglion enhances cortical blood flow in the rat. *J. Cereb. Blood Flow Metab. Off. J. Int. Soc. Cereb. Blood Flow Metab.* 1990;10:383–391.

105. Hennerici MG, Kern R, Szabo K. Non-pharmacological strategies for the treatment of acute ischaemic stroke. *Lancet Neurol.* 2013;12:572–584.

106. Baron J-C. Protecting the ischaemic penumbra as an adjunct to thrombectomy for acute stroke. *Nat. Rev. Neurol.* 2018;14:325–337.

107. Seylaz J, Hara H, Pinard E, Mraovitch S, MacKenzie ET, Edvinsson L. Effect of stimulation of the sphenopalatine ganglion on cortical blood flow in the rat. *J. Cereb. Blood Flow Metab. Off. J. Int. Soc. Cereb. Blood Flow Metab.*

1988;8:875–878.

108. Levi H, Schoknecht K, Prager O, Chassidim Y, Weissberg I, Serlin Y, et al. Stimulation of the sphenopalatine ganglion induces reperfusion and blood-brain barrier protection in the photothrombotic stroke model. *PloS One*. 2012;7:e39636.

109. Bar-Shir A, Shemesh N, Nossin-Manor R, Cohen Y. Late stimulation of the sphenopalatine-ganglion in ischemic rats: improvement in N-acetyl-aspartate levels and diffusion weighted imaging characteristics as seen by MR. *J. Magn. Reson. Imaging JMRI*. 2010;31:1355–1363.

110. Henninger N, Fisher M. Stimulating circle of Willis nerve fibers preserves the diffusion-perfusion mismatch in experimental stroke. *Stroke*. 2007;38:2779–2786.

111. Khurana D, Kaul S, Bornstein NM, ImpACT-1 Study Group. Implant for augmentation of cerebral blood flow trial 1: a pilot study evaluating the safety and effectiveness of the Ischaemic Stroke System for treatment of acute ischaemic stroke. *Int. J. Stroke Off. J. Int. Stroke Soc.* 2009;4:480–485.

112. Bornstein NM, Saver JL, Diener HC, Gorelick PB, Shuaib A, Solberg Y, et al. An injectable implant to stimulate the sphenopalatine ganglion for treatment of acute ischaemic stroke up to 24 h from onset (ImpACT-24B): an international, randomised, double-blind, sham-controlled, pivotal trial. *The Lancet* [Internet].

2019 [cited 2019 Jun 21];Available from: http://www.sciencedirect.com/science/article/pii/S0140673619311924

113. Bornstein NM, Saver JL, Diener H-C, Gorelick PB, Shuaib A, Solberg Y, et al. Sphenopalatine Ganglion Stimulation to Augment Cerebral Blood Flow: A Randomized, Sham-Controlled Trial. *Stroke* [Internet]. 2019 [cited 2019 Jun 21];Available from: https://www.ahajournals.org/doi/10.1161/STROKEAHA.118.024582

114. Noor R, Wang CX, Todd K, Elliott C, Wahr J, Shuaib A. Partial Intra-Aortic Occlusion Improves Perfusion Deficits and Infarct Size Following Focal Cerebral Ischemia. *J. Neuroimaging*. 2010;20:272–276.

115. Hammer M, Jovin T, Wahr JA, Heiss W-D. Partial occlusion of the descending aorta increases cerebral blood flow in a nonstroke porcine model. *Cerebrovasc. Dis. Basel Switz.* 2009;28:406–410.

116. Stokland O, Miller MM, Ilebekk A, Kiil F. Mechanism of hemodynamic responses to occlusion of the descending thoracic aorta. *Am. J. Physiol.* 1980;238:H423-429.

117. Shuaib A, Bornstein NM, Diener H-C, Dillon W, Fisher M, Hammer MD, et al. Partial aortic occlusion for cerebral perfusion augmentation: safety and efficacy of NeuroFlo in Acute Ischemic Stroke trial. *Stroke*. 2011;42:1680–1690.

118. Emery DJ, Schellinger PD, Selchen D, Douen AG, Chan R, Shuaib A, et al.

Safety and feasibility of collateral blood flow augmentation after intravenous thrombolysis. *Stroke*. 2011;42:1135–1137.

119. Lutsep HL, Altafullah IM, Roberts R, Silverman IE, Turco MA, Vaishnav AG. Neurologic safety event rates in the SENTIS trial control population. *Acta Neurol. Scand.* 2013;127:e5-7.

120. Shuaib A, Schwab S, Rutledge JN, Starkman S, Liebeskind DS, Bernardini GL, et al. Importance of proper patient selection and endpoint selection in evaluation of new therapies in acute stroke: further analysis of the SENTIS trial. *J. Neurointerventional Surg.* 2013;5 Suppl 1:i21-24.

121. Leker RR, Molina C, Cockroft K, Liebeskind DS, Concha M, Shuaib A, et al. Effects of Age on Outcome in the SENTIS Trial: Better Outcomes in Elderly Patients. *Cerebrovasc. Dis. Basel Switz.* 2012;34:263–271.

122. Schellinger PD, Shuaib A, Köhrmann M, Liebeskind DS, Jovin T, Hammer MD, et al. Reduced mortality and severe disability rates in the SENTIS trial. *AJNR Am. J. Neuroradiol.* 2013;34:2312–2316.

123. Arora RR, Chou TM, Jain D, Fleishman B, Crawford L, McKiernan T, et al. The multicenter study of enhanced external counterpulsation (MUST-EECP): effect of EECP on exercise-induced myocardial ischemia and anginal episodes. *J. Am. Coll. Cardiol.* 1999;33:1833–1840.

124. Michaels AD, Linnemeier G, Soran O, Kelsey SF, Kennard ED. Two-year

outcomes after enhanced external counterpulsation for stable angina pectoris (from the International EECP Patient Registry [IEPR]). *Am. J. Cardiol.* 2004;93:461–464.

125. Bonetti PO, Holmes DR, Lerman A, Barsness GW. Enhanced external counterpulsation for ischemic heart disease: what's behind the curtain? *J. Am. Coll. Cardiol.* 2003;41:1918–1925.

126. Werner D, Schneider M, Weise M, Nonnast-Daniel B, Daniel WG. Pneumatic external counterpulsation: a new noninvasive method to improve organ perfusion. *Am. J. Cardiol.* 1999;84:950–952, A7-8.

127. Lin W, Xiong L, Han J, Leung TWH, Soo YOY, Chen X, et al. External counterpulsation augments blood pressure and cerebral flow velocities in ischemic stroke patients with cerebral intracranial large artery occlusive disease. *Stroke*. 2012;43:3007–3011.

128. Masuda D, Nohara R, Hirai T, Kataoka K, Chen LG, Hosokawa R, et al. Enhanced external counterpulsation improved myocardial perfusion and coronary flow reserve in patients with chronic stable angina; evaluation by(13)N-ammonia positron emission tomography. *Eur. Heart J.* 2001;22:1451–1458.

129. Han JH, Wong KS. Is counterpulsation a potential therapy for ischemic stroke? *Cerebrovasc. Dis. Basel Switz.* 2008;26:97–105.

130. Alexandrov AW, Ribo M, Wong KS, Sugg RM, Garami Z, Jesurum JT, et al.

Perfusion augmentation in acute stroke using mechanical counter-pulsation-phase IIa: effect of external counterpulsation on middle cerebral artery mean flow velocity in five healthy subjects. *Stroke*. 2008;39:2760–2764.

131. Han JH, Leung TW, Lam WW, Soo YO, Alexandrov AW, Mok V, et al. Preliminary findings of external counterpulsation for ischemic stroke patient with large artery occlusive disease. *Stroke*. 2008;39:1340–1343.

132. Guluma KZ, Liebeskind DS, Raman R, Rapp KS, Ernstrom KB, Alexandrov AV, et al. Feasibility and Safety of Using External Counterpulsation to Augment Cerebral Blood Flow in Acute Ischemic Stroke-The Counterpulsation to Upgrade Forward Flow in Stroke (CUFFS) Trial. *J. Stroke Cerebrovasc. Dis. Off. J. Natl. Stroke Assoc.* 2015;24:2596–2604.

133. Lin S, Liu M, Wu B, Hao Z, Yang J, Tao W. External counterpulsation for acute ischaemic stroke. *Cochrane Database Syst. Rev.* 2012;1:CD009264.

134. Murry CE, Jennings RB, Reimer KA. Preconditioning with ischemia: a delay of lethal cell injury in ischemic myocardium. *Circulation*. 1986;74:1124–1136.

135. Hess DC, Hoda MN, Bhatia K. Remote limb perconditioning [corrected] and postconditioning: will it translate into a promising treatment for acute stroke? *Stroke*. 2013;44:1191–1197.

136. Lim SY, Hausenloy DJ. Remote Ischemic Conditioning: From Bench to Bedside. *Front. Physiol.* [Internet]. 2012 [cited 2017 Apr 15];3. Available from:

http://www.ncbi.nlm.nih.gov/pmc/articles/PMC3282534/

137. Hougaard KD, Hjort N, Zeidler D, Sørensen L, Nørgaard A, Thomsen RB, et al. Remote Ischemic Perconditioning in Thrombolysed Stroke Patients: Randomized Study of Activating Endogenous Neuroprotection – Design and MRI Measurements. *Int. J. Stroke*. 2013;8:141–146.

138. Hahn CD, Manlhiot C, Schmidt MR, Nielsen TT, Redington AN. Remote ischemic per-conditioning: a novel therapy for acute stroke? *Stroke*. 2011;42:2960–2962.

139. Hoda MN, Siddiqui S, Herberg S, Periyasamy-Thandavan S, Bhatia K, Johnson MH, et al. Remote Ischemic Perconditioning is Effective Alone and in Combination with Intravenous Tissue Plasminogen Activator in Murine Model of Embolic Stroke. *Stroke J. Cereb. Circ.* 2012;43:2794–2799.

140. Hoda MN, Fagan SC, Khan MB, Vaibhav K, Chaudhary A, Wang P, et al. A 2 × 2 factorial design for the combination therapy of minocycline and remote ischemic perconditioning: efficacy in a preclinical trial in murine thromboembolic stroke model. *Exp. Transl. Stroke Med.* 2014;6:10.

141. Hoda MN, Bhatia K, Hafez SS, Johnson MH, Siddiqui S, Ergul A, et al. Remote ischemic perconditioning is effective after embolic stroke in ovariectomized female mice. *Transl. Stroke Res.* 2014;5:484–490.

142. Jesudasan SJB, Todd KG, Winship IR. Reduced Inflammatory Phenotype in

Microglia Derived from Neonatal Rat Spinal Cord versus Brain. *PLOS ONE*. 2014;9:e99443.

143. Ren C, Li N, Wang B, Yang Y, Gao J, Li S, et al. Limb Ischemic Perconditioning Attenuates Blood-Brain Barrier Disruption by Inhibiting Activity of MMP-9 and Occludin Degradation after Focal Cerebral Ischemia. *Aging Dis.* 2015;6:406.

144. Hougaard KD, Hjort N, Zeidler D, Sørensen L, Nørgaard A, Hansen TM, et al. Remote ischemic perconditioning as an adjunct therapy to thrombolysis in patients with acute ischemic stroke: a randomized trial. *Stroke*. 2014;45:159–167.

145. Park JM, Hess DC. Breaking out from the neuroprotective logjam: combined treatment with remote ischemic conditioning and minocycline in the prehospital setting. *Neural Regen. Res.* 2015;10:537–539.

146. Hess DC, Blauenfeldt RA, Andersen G, Hougaard KD, Hoda MN, Ding Y, et al. Remote ischaemic conditioning—a new paradigm of self-protection in the brain. *Nat. Rev. Neurol.* 2015;11:698–710.

147. Hess DC, Hoda MN, Khan MB. Humoral Mediators of Remote Ischemic Conditioning: Important Role of eNOS/NO/Nitrite. *Acta Neurochir. Suppl.* 2016;121:45–48.

148. Kitagawa K, Saitoh M, Ishizuka K, Shimizu S. Remote Limb Ischemic Conditioning during Cerebral Ischemia Reduces Infarct Size through Enhanced Collateral Circulation in Murine Focal Cerebral Ischemia. *J. Stroke Cerebrovasc.*

Dis. 2018;27:831–838.

149. Bury SD, Jones TA. Unilateral sensorimotor cortex lesions in adult rats facilitate motor skill learning with the “unaffected” forelimb and training-induced dendritic structural plasticity in the motor cortex. *J. Neurosci. Off. J. Soc. Neurosci.* 2002;22:8597–8606.

150. Li J, Shan W, Zuo Z. Age-Related Upregulation of Carboxyl Terminal Modulator Protein Contributes to the Decreased Brain Ischemic Tolerance in Older Rats. *Mol. Neurobiol.* 2018;55:6145–6154.

151. Ay H, Koroshetz WJ, Vangel M, Benner T, Melinosky C, Zhu M, et al. Conversion of ischemic brain tissue into infarction increases with age. *Stroke*. 2005;36:2632–2636.

152. Popa-Wagner A, Badan I, Walker L, Groppa S, Patrana N, Kessler C. Accelerated infarct development, cytogenesis and apoptosis following transient cerebral ischemia in aged rats. *Acta Neuropathol. (Berl.)*. 2007;113:277–293.

153. Uchida M, Iida H, Iida M, Kumazawa M, Sumi K, Takenaka M, et al. Both milrinone and colforsin daropate attenuate the sustained pial arteriolar constriction seen after unclamping of an abdominal aortic cross-clamp in rabbits. *Anesth. Analg.* 2005;101:9–16, table of contents.

154. Pi Y, Zhang D, Kemnitz KR, Wang H, Walker JW. Protein kinase C and A sites on troponin I regulate myofilament Ca2+ sensitivity and ATPase activity in the

mouse myocardium. *J. Physiol.* 2003;552:845–857.

155. Guglin M, Kaufman M. Inotropes do not increase mortality in advanced heart failure. *Int. J. Gen. Med.* 2014;7:237–251.

156. Olson EM, Kim D, Smith TW, Marsh JD. Mechanism of the positive inotropic effect of milrinone in cultured embryonic chick ventricular cells. *J. Mol. Cell. Cardiol.* 1987;19:95–104.

157. Nishiguchi M, Ono S, Iseda K, Manabe H, Hishikawa T, Date I. Effect of Vasodilation by Milrinone, a Phosphodiesterase III Inhibitor, on Vasospastic Arteries After a Subarachnoid Hemorrhage in Vitro and in Vivo: Effectiveness of Cisternal Injection of Milrinone. *Neurosurgery*. 2010;66:158–164.

158. Shankar JJS, Santos MP dos, Deus-Silva L, Lum C. Angiographic evaluation of the effect of intra-arterial milrinone therapy in patients with vasospasm from aneurysmal subarachnoid hemorrhage. *Neuroradiology*. 2011;53:123–128.

159. Vroom MB, Pfaffendorf M, van Wezel HB, van Zwieten PA. Effect of phosphodiesterase inhibitors on human arteries in vitro. *Br. J. Anaesth.* 1996;76:122–129.

160. Lannes M, Teitelbaum J, Cortés M del P, Cardoso M, Angle M. Milrinone and Homeostasis to Treat Cerebral Vasospasm Associated with Subarachnoid Hemorrhage: The Montreal Neurological Hospital Protocol. *Neurocrit. Care*. 2012;16:354–362.

161. Ramakrishnan G, Armitage GA, Winship IR. Understanding and Augmenting Collateral Blood Flow During Ischemic Stroke. 2012 [cited 2017 Apr 11];Available from: http://www.intechopen.com/books/acute-ischemic-stroke/understanding-and-augmenting-collateral-blood-flow-during-ischemic-stroke

162. Campbell BCV, Christensen S, Tress BM, Churilov L, Desmond PM, Parsons MW, et al. Failure of collateral blood flow is associated with infarct growth in ischemic stroke. *J. Cereb. Blood Flow Metab. Off. J. Int. Soc. Cereb. Blood Flow Metab.* 2013;33:1168–1172.

163. Goyal M, Demchuk AM, Menon BK, Eesa M, Rempel JL, Thornton J, et al. Randomized assessment of rapid endovascular treatment of ischemic stroke. *N. Engl. J. Med.* 2015;372:1019–1030.

164. Berkhemer OA, Fransen PSS, Beumer D, van den Berg LA, Lingsma HF, Yoo AJ, et al. A randomized trial of intraarterial treatment for acute ischemic stroke. *N. Engl. J. Med.* 2015;372:11–20.

165. Campbell BCV, Mitchell PJ, Kleinig TJ, Dewey HM, Churilov L, Yassi N, et al. Endovascular Therapy for Ischemic Stroke with Perfusion-Imaging Selection. *N. Engl. J. Med.* 2015;372:1009–1018.

166. Saver JL, Goyal M, Bonafe A, Diener H-C, Levy EI, Pereira VM, et al. Stent-retriever thrombectomy after intravenous t-PA vs. t-PA alone in stroke. *N. Engl.*

J. Med. 2015;372:2285–2295.

167. Jovin TG, Chamorro A, Cobo E, de Miquel MA, Molina CA, Rovira A, et al. Thrombectomy within 8 Hours after Symptom Onset in Ischemic Stroke. *N. Engl. J. Med.* 2015;372:2296–2306.

168. Kilkenny C, Browne W, Cuthill IC, Emerson M, Altman DG. Animal research: Reporting in vivo experiments: The ARRIVE guidelines. *Br. J. Pharmacol.* 2010;160:1577–1579.

169. Armitage GA, Todd KG, Shuaib A, Winship IR. Laser speckle contrast imaging of collateral blood flow during acute ischemic stroke. *J. Cereb. Blood Flow Metab. Off. J. Int. Soc. Cereb. Blood Flow Metab.* 2010;30:1432–1436.

170. Chen ST, Hsu CY, Hogan EL, Maricq H, Balentine JD. A model of focal ischemic stroke in the rat: reproducible extensive cortical infarction. *Stroke*. 1986;17:738–743.

171. Li N, Thakor NV, Jia X. Laser speckle imaging reveals multiple aspects of cerebral vascular responses to whole body mild hypothermia in rats. In: 2011 Annual International Conference of the IEEE Engineering in Medicine and Biology Society. 2011. p. 2049–2052.

172. Boas DA, Dunn AK. Laser speckle contrast imaging in biomedical optics. *J. Biomed. Opt.* [Internet]. 2010 [cited 2017 Apr 10];15. Available from: http://www.ncbi.nlm.nih.gov/pmc/articles/PMC2816990/

173. Dunn AK. Laser Speckle Contrast Imaging of Cerebral Blood Flow. *Ann. Biomed. Eng.* 2012;40:367–377.

174. Zhu S, Li Y, Lu H, Li H, Tong S. Imaging the early cerebral blood flow changes in rat middle cerebral artery occlusion stroke model. *Conf. Proc. Annu. Int. Conf. IEEE Eng. Med. Biol. Soc. IEEE Eng. Med. Biol. Soc. Annu. Conf.* 2012;2012:2655–2658.

175. Briers JD, Richards G, He XW. Capillary Blood Flow Monitoring Using Laser Speckle Contrast Analysis (LASCA). *J. Biomed. Opt.* 1999;4:164–175.

176. Zhao L, Li Y, Li H, Omire-Mayor D, Tong S. The cerebral blood flow response dependency on stimulus pulse width is affected by stimulus current amplitude - a study of activation flow coupling. In: 2015 37th Annual International Conference of the IEEE Engineering in Medicine and Biology Society (EMBC). 2015. p. 5888–5891.

177. Miao P, Rege A, Li N, Thakor NV, Tong S. High Resolution Cerebral Blood Flow Imaging by Registered Laser Speckle Contrast Analysis. *IEEE Trans. Biomed. Eng.* 2010;57:1152–1157.

178. Liu Q, Li Y, Lu H, Tong S. Real-time high resolution laser speckle imaging of cerebral vascular changes in a rodent photothrombosis model. *Biomed. Opt. Express*. 2014;5:1483–1493.

179. Fischer MJM, Uchida S, Messlinger K. Measurement of meningeal blood vessel

diameter in vivo with a plug-in for ImageJ. *Microvasc. Res.* 2010;80:258–266.

180. Swanson RA, Morton MT, Tsao-Wu G, Savalos RA, Davidson C, Sharp FR. A Semiautomated Method for Measuring Brain Infarct Volume. *J. Cereb. Blood Flow Metab.* 1990;10:290–293.

181. Lin TN, He YY, Wu G, Khan M, Hsu CY. Effect of brain edema on infarct volume in a focal cerebral ischemia model in rats. *Stroke*. 1993;24:117–121.

182. Huang J-Y, Li L-T, Wang H, Liu S-S, Lu Y-M, Liao M-H, et al. In vivo two-photon fluorescence microscopy reveals disturbed cerebral capillary blood flow and increased susceptibility to ischemic insults in diabetic mice. *CNS Neurosci. Ther.* 2014;20:816–822.

183. Dong P, Zhao J, Zhang Y, Dong J, Zhang L, Li D, et al. Aging causes exacerbated ischemic brain injury and failure of sevoflurane post-conditioning: role of B-cell lymphoma-2. *Neuroscience*. 2014;275:2–11.

184. Tang Y, Wang L, Wang J, Lin X, Wang Y, Jin K, et al. Ischemia-induced Angiogenesis is Attenuated in Aged Rats. *Aging Dis.* 2016;7:326–335.

185. Dinapoli VA, Benkovic SA, Li X, Kelly KA, Miller DB, Rosen CL, et al. Age exaggerates proinflammatory cytokine signaling and truncates signal transducers and activators of transcription 3 signaling following ischemic stroke in the rat. *Neuroscience*. 2010;170:633–644.

186. Xu X, Wang B, Ren C, Hu J, Greenberg DA, Chen T, et al. Age-related Impairment of Vascular Structure and Functions. *Aging Dis.* 2017;8:590–610.

187. Farkas E, Luiten PG. Cerebral microvascular pathology in aging and Alzheimer's disease. *Prog. Neurobiol.* 2001;64:575–611.

188. Farkas E, de Vos RAI, Donka G, Jansen Steur EN, Mihály A, Luiten PGM. Age-related microvascular degeneration in the human cerebral periventricular white matter. *Acta Neuropathol. (Berl.)*. 2006;111:150–157.

189. Villena A, Vidal L, Díaz F, Pérez De Vargas I. Stereological changes in the capillary network of the aging dorsal lateral geniculate nucleus. *Anat. Rec. A. Discov. Mol. Cell. Evol. Biol.* 2003;274:857–861.

190. Hunter JM, Kwan J, Malek-Ahmadi M, Maarouf CL, Kokjohn TA, Belden C, et al. Morphological and Pathological Evolution of the Brain Microcirculation in Aging and Alzheimer's Disease. *PLOS ONE*. 2012;7:e36893.

191. Burns EM, Kruckeberg TW, Gaetano PK. Changes with age in cerebral capillary morphology. *Neurobiol. Aging*. 1981;2:283–291.

192. Klein AW, Michel ME. A morphometric study of the neocortex of young adult and old maze-differentiated rats. *Mech. Ageing Dev.* 1977;6:441–452.

193. Knox CA, Oliveira A. Brain aging in normotensive and hypertensive strains of rats. III. A quantitative study of cerebrovasculature. *Acta Neuropathol. (Berl.)*.

1980;52:17–25.

194. Wilkinson JH, Hopewell JW, Reinhold HS. A quantitative study of age-related changes in the vascular architecture of the rat cerebral cortex. *Neuropathol. Appl. Neurobiol.* 1981;7:451–462.

195. Shaul ME, Hallacoglu B, Sassaroli A, Shukitt-Hale B, Fantini S, Rosenberg IH, et al. Cerebral blood volume and vasodilation are independently diminished by aging and hypertension: a near infrared spectroscopy study. *J. Alzheimers Dis. JAD*. 2014;42 Suppl 3:S189-198.

196. Thore CR, Anstrom JA, Moody DM, Challa VR, Marion MC, Brown WR. Morphometric analysis of arteriolar tortuosity in human cerebral white matter of preterm, young, and aged subjects. *J. Neuropathol. Exp. Neurol.* 2007;66:337–345.

197. Brown WR, Moody DM, Challa VR, Thore CR, Anstrom JA. Venous collagenosis and arteriolar tortuosity in leukoaraiosis. *J. Neurol. Sci.* 2002;203–204:159–163.

198. Arsava EM, Vural A, Akpinar E, Gocmen R, Akcalar S, Oguz KK, et al. The detrimental effect of aging on leptomeningeal collaterals in ischemic stroke. *J. Stroke Cerebrovasc. Dis. Off. J. Natl. Stroke Assoc.* 2014;23:421–426.

199. Wagner M, Jurcoane A, Volz S, Magerkurth J, Zanella FE, Neumann-Haefelin T, et al. Age-related changes of cerebral autoregulation: new insights with

quantitative T2’-mapping and pulsed arterial spin-labeling MR imaging. *AJNR Am. J. Neuroradiol.* 2012;33:2081–2087.

200. Leoni RF, Oliveira I a. F, Pontes-Neto OM, Santos AC, Leite JP. Cerebral blood flow and vasoreactivity in aging: an arterial spin labeling study. *Braz. J. Med. Biol. Res. Rev. Bras. Pesqui. Medicas E Biol.* 2017;50:e5670.

201. Behnke BJ, Delp MD. Aging blunts the dynamics of vasodilation in isolated skeletal muscle resistance vessels. *J. Appl. Physiol. Bethesda Md 1985*. 2010;108:14–20.

202. Wang Z, Luo W, Zhou F, Li P, Luo Q. Dynamic change of collateral flow varying with distribution of regional blood flow in acute ischemic rat cortex. *J. Biomed. Opt.* 2012;17:125001–125001.

203. Wang S, Zhang H, Dai X, Sealock R, Faber JE. Genetic architecture underlying variation in extent and remodeling of the collateral circulation. *Circ. Res.* 2010;107:558–568.

204. Meier P, Gloekler S, Zbinden R, Beckh S, de Marchi SF, Zbinden S, et al. Beneficial effect of recruitable collaterals: a 10-year follow-up study in patients with stable coronary artery disease undergoing quantitative collateral measurements. *Circulation*. 2007;116:975–983.

205. Chalothorn D, Faber JE. Formation and maturation of the native cerebral collateral circulation. *J. Mol. Cell. Cardiol.* 2010;49:251–259.

206. Lucitti JL, Mackey JK, Morrison JC, Haigh JJ, Adams RH, Faber JE. Formation of the collateral circulation is regulated by vascular endothelial growth factor-A and a disintegrin and metalloprotease family members 10 and 17. *Circ. Res.* 2012;111:1539–1550.

207. Chalothorn D, Zhang H, Smith JE, Edwards JC, Faber JE. Chloride intracellular channel-4 is a determinant of native collateral formation in skeletal muscle and brain. *Circ. Res.* 2009;105:89–98.

208. Clayton JA, Chalothorn D, Faber JE. Vascular endothelial growth factor-A specifies formation of native collaterals and regulates collateral growth in ischemia. *Circ. Res.* 2008;103:1027–1036.

209. Beard DJ, McLeod DD, Logan CL, Murtha LA, Imtiaz MS, van Helden DF, et al. Intracranial pressure elevation reduces flow through collateral vessels and the penetrating arterioles they supply. A possible explanation for ‘collateral failure’’ and infarct expansion after ischemic stroke.’ *J. Cereb. Blood Flow Metab.* 2015;35:861–872.

210. Beard DJ, Murtha LA, McLeod DD, Spratt NJ. Intracranial Pressure and Collateral Blood Flow. *Stroke*. 2016;47:1695–1700.

211. Beard DJ, Logan CL, McLeod DD, Hood RJ, Pepperall D, Murtha LA, et al. Ischemic penumbra as a trigger for intracranial pressure rise - A potential cause for collateral failure and infarct progression? *J. Cereb. Blood Flow Metab. Off.*

J. Int. Soc. Cereb. Blood Flow Metab. 2016;36:917–927.

212. Menon BK, Smith EE, Coutts SB, Welsh DG, Faber JE, Goyal M, et al. Leptomeningeal collaterals are associated with modifiable metabolic risk factors. *Ann. Neurol.* 2013;74:241–248.

213. Winship IR, Armitage GA, Ramakrishnan G, Dong B, Todd KG, Shuaib A. Augmenting collateral blood flow during ischemic stroke via transient aortic occlusion. *J. Cereb. Blood Flow Metab.* 2014;34:61–71.

214. Liebeskind DS. Collateral Circulation. *Stroke*. 2003;34:2279–2284.

215. Shuaib A, Butcher K, Mohammad AA, Saqqur M, Liebeskind DS. Collateral blood vessels in acute ischaemic stroke: a potential therapeutic target. *Lancet Neurol.* 2011;10:909–921.

216. Ramakrishnan G, A. G, R. I. Understanding and Augmenting Collateral Blood Flow During Ischemic Stroke [Internet]. In: Garcia Rodriguez JC, editor. Acute Ischemic Stroke. InTech; 2012 [cited 2019 Feb 15]. Available from: http://www.intechopen.com/books/acute-ischemic-stroke/understanding-and-augmenting-collateral-blood-flow-during-ischemic-stroke

217. Hendrikse J, van Raamt AF, van der Graaf Y, Mali WPTM, van der Grond J. Distribution of Cerebral Blood Flow in the Circle of Willis. *Radiology*. 2005;235:184–189.

218. Winship IR. Cerebral Collaterals and Collateral Therapeutics for Acute Ischemic Stroke. *Microcirculation*. 2015;22:228–236.

219. Bang OY, Saver JL, Buck BH, Alger JR, Starkman S, Ovbiagele B, et al. Impact of collateral flow on tissue fate in acute ischaemic stroke. *J. Neurol. Neurosurg. Psychiatry*. 2008;79:625–629.

220. Christoforidis GA, Mohammad Y, Kehagias D, Avutu B, Slivka AP. Angiographic assessment of pial collaterals as a prognostic indicator following intra-arterial thrombolysis for acute ischemic stroke. *AJNR Am. J. Neuroradiol.* 2005;26:1789–1797.

221. Schellinger PD, Köhrmann M, Liu S, Dillon WP, Nogueira RG, Shuaib A, et al. Favorable vascular profile is an independent predictor of outcome: a post hoc analysis of the safety and efficacy of NeuroFlo Technology in Ischemic Stroke trial. *Stroke*. 2013;44:1606–1608.

222. Liebeskind DS. Of mice and men: essential considerations in the translation of collateral therapeutics. *Stroke*. 2008;39:e187-188; author reply e189.

223. Hoda MN, Bhatia K, Hafez SS, Johnson MH, Siddiqui S, Ergul A, et al. Remote Ischemic Perconditioning is Effective After Embolic Stroke in Ovariectomized Female Mice. *Transl. Stroke Res.* 2014;5:484–490.

224. Ren C, Li N, Wang B, Yang Y, Gao J, Li S, et al. Limb Ischemic Perconditioning Attenuates Blood-Brain Barrier Disruption by Inhibiting Activity of MMP-9 and

Occludin Degradation after Focal Cerebral Ischemia. *Aging Dis.* 2015;6:406–417.

225. Hanss M. Letter by Hanss Regarding Article, "Remote Ischemic Perconditioning Is Effective Alone and in Combination With Intravenous Tissue-type Plasminogen Activator in Murine Model of Embolic Stroke." *Stroke*. 2013;44:e36–e36.

226. Kim T, Masamoto K, Fukuda M, Vazquez A, Kim S-G. Frequency-dependent neural activity, CBF, and BOLD fMRI to somatosensory stimuli in isoflurane-anesthetized rats. *NeuroImage*. 2010;52:224–233.

227. Masamoto K, Fukuda M, Vazquez A, Kim S-G. Dose-dependent effect of isoflurane on neurovascular coupling in rat cerebral cortex. *Eur. J. Neurosci.* 2009;30:242–250.

228. Masamoto K, Kim T, Fukuda M, Wang P, Kim S-G. Relationship between neural, vascular, and BOLD signals in isoflurane-anesthetized rat somatosensory cortex. *Cereb. Cortex N. Y. N 1991*. 2007;17:942–950.

229. Santisakultarm TP, Kersbergen CJ, Bandy DK, Ide DC, Choi S-H, Silva AC. Two-photon imaging of cerebral hemodynamics and neural activity in awake and anesthetized marmosets. *J. Neurosci. Methods*. 2016;271:55–64.

230. Seto A, Taylor S, Trudeau D, Swan I, Leung J, Reeson P, et al. Induction of ischemic stroke in awake freely moving mice reveals that isoflurane anesthesia

can mask the benefits of a neuroprotection therapy. *Front. Neuroenergetics* [Internet]. 2014 [cited 2017 Feb 14];6. Available from: http://www.ncbi.nlm.nih.gov/pmc/articles/PMC3982055/

231. Lay CC, Frostig RD. Complete protection from impending stroke following permanent middle cerebral artery occlusion in awake, behaving rats. *Eur. J. Neurosci.* 2014;40:3413–3421.

232. Lay CC, Jacobs N, Hancock AM, Zhou Y, Frostig RD. Early stimulation treatment provides complete sensory-induced protection from ischemic stroke under isoflurane anesthesia. *Eur. J. Neurosci.* 2013;38:2445–2452.

233. Hara K, Harris RA. The anesthetic mechanism of urethane: the effects on neurotransmitter-gated ion channels. *Anesth. Analg.* 2002;94:313–318, table of contents.

234. Maggi CA, Meli A. Suitability of urethane anesthesia for physiopharmacological investigations in various systems. Part 2: Cardiovascular system. *Experientia*. 1986;42:292–297.

235. Maggi CA, Meli A. Suitability of urethane anesthesia for physiopharmacological investigations in various systems. Part 1: General considerations. *Experientia*. 1986;42:109–114.

236. Paasonen J, Salo RA, Shatillo A, Forsberg MM, Närväinen J, Huttunen JK, et al. Comparison of seven different anesthesia protocols for nicotine pharmacologic

magnetic resonance imaging in rat. *Eur. Neuropsychopharmacol. J. Eur. Coll. Neuropsychopharmacol.* 2016;26:518–531.

237. Winship IR. Laser speckle contrast imaging to measure changes in cerebral blood flow. *Methods Mol. Biol. Clifton NJ*. 2014;1135:223–235.

238. Li N, Thakor NV, Jia X. Laser speckle imaging reveals multiple aspects of cerebral vascular responses to whole body mild hypothermia in rats. *Conf. Proc. Annu. Int. Conf. IEEE Eng. Med. Biol. Soc. IEEE Eng. Med. Biol. Soc. Annu. Conf.* 2011;2011:2049–2052.

239. Strong AJ, Bezzina EL, Anderson PJ, Boutelle MG, Hopwood SE, Dunn AK. Evaluation of Laser Speckle Flowmetry for Imaging Cortical Perfusion in Experimental Stroke Studies: Quantitation of Perfusion and Detection of Peri-Infarct Depolarisations. *J. Cereb. Blood Flow Metab.* 2006;26:645–653.

240. Ayata C, Dunn AK, Gursoy-OZdemir Y, Huang Z, Boas DA, Moskowitz MA. Laser speckle flowmetry for the study of cerebrovascular physiology in normal and ischemic mouse cortex. *J. Cereb. Blood Flow Metab. Off. J. Int. Soc. Cereb. Blood Flow Metab.* 2004;24:744–755.

241. Ren C, Gao M, Dornbos D, Ding Y, Zeng X, Luo Y, et al. Remote ischemic post-conditioning reduced brain damage in experimental ischemia/reperfusion injury. *Neurol. Res.* 2011;33:514–519.

242. Bøtker HE, Kharbanda R, Schmidt MR, Bøttcher M, Kaltoft AK, Terkelsen CJ,

et al. Remote ischaemic conditioning before hospital admission, as a complement to angioplasty, and effect on myocardial salvage in patients with acute myocardial infarction: a randomised trial. *Lancet Lond. Engl.* 2010;375:727–734.

243. White SK, Frohlich GM, Sado DM, Maestrini V, Fontana M, Treibel TA, et al. Remote ischemic conditioning reduces myocardial infarct size and edema in patients with ST-segment elevation myocardial infarction. *JACC Cardiovasc. Interv.* 2015;8:178–188.

244. Hacke W, Kaste M, Bluhmki E, Brozman M, Dávalos A, Guidetti D, et al. Thrombolysis with alteplase 3 to 4.5 hours after acute ischemic stroke. *N. Engl. J. Med.* 2008;359:1317–1329.

245. Thrift AG, Thayabaranathan T, Howard G, Howard VJ, Rothwell PM, Feigin VL, et al. Global stroke statistics. *Int. J. Stroke*. 2017;12:13–32.

246. Fisher M, Feuerstein G, Howells DW, Hurn PD, Kent TA, Savitz SI, et al. Update of the stroke therapy academic industry roundtable preclinical recommendations. *Stroke*. 2009;40:2244–2250.

247. Pan J, Li X, Peng Y. Remote ischemic conditioning for acute ischemic stroke: dawn in the darkness. *Rev. Neurosci.* 2016;27:501–510.

248. Szijártó A, Czigány Z, Turóczi Z, Harsányi L. Remote ischemic perconditioning—a simple, low-risk method to decrease ischemic reperfusion injury: Models, protocols and mechanistic background. A review. *J. Surg. Res.*

2012;178:797–806.

249. Coelho JC, Sigel B, Flanigan DP, Schuler JJ, Justin J, Machi J. Arteriographic and ultrasonic evaluation of vascular clamp injuries using an in vitro human experimental model. *Surg. Gynecol. Obstet.* 1982;155:506–512.

250. Chen K, Pittman RN, Popel AS. Nitric Oxide in the Vasculature: Where Does It Come From and Where Does It Go? A Quantitative Perspective. *Antioxid. Redox Signal.* 2008;10:1185–1198.

251. Abu-Amara M, Yang SY, Quaglia A, Rowley P, Fuller B, Seifalian A, et al. Role of endothelial nitric oxide synthase in remote ischemic preconditioning of the mouse liver. *Liver Transplant. Off. Publ. Am. Assoc. Study Liver Dis. Int. Liver Transplant. Soc.* 2011;17:610–619.

252. Abu-Amara M, Yang SY, Quaglia A, Rowley P, De Mel A, Tapuria N, et al. Nitric oxide is an essential mediator of the protective effects of remote ischaemic preconditioning in a mouse model of liver ischaemia/reperfusion injury. *Clin. Sci.* 2011;121:257–266.

253. Rassaf T, Totzeck M, Hendgen-Cotta UB, Shiva S, Heusch G, Kelm M. Circulating Nitrite Contributes to Cardioprotection by Remote Ischemic PreconditioningNovelty and Significance. *Circ. Res.* 2014;114:1601–1610.

254. Qazi MA, Rizzatti F, Piknova B, Sibmooh N, Stroncek DF, Schechter AN. Effect of storage levels of nitric oxide derivatives in blood components. *F1000Research*

[Internet]. 2012 [cited 2019 Apr 3];1. Available from: https://www.ncbi.nlm.nih.gov/pmc/articles/PMC3814924/

255. Shiva S. Nitrite: A physiological store of nitric oxide and modulator of mitochondrial function. *Redox Biol.* 2013;1:40–44.

256. Lundberg JO, Weitzberg E. NO generation from nitrite and its role in vascular control. *Arterioscler. Thromb. Vasc. Biol.* 2005;25:915–922.

257. Hoda MN, Hess DC, Ergul A, Fagan SC. Response to Letter Regarding Article, “Remote Ischemic Perconditioning Is Effective Alone and in Combination With Intravenous Tissue-Type.” *Stroke*. 2013;44:e37–e37.

258. Ahmad F, Murata T, Shimizu K, Degerman E, Maurice D, Manganiello V. Cyclic Nucleotide Phosphodiesterases: important signaling modulators and therapeutic targets. *Oral Dis.* 2015;21:e25–e50.

259. Knott E, Assi M, Rao S, Ghosh M, Pearse D. Phosphodiesterase Inhibitors as a Therapeutic Approach to Neuroprotection and Repair. *Int. J. Mol. Sci.* 2017;18:696.

260. Atalay B, Caner H, Cekinmez M, Ozen O, Celasun B, Altinors N. Systemic Administration Of Phosphodiesterase V Inhibitor, Sildenafil Citrate, Forattenuation Of Cerebral Vasospasm Afterexperimental Subarachnoid Hemorrhage. *Neurosurgery*. 2006;59:1102–1108.

261. Birk S, Edvinsson L, Olesen J, Kruuse C. Analysis of the effects of phosphodiesterase type 3 and 4 inhibitors in cerebral arteries. *Eur. J. Pharmacol.* 2004;489:93–100.

262. Beavo JA. Cyclic nucleotide phosphodiesterases: functional implications of multiple isoforms. *Physiol. Rev.* 1995;75:725–748.

263. Zimmerman AL. Cyclic Nucleotide-Gated Ion Channels [Internet]. In: Cell Physiology Source Book. Elsevier; 2012 [cited 2019 May 2]. p. 621–632.Available from: https://linkinghub.elsevier.com/retrieve/pii/B9780123877383000354

264. Ma L, Gibson DA. Chapter 3 - Axon Growth and Branching [Internet]. In: Rubenstein JLR, Rakic P, editors. Cellular Migration and Formation of Neuronal Connections. Oxford: Academic Press; 2013 [cited 2019 May 3]. p. 51–68.Available from: http://www.sciencedirect.com/science/article/pii/B9780123972668000016

265. Yan K, Gao L-N, Cui Y-L, Zhang Y, Zhou X. The cyclic AMP signaling pathway: Exploring targets for successful drug discovery (Review). *Mol. Med. Rep.* 2016;13:3715–3723.

266. Bridges, D; Fraser ME; Moorhead GB. Cyclic nucleotide binding proteins in the Arabidopsis thaliana and Oryza sativa genomes | BMC Bioinformatics. 2005;

267. Beavo JA, Brunton LL. Cyclic nucleotide research — still expanding after half

a century. *Nat. Rev. Mol. Cell Biol.* 2002;3:710–717.

268. J B Polson, Strada and SJ. Cyclic Nucleotide Phosphodiesterases and Vascular Smooth Muscle. *Annu. Rev. Pharmacol. Toxicol.* 1996;36:403–427.

269. Kondo R, Matsumoto Y, Furui E, Itabashi R, Sato S, Yazawa Y, et al. Effect of Cilostazol in the Treatment of Acute Ischemic Stroke in the Lenticulostriate Artery Territory. *Eur. Neurol.* 2013;69:122–128.

270. Torii H, Kubota H, Ishihara H, Suzuki M. Cilostazol inhibits the redistribution of the actin cytoskeleton and junctional proteins on the blood–brain barrier under hypoxia/reoxygenation. *Pharmacol. Res.* 2007;55:104–110.

271. Anderson JL. Hemodynamic and clinical benefits with intravenous milrinone in severe chronic heart failure: Results of a multicenter study in the United States. *Am. Heart J.* 1991;121:1956–1964.

272. Nishiguchi M, Ono S, Iseda K, Manabe H, Hishikawa T, Date I. Effect of Vasodilation by Milrinone, a Phosphodiesterase III Inhibitor, on Vasospastic Arteries After a Subarachnoid Hemorrhage in Vitro and in Vivo: Effectiveness of Cisternal Injection of Milrinone. *Neurosurgery*. 2010;66:158–164.

273. Lannes M, Teitelbaum J, Cortés M del P, Cardoso M, Angle M. Milrinone and Homeostasis to Treat Cerebral Vasospasm Associated with Subarachnoid Hemorrhage: The Montreal Neurological Hospital Protocol. *Neurocrit. Care*. 2012;16:354–362.

274. Monrad ES, Baim DS, Smith HS, Lanoue AS. Milrinone, dobutamine, and nitroprusside: Comparative effects of hemodynamics and myocardial energetics in patients with severe congestive heart failure. *Circulation* [Internet]. 1986 [cited 2019 May 3];73. Available from: https://einstein.pure.elsevier.com/en/publications/milrinone-dobutamine-and-nitroprusside-comparative-effects-of-hem-2

275. Shankar JJS, Santos MP dos, Deus-Silva L, Lum C. Angiographic evaluation of the effect of intra-arterial milrinone therapy in patients with vasospasm from aneurysmal subarachnoid hemorrhage. *Neuroradiology*. 2011;53:123–128.

276. Drexler H, Höing S, Faude F, Wollschläger H, Just H. Central and regional vascular hemodynamics following intravenous milrinone in the conscious rat: comparison with dobutamine. *J. Cardiovasc. Pharmacol.* 1987;9:563–569.

277. Iida H, Iida M, Takenaka M, Oda A, Uchida M, Fujiwara H, et al. The effects of alpha-human atrial natriuretic peptide and milrinone on pial vessels during blood-brain barrier disruption in rabbits. *Anesth. Analg.* 2001;93:177–182.

278. Sulek CA, Blas ML, Lobato EB. Milrinone increases middle cerebral artery blood flow velocity after cardiopulmonary bypass. *J. Cardiothorac. Vasc. Anesth.* 2002;16:64–69.

279. Zeiler FA, Silvaggio J, Kaufmann AM, Gillman LM, West M. Norepinephrine as a potential aggravator of symptomatic cerebral vasospasm: two cases and

argument for milrinone therapy. *Case Rep. Crit. Care*. 2014;2014:630970.

280. Arakawa Y, Kikuta K, Hojo M, Goto Y, Ishii A, Yamagata S. Milrinone for the treatment of cerebral vasospasm after subarachnoid hemorrhage: report of seven cases. *Neurosurgery*. 2001;48:723–728; discussion 728-730.

281. Yoshida K, Watanabe H, Nakamura S. Intraarterial injection of amrinone for vasospasm induced by subarachnoid hemorrhage. *AJNR Am. J. Neuroradiol.* 1997;18:492–496.

282. Crespy T, Heintzelmann M, Chiron C, Vinclair M, Tahon F, Francony G, et al. Which Protocol for Milrinone to Treat Cerebral Vasospasm Associated With Subarachnoid Hemorrhage? *J. Neurosurg. Anesthesiol.* 2018;

283. Fraticelli AT, Cholley BP, Losser M-R, Maurice J-PS, Payen D. Milrinone for the Treatment of Cerebral Vasospasm After Aneurysmal Subarachnoid Hemorrhage. *Stroke*. 2008;39:893–898.

284. Romero CM, Morales D, Reccius A, Mena F, Prieto J, Bustos P, et al. Milrinone as a rescue therapy for symptomatic refractory cerebral vasospasm in aneurysmal subarachnoid hemorrhage. *Neurocrit. Care*. 2009;11:165–171.

285. Velly LJ, Bilotta F, Fàbregas N, Soehle M, Bruder NJ, Nathanson MH, et al. Anaesthetic and ICU management of aneurysmal subarachnoid haemorrhage: a survey of European practice. *Eur. J. Anaesthesiol.* 2015;32:168–176.

286. Davis MF, Lay C, Frostig RD. Permanent Cerebral Vessel Occlusion via Double Ligature and Transection. *J. Vis. Exp. JoVE* [Internet]. 2013 [cited 2017 Apr 15];Available from: http://www.ncbi.nlm.nih.gov/pmc/articles/PMC3845834/

287. Van Den Buuse M. Circadian rhythms of blood pressure, heart rate, and locomotor activity in spontaneously hypertensive rats as measured with radio-telemetry. *Physiol. Behav.* 1994;55:783–787.

288. Auriat AM, Klahr AC, Silasi G, Maclellan CL, Penner M, Clark DL, et al. Prolonged hypothermia in rat: a safety study using brain-selective and systemic treatments. *Ther. Hypothermia Temp. Manag.* 2012;2:37–43.

289. Radak D, Katsiki N, Resanovic I, Jovanovic A, Sudar-Milovanovic E, Zafirovic S, et al. Apoptosis and Acute Brain Ischemia in Ischemic Stroke. *Curr. Vasc. Pharmacol.* 2017;15:115–122.

290. Tang X, Liu P, Li R, Jing Q, Lv J, Liu L, et al. Milrinone for the Treatment of Acute Heart Failure After Acute Myocardial Infarction: A Systematic Review and Meta-Analysis. *Basic Clin. Pharmacol. Toxicol.* 2015;117:186–194.

291. Jeng J-S, Sun Y, Lee J-T, Lin R-T, Chen C-H, Po HL, et al. The Efficacy and Safety of Cilostazol in Ischemic Stroke Patients with Peripheral Arterial Disease (SPAD): Protocol of a Randomized, Double-Blind, Placebo-Controlled Multicenter Trial. *Int. J. Stroke*. 2015;10:123–127.

292. Shi L, Pu J, Xu L, Malaguit J, Zhang J, Chen S. The efficacy and safety of

cilostazol for the secondary prevention of ischemic stroke in acute and chronic phases in Asian population- an updated meta-analysis. *BMC Neurol.* [Internet]. 2014 [cited 2017 Apr 16];14. Available from: http://www.ncbi.nlm.nih.gov/pmc/articles/PMC4301843/

293. ALZET® Osmotic Pumps - Implantable pumps for research [Internet]. [cited 2019 Mar 4];Available from: http://www.alzet.com/

294. Schoemaker RG, Debets JJM, Struyker-Boudier HAJ, Smits JFM. Beneficial hemodynamic effects of two weeks' milrinone treatment in conscious rats with heart failure. *Eur. J. Pharmacol.* 1990;182:527–535.

295. Su J, Zhang T, Wang K, Zhu T, Li X. Autophagy activation contributes to the neuroprotection of remote ischemic perconditioning against focal cerebral ischemia in rats. *Neurochem. Res.* 2014;39:2068–2077.

296. Wang J, Han D, Sun M, Feng J. A Combination of Remote Ischemic Perconditioning and Cerebral Ischemic Postconditioning Inhibits Autophagy to Attenuate Plasma HMGB1 and Induce Neuroprotection Against Stroke in Rat. *J. Mol. Neurosci. MN*. 2016;58:424–431.

297. Beard DJ, McLeod DD, Logan CL, Murtha LA, Imtiaz MS, van Helden DF, et al. Intracranial pressure elevation reduces flow through collateral vessels and the penetrating arterioles they supply. A possible explanation for 'collateral failure'' and infarct expansion after ischemic stroke.' *J. Cereb. Blood Flow Metab.*

2015;35:861–872.

298. Williamson MR, Wilkinson CM, Dietrich K, Colbourne F. Acetazolamide Mitigates Intracranial Pressure Spikes Without Affecting Functional Outcome After Experimental Hemorrhagic Stroke. *Transl. Stroke Res.* [Internet]. 2018 [cited 2019 Jun 8];Available from: https://doi.org/10.1007/s12975-018-0663-6

299. Tatebayashi K, Asai Y, Maeda T, Shiraishi Y, Miyoshi M, Kawai Y. Effects of head-down tilt on the intracranial pressure in conscious rabbits. *Brain Res.* 2003;977:55–61.

300. Beretta S, Versace A, Carone D, Riva M, Dell'Era V, Cuccione E, et al. Cerebral collateral therapeutics in acute ischemic stroke: A randomized preclinical trial of four modulation strategies. *J. Cereb. Blood Flow Metab. Off. J. Int. Soc. Cereb. Blood Flow Metab.* 2017;37:3344–3354.

301. Ishida S, Miyati T, Ohno N, Hiratsuka S, Alperin N, Mase M, et al. MRI-based assessment of acute effect of head-down tilt position on intracranial hemodynamics and hydrodynamics. *J. Magn. Reson. Imaging JMRI.* 2018;47:565–571.

302. Tomiyama H, Higashi Y, Takase B, Node K, Sata M, Inoue T, et al. Relationships among hyperuricemia, metabolic syndrome, and endothelial function. *Am. J. Hypertens.* 2011;24:770–774.

303. Hattori T, Murase T, Ohtake M, Inoue T, Tsukamoto H, Takatsu M, et al.

Characterization of a new animal model of metabolic syndrome: the DahlS.Z-Leprfa/Leprfa rat. *Nutr. Diabetes*. 2011;1:e1.

304. Panchal SK, Brown L. Rodent models for metabolic syndrome research. *J. Biomed. Biotechnol.* 2011;2011:351982.

305. Zhang S, Zhuang J, Yue G, Wang Y, Liu M, Zhang B, et al. Lipidomics to investigate the pharmacologic mechanisms of ginkgo folium in the hyperuricemic rat model. *J. Chromatogr. B Analyt. Technol. Biomed. Life. Sci.* 2017;1060:407–415.

306. Liu Z, Chen T, Niu H, Ren W, Li X, Cui L, et al. The Establishment and Characteristics of Rat Model of Atherosclerosis Induced by Hyperuricemia. *Stem Cells Int.* 2016;2016:1365257.

307. Li Y, Lapina N, Weinzierl N, Bonde L, Boedtkjer E, Schubert R, et al. A novel method to isolate retinal and brain microvessels from individual rats: Microscopic and molecular biological characterization and application in hyperglycemic animals. *Vascul. Pharmacol.* 2018;110:24–30.

308. Wang J, Peng X, Lassance-Soares RM, Najafi AH, Alderman LO, Sood S, et al. Aging-Induced Collateral Dysfunction: Impaired Responsiveness of Collaterals and Susceptibility to Apoptosis via Dysfunctional eNOS signaling. *J Cardiovasc. Transl. Res.* 2011;4:779–789.

309. Pico F, Rosso C, Meseguer E, Chadenat M-L, Cattenoy A, Aegerter P, et al. A

multicenter, randomized trial on neuroprotection with remote ischemic per-conditioning during acute ischemic stroke: the REmote iSchemic Conditioning in acUtE BRAin INfarction study protocol. *Int. J. Stroke*. 2016;11:938–943.

310. Shahjouei S, Cai PY, Ansari S, Sharififar S, Azari H, Ganji S, et al. Middle Cerebral Artery Occlusion Model of Stroke in Rodents: A Step-by-Step Approach. *J. Vasc. Interv. Neurol.* 2016;8:1–8.

311. Sommer CJ. Ischemic stroke: experimental models and reality. *Acta Neuropathol. (Berl.)*. 2017;133:245–261.

312. Chi Y-W, Lavie CJ, Milani RV, White CJ. Safety and efficacy of cilostazol in the management of intermittent claudication. *Vasc. Health Risk Manag.* 2008;4:1197–1203.

313. Ding D. Cilostazol reduces morbidity but not mortality secondary to cerebral vasospasm following aneurysmal subarachnoid hemorrhage. *J. Neurol. Sci.* 2014;340:243–244.

314. Tanahashi N. [Antiplatelet therapy for secondary prevention of cerebral infarction]. *Nihon Rinsho Jpn. J. Clin. Med.* 2014;72:1270–1275.

315. Yamazaki T, Anraku T, Matsuzawa S. Ibudilast, a mixed PDE3/4 inhibitor, causes a selective and nitric oxide/cGMP-independent relaxation of the intracranial vertebrobasilar artery. *Eur. J. Pharmacol.* 2011;650:605–611.

316. Kishi Y, Ohta S, Kasuya N, Sakita S, Ashikaga T, Isobe M. Ibudilast: a non-selective PDE inhibitor with multiple actions on blood cells and the vascular wall. *Cardiovasc. Drug Rev.* 2001;19:215–225.

317. Li H, Zuo J, Tang W. Phosphodiesterase-4 Inhibitors for the Treatment of Inflammatory Diseases. *Front. Pharmacol.* [Internet]. 2018 [cited 2019 Jun 9];9. Available from: https://www.ncbi.nlm.nih.gov/pmc/articles/PMC6199465/